Universidade de Aveiro Departamento de Química
2017

Suzanne Christé

Preparação de nanoestruturas multifuncionais de polímero@ouro e preparação de filmes finos em multicamadas para biodeteção

Preparation of multifunctional polymer@gold nanostructures and assembly into multilayered thin films for biosensing

Universidade de Aveiro Departamento de Química
2017

Suzanne Christé

Preparação de nanoestruturas multifuncionais de polímero@ouro e preparação de filmes finos em multicamadas para biodeteção

Preparation of multifunctional polymer@gold nanostructures and assembly into multilayered thin films for biosensing

Dissertação apresentada à Universidade de Aveiro para cumprimento dos requisitos necessários à obtenção do grau de Mestre em Química/Functionalized Advanced Materials and Engineering (FAME), realizada sob a orientação científica da Doutora Ana Margarida Madeira Viegas de Barros Timmons, Professora auxiliar do Departamento de Química da Universidade de Aveiro e da Doutora Sónia Oliveira Pereira, Bolseira de Pós-Doutoramento do Departamento de Física da Universidade de Aveiro

o júri

presidente

Prof. Doutor Vitor Brás Sequeira Amaral
professor catedrático com agregação do Departamento de Física da Universidade de Aveiro

Prof. Doutor Tito Trindade
professor associado com agregação do Departamento de Química da Universidade de Aveiro

Doutora Sónia Oliveira Pereira
investigadora de pós-doutoramento do Departamento de Física da Universidade de Aveiro

agradecimentos

Em primeiro lugar, gostaria de agradecer às minhas orientadoras, pela ajuda e apoio durante este projeto e pelas várias discussões e sugestões. À Professora Ana Barros-Timmons pela sua disponibilidade e conselhos. À Doutora Sónia Oliveira Pereira pela sua disponibilidade e apoio, especialmente pela sua ajuda nas reações e discussao dos resultados, pelos seus preciosos conselhos no uso de software e outras técnicas de laboratório.

Agradeço também à Maria Celeste Azevedo pelo seu bom humor, a sua disponibilidade e pela sua ajuda em técnicas de espectroscopia: UV-Visível, fotoluminescência e infravermelho. À Marta Ferro pela sua ajuda e experiência em microscopia electrónica: TEM, SEM e STEM. Ao Professor Dmitry Evtyugin, pelo seu tempo e explicações sobre a caracterização por GPC-SEC. À Engenheira Ana Caço, pelo uso do espectrómetro UV-Visível do complexo dos Laboratórios Tecnológicos, e a sua ajuda na pesquisa de reagentes.

Gostaria também de agradecer à equipa que trabalha no laboratório do complexo dos Laboratórios Tecnológicos: ao Nuno Gama pela sua ajuda na minha integração no laboratório, à Marina Matos e à Doutora Patrícia Ramos pelos seus sorrisos e bom humor de todos os dias. À equipa do departamento de Química: Doutoras Ana Luísa Silva e Ana Estrada pela ajuda e pelo material de laboratório disponibilizado, e aos outros estudantes amigáveis que trabalham no laboratório.

Finalmente, aos meus pais pelo apoio e encorajamento, e também às preciosas amizades criadas durante este ano em Aveiro.

palavras-chave

Nanoparticulas de ouro, modificação e funcionalização de superfícies, nanoestruturas do tipo coroa@núcleo, polimerização RAFT, filmes finos multicamadas, biodeteção.

resumo

O objetivo desta tese de mestrado era desenvolver nanoestruturas robustas e multifuncionais do tipo coroa@núcleo para servir como base num sensor biológico. A estabilidade e as propriedades óticas das nanopartículas de ouro (Au NPs), nomeadamente a ressonância de plasmão de superfície localizada (LSPR), tornam as excelentes candidatos para o desenvolvimento de biossensores baseados em SPR. No seguimento de um trabalho anterior, procedeu-se primeiro à otimização da encapsulação e funcionalização dasAu NPs. Em segundo lugar, preparou-se filmes finos de multicamadas que incorporam as nanopartículas encapsuladas.

Au NPs (15 $\pm$ 4 nm) foram sintetizadas pelo método de Turkevich, e sua superfície foi revestida por polimerização de transferência de cadeia reversível por adição-fragmentação (RAFT) assistida em encapsulante emulsão (REEP). Foram explorados dois tipos de nanoestruturas: i) nanoestruturas não funcionalizadas foram preparadas com sucesso adsorvendo um agente macroRAFT (MR) P($PEGA_{40}$)-TTC) não funcionalizado nas Au NPs, seguido pelo crescimento do bloco hidrofóbico usando uma mixtura (10:1 w/w) de metacrilato de metilo (MMA) e de acrilato de butilo (BA) a partir de MR@Au NPs; e ii) nanoestruturas funcionalizadas foram preparadas usando um agente MR funcionalizado com um bioreceptor (biotina) e um fluoróforo (isotiocianato de fluoresceína - FITC). Foram realizadas tentativas para crescer o bloco hidrofóbico apartir das nanoestruturas multifuncionais MR@Au com o objetivo de melhorar a sua resposta óptica aumentando a distância entre o núcleo e o fluoróforo. No entanto, concluiu-se que a estratégia seguida para preparar estas nanoestruturas multifuncionais tem de ser revista. O tamanho e a estabilidade das nanoestruturas de ouro foi avaliado por espectroscopia UV-Visível e fluorescência, STEM (microscopia eletrónica de transmissão de varrimento), DLS (dispersão dinâmica de luz) e medidas de potencial zeta. A caracterização química e estrutural dos polímeros foi feita por espectroscopias de ^{1}H-RMN (ressonância magnética nuclear de protões) e de infravermelho, e cromatografia de permeação de gel – cromatografia de exclusão por tamanho (GPC-SEC). Em seguida, foram realizados testes de biodeteção usando a nanoestrutura multifuncional de coroa@núcleo no sentido de avaliar a sua resposta óptica na presença de um bioanalito específico - avidin. No entanto, estes testes não foram conclusivos devido às limitações da estratégia seguida para preparar as nanoestruturas multifuncionais.

Paralelamente ao trabalho descrito acima, estudou-se a preparação de filmes finos usando o método camada a camada (Layer-by-Layber, LbL) baseado em interações electrostáticas, para isso foi usado o hidrocloreto de polialilamina (PAH) e as nanoestruturas de Au. Foram estudados alguns parâmetros nomeadamente o peso molecular, tempo de deposição, pH e força iónica, e o número de camadas. O objetivo final era depositar na última camada as nanoestruturas de ouro funcionalizadas com biotina-FITC. O procedimento para a deposição por LbL das NPs de Au encapsuladas foi realizado com sucesso, mas uma vez que os testes de biodeteção não foram conclusivos este último passo não foi efectuado.

keywords

Gold nanoparticles, surface modification and functionalization, shell@core nanostructure, RAFT polymerization, multilayered thin films, Layer-by-Layer, biosensing.

abstract

The aim of this master thesis was to develop robust, easily prepared multifunctional shell@core gold nanostructures to serve as a basis for customization into a specific biological sensor. The stability and optical properties of gold nanoparticles (Au NPs), namely the localized surface plasmon resonance (LSPR), makes them excellent candidates for the development of SPR-based biosensors. In this work, the preparation and functionalization of the gold nanoparticles was first optimized, on the basis of the previous work. Next, multilayered thin-films embedding these gold nanostructures were prepared.

Au NPs (15 $\pm$ 4 nm) were synthetized by the Turkevich method, and their surface was coated via reversible addition fragmentation chain transfer (RAFT) assisted encapsulating emulsion polymerization (REEP). The preparation of two types of nanostructures was explored: i) non-functionalized nanostructures were successfully prepared using the macroRAFT (MR) agent P($PEGA_{40}$)-TTC) adsorbed onto Au NPs, followed the growth of a hydrophobic block using a 10:1 (w/w) mixture of methyl methacrylate and butyl acrylate from MR@Au NPs; and ii) functionalized nanostructures were prepared using a MR agent functionalized with a bio-receptor (biotin) and a fluorophore (fluorescein isothiocyanate - FITC). Attempts to grow a hydrophobic block from the multifunctional MR@Au NPs were carried out to enhance the optical response by increasing the distance between the core and fluorophore. Yet, the synthetic strategy followed to prepare this type of multifunctional nanostructures needs to be revised.

The size and stability of gold nanostructures were characterized by UV-Visible and fluorescence spectroscopy, STEM (scanning transmission electron microscopy), DLS (dynamic light scattering) and Zeta potential measurements. The chemical and structural characterization of polymers was carried out by ^{1}HNMR (proton nuclear magnetic resonance), infrared spectroscopies and gel permeation chromatography – size exclusion chromatography (GPC-SEC). Then, biosensing tests were performed on the multifunctional shell@core nanostructures synthetized to assess their optical response towards a specific bioanalyte - avidin. However, these tests were inconclusive due to the limitations of the synthetic strategy followed to prepare the Au nanostructures.

Parallel to the synthetic work described above, the preparation of thin films via electrostatic interactions using the Layer-by-Layer (LbL) method was studied, using poly(allylamine hydrochloride) (PAH) and carboxylic acid terminated non-functionalized Au nanostructures. Various parameters were studied such as molecular weight, deposition time, pH and ionic strength, as well as the number of layers. The final goal was to deposit the biotin-FITC-functionalized gold nanostructure as last layer. The optimized procedure for LbL deposition of the encapsulated Au NPs was fully accomplished, in view of the fact that the biosensing tests were inconclusive, this last step was not carried out.

CONTENTS

ABBREVIATIONS

ATR-FTIR	Attenuated Total Reflectance - Fourier Transform InfraRed
BSA	Bovine Serum Albumin
C-NMR	C (Carbon)-Nuclear Magnetic Resonance
CMC	Critical Micellar Concentration
CSIRO	Commonwealth Scientific and Industrial Research Organization
CTA	Chain Transfer Agent
CuAAC	Copper-catalyzed (Cu(I)) Azide-Alkyne Cycloaddition
d	Diameter
$d_{average}$	Hydrodynamic average diameter
DLS	Dynamic Light Scattering
DMSO	Dimethyl Sulfoxide
DNA	DeoxyriboNucleic Acid
DP	Degree of Polymerization
FRET	Förster Resonance Energy Transfer
FTIR	Fourier Transformed InfraRed
GPC-SEC	Gel Permeation Chromatography - Size Exclusion Chromatography
H-NMR	H (Proton)-Nuclear Magnetic Resonance
IgG	Immunoglobulin G
LB	Langmuir-Blodgett
LbL	Layer-by-Layer
LSPCF	Localized Surface Plasmon Coupled Fluorescence
LSPR	Localized Surface Plasmon Resonance
M_n	Number average Molecular weight
MR	MacroRAFT
M_w	Weight average Molecular weight
MW	Molecular Weight
NPs	NanoParticles
NSET	Nanoparticle Surface Energy Transfer
PBS	Phosphate Buffer Saline
PdI	Polydispersity Index (DLS measurements)
PE	Polyelectrolyte
PL	Photoluminescence
QDs	Quantum Dots
RAFT	Reversible Addition−Fragmentation chain Transfer
RDRP	Reversible-Deactivation Radical Polymerization
SEM	Scanning Electron Microscopy
SERS	Surface-Enhanced Raman Spectroscopy
STEM	Scanning Transmission Electron Microscopy
TEM	Transmission Electron Microscopy
UV-Vis	Ultraviolet-Visible

Chemicals

AA	acrylic acid
ACPA	4,4'-azobis(4-cyanopentanoic acid)
AEM	2-aminoethyl methacrylate
AIBN	2,2'-azobis(isobutyronitrile)
BA	Butyl acrylate
DMF	Dimethylformamide
FITC	Fluorescein isothiocyanate
MMA	Methyl methacrylate
P(AA_2-*b*-$PEGA_{40}$)-*b*-(MMA-*co*-BA)-TTC	Poly[(acrylic acid)-*b*-(poly(ethylene glycol) methyl ether acrylate]-*b*-(methyl methacrylate-*co*-butyl acrylate)] synthetized from TTC
P(AA_2-*b*-$PEGA_{40}$)-TTC	Poly[(acrylic acid)-*b*-(poly(ethylene glycol) methyl ether acrylate)] synthetized from TTC
P($PEGA_{40}$)-*b*-(MMA-*co*-BA)-TTC	Poly[(poly(ethylene glycol) methyl ether acrylate)-*b*-(methyl methacrylate-*co*-butyl acrylate)] synthetized from TTC
P($PEGA_{40}$)-TTC	Poly[poly(ethylene glycol) methyl ether acrylate] synthetized from TTC
PAA	Poly(acrylic acid)
PAH	Poly(allylamine hydrochloride)
PEGA	Poly(ethylene glycol) methyl ether acrylate
PPE	Poly(*p*-phenyleneethynylene)
PSS	Poly(styrene sulfonic acid)
THF	Tetrahydrofuran
TTC-A	2-(dodecylthiocarbonothioylthio)-2-methylpropionic acid
VA-044	2,2'-azobis[2-(2-imidazolin-2-yl)propane] dihrydrochloride

Symbols

Đ	Dispersity (for GPC-SEC measurements)
Δλ	Wavelength shift (nm)
ζ	Zeta potential (mV)
λ	Wavelength (nm)
λ_{exc}	Excitation wavelength (nm)
λ_{LSPR}	Wavelength of Localized Surface Plasmon Resonance (nm)

LIST OF FIGURES

LIST OF SCHEMES

LIST OF TABLES

CHAPTER 1. GENERAL INTRODUCTION

1.1. Introduction

In this chapter, the theoretical basis related to the present dissertation will be outlined. First, the definition of a biosensor device and basic principles will be given. The use of nanomaterials in the preparation of such devices, and in particular noble metal nanoparticles such as gold, present advantages in the improvement of sensitivity and detection. Therefore, the synthesis and preparation of gold nanoparticles (Au NPs), their main optical properties, namely the localized surface plasmon resonance (LSPR) will be briefly presented. Moreover, their surface modification and functionalization make them interesting candidates for biosensing applications. Among functionalization routes for Au NPs, the polymerization methods used in this work, namely emulsion polymerization and click chemistry will be described. Finally, the physical preparation of multilayers films that includes functionalized Au NPs can be obtained using the layer-by-layer deposition technique, which will be presented in the last part of this introductory chapter.

1.2. Nanomaterials for biosensing applications

According to the IUPAC definition, a biosensor is ‘‘a self-contained integrated device which is capable of providing specific quantitative or semi-quantitative analytical information using a biological recognition element which is in direct spatial contact with a transducer’’ [1, 2]. In other words, a biosensor is a system that reports the presence of an analyte of biological relevance. The transducer is made up of two moieties. The “bio” moiety is a recognition system able to bind to or react with the analyte. It is by interacting with the “sensor” moiety that a transducer system is able to transform this recognition event into a signal that can be then visualized and/or quantified via signal processing. Depending on the type of transducer, the translated signal can be read in the form of electrochemical, electrochemiluminescent, magnetic, gravimetric or optical signals [3].

Nanomaterials are promising candidates to increase the sensitivity and lower detection limits of biosensing devices. They can help to enhance the biorecognition event signal at reduced volumes or even act themselves as transducers. Among such nanomaterials, gold nanoparticles, semi-conductor quantum dots, polymer nanoparticles, carbon nanotubes, nanodiamonds, and graphene have been and continue to be intensively studied as biosensing materials [3].

The properties of noble metal nanoparticles, namely their physicochemical properties such as their ease of functionalization and high surface-to-volume ratios, combined with their unique optical properties, allowed the development of new biosensing platforms with enhanced capabilities for the detection of bioanalytes. Additionally, they present advantages for commonly used techniques, such as fluorescence and Raman spectroscopy [4, 5].

1.3. Gold nanoparticles (Au NPs) as biosensors

Due to their biocompatibility, their tunability in particle size and shape, ease of synthesis and surface modification, and their particular optical properties, colloidal gold nanoparticles (Au NPs) have been extensively studied for applications in biomedicine, biosensing, imaging and therapy [4, 5]. However, to be used in biological systems, Au NPs require surface modification and functionalization to enable their use as biosensors, as well maintaining their colloidal stability in physiological medium. The surface modification and functionalization permits to chemically design the Au NPs surface, while maintaining their optical properties [6].

1.3.1. Synthesis and stabilization of Au NPs

Several methods exist for the synthesis of metallic nanoparticles such as gold and silver (Au and Ag NPs), resulting in particles of different sizes and shapes, as represented in Figure 1.1 [7].

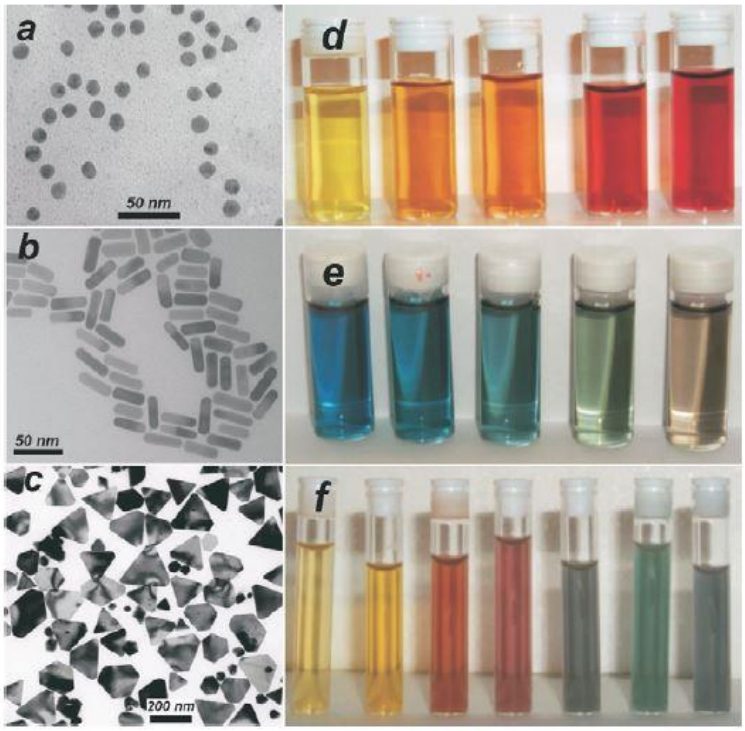

Figure 1.1: Aspect and colours of metallic nanoparticles
Left: Transmission electron micrographs of Au nanospheres and nanorods (a,b) and Ag nanoprisms (c) formed using citrate reduction, seeded growth, and DMF (dimethylformamide) reduction, respectively. Right: Photographs of colloidal dispersions of AuAg alloy nanoparticles with increasing Au concentration (d), Au nanorods of increasing aspect ratio (e), and Ag nanoprisms with increasing lateral size (f). Taken from [7]

As early as 1857, it has been described by Faraday that the colour properties of small Au particles were highly dependent on their size. Faraday was also the first to establish a scientific recipe for the production

of gold colloids [8]. One of the most common methods to produce colloidal gold solution is the citrate method, developed by Turkevich and co-workers in 1951 [9], leading to the formation of quasi-spherical nanoparticles with diameters from around 10 to 50 nm. It is based on chemical reduction of Au(III) to Au(0) ions using sodium citrate as a reducing agent. In this approach, the citrate acts both as reducing agent and as capping agent, thus forming citrate-capped gold NPs stabilized by electrostatic repulsion [4]. The method was later refined by Frens, to better monitor the particle size by controlling the citrate concentration [10]. In 2006, Kimling and his group have shown that the exposure to UV radiation in citrate, or using ascorbate as a reducing agent enabled the preparation of Au NPs at room temperature [11].

1.3.2. Localized surface plasmon resonance (LSPR) of Au NPs

The unique optical properties of metal nanoparticles (1 to 100 nm in diameter) such as Au and Ag NPs arise from their size confinement effect, which provides new electronic and optical properties. A distinct feature is the intense visible color of their colloidal solution that is caused by the surface plasmon resonance (SPR) absorption, also called localized surface plasmon resonance (LSPR). The origin of the light absorption by Au NPs is the coherent oscillation of the conduction band electrons induced by interacting with the electromagnetic field, as illustrated in Figure 1.2 (A) [7, 12]. The LSPR absorption peak red shifts to longer wavelength with increasing particle size, as shown in Figure 1.2 (B). The LSPR not only depends on the size of the particles but also on their shape, aggregation state and surface modifications, as well as the dielectric properties and refractive index of the surrounding medium [12–15].

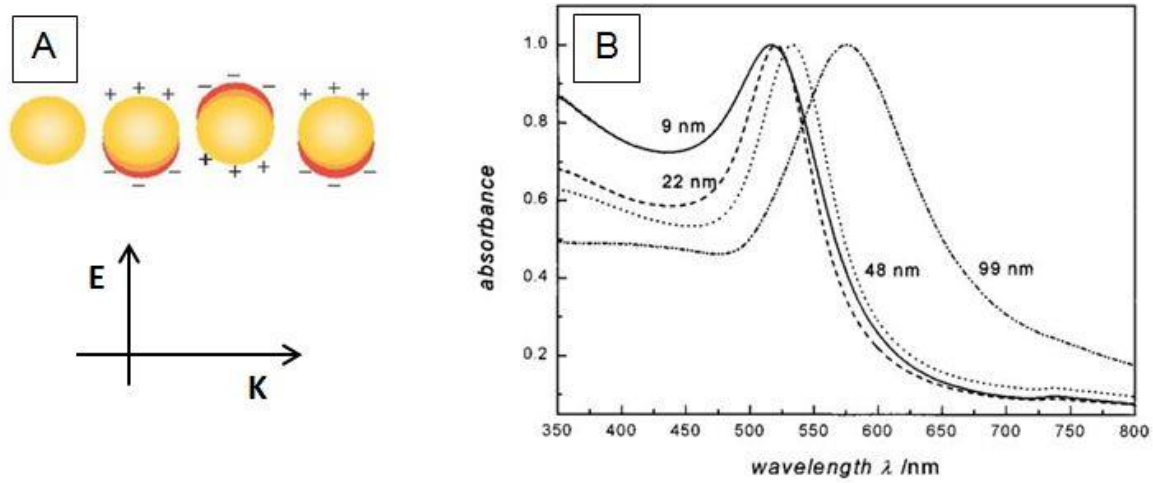

Figure 1.2: Surface plasmon resonance of Au nanospheres
(A) Schematic illustration of surface plasmon resonance in plasmonic nanospheres. Adjusted from [7] (B) UV-Vis spectra of gold nanospheres of different sizes. Adjusted from [13]

An example of the use of red-shift in LSPR as a refractive index sensor is presented in Figure 1.3, in which the local refractive index changes such as those induced by biomolecular interactions at the surface of the nanostructures can be monitored via the LSPR peak shift [16].

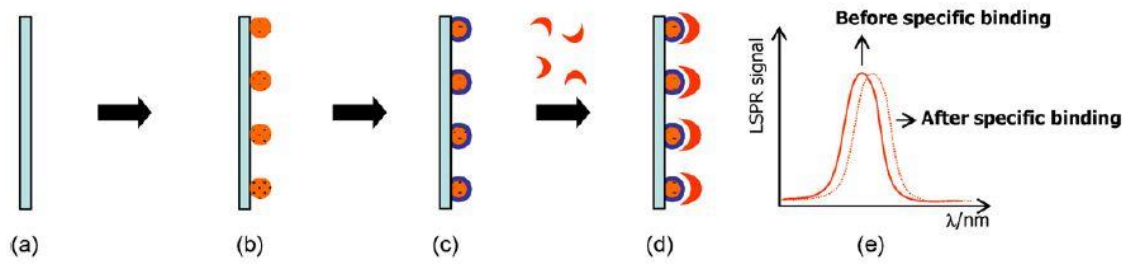

Figure 1.3: Schematic representation of the preparation and response of LSPR biosensors based on refractive index changes.
(a) a substrate is chosen, (b) metal nanoparticles are attached to it by means of chemical linkers or prepared by nanolithography, (c) the metal particles are modified with the sensor moiety, (d) the analyte attaches from solution specifically onto the recognition function adsorbed onto the particles, causing a change in the refractive index around the particle resulting in an LSPR shift (e). Taken from [16]

Plasmonic biosensors have also been combined with other techniques such as the surface-enhanced Raman spectroscopy (SERS) and laser desorption ionization mass spectroscopy [17]. Another interesting example of a biorecognition experiment using Au NPs as LSPR transducers was reported in 2003 by Raschke and co-workers, as shown in Figure 1.4, in which single Au NPs were functionalized with biotin. The addition of streptavidin and subsequent specific binding events alter the dielectric environment of the nanoparticle, resulting in a spectral shift of the particle plasmon resonance [18].

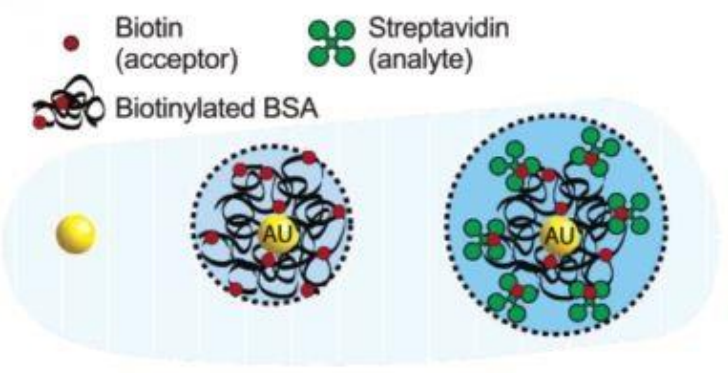

Figure 1.4: Schematic representation of a biosensor based on light scattering from a single gold nanoparticle functionalized with biotinylated BSA which subsequently binds streptavidin. Taken from [18]

1.3.3. Fluorescence quenching combined with Au NPs

The fluorescence quenching is a phenomenon attributed to Förster resonance energy transfer (FRET), also known as fluorescence resonance energy transfer, which occurs at distances up to 10 nm between a donor and an acceptor. In the case of nanoparticles, another phenomenon called nanoparticle surface energy transfer (NSET) can take place, in which the energy transfer occurs between the fluorophore (donor) and the nanoparticle surface (acceptor). In this case the phenomenon occurs for distances from 2 to 30 nm (nearly twice as far as FRET) [19]. Thus, the fluorescence quenching has been explored in biosensing, by monitoring the receptor/ligand binding through changes in fluorescence intensity [4, 20–22].

The combination of LSPR of Au NPs and fluorescence quenching properties into a biosensor device was reported for the detection of immunoglobulin by Hsieh and co-workers in 2007. In their work, a fiber-optic biosensor was prepared based on the coupling of LSPR and fluorescence (LSPCF). Experimentally, the LSPCF biosensor could detect mouse immunoglobulin G (IgG) at a minimum concentration of 1 pg/mL [23]. In 2007, You *et al* used the principle of fluorescence quenching for a prototype sensor array using functionalized Au NPs with a fluorescent polymer: poly-(*p*-phenylene ethynylene) (PPE). As illustrated in Figure 1.5, the electrostatic complexation of the Au NPs and polymer results in fluorescence quenching of the polymer (fluorescence "OFF"). Upon addition of protein analytes, the quenched polymer-Au NPs complexes is then disrupted, causing recovery of fluorescence signal (fluorescence "ON") [24].

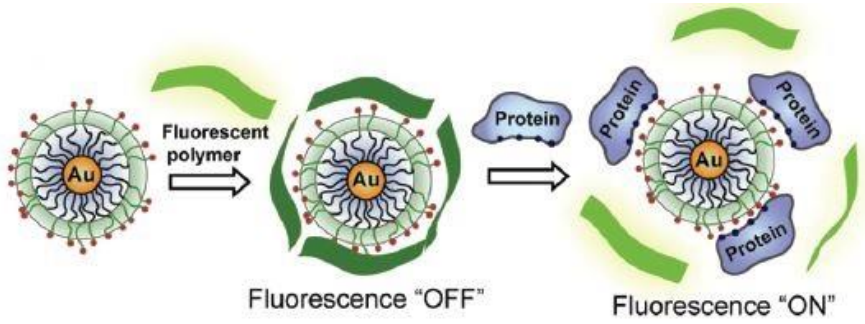

Figure 1.5: Schematic illustration of sensor array based on AuNP-fluorescent polymer conjugates. Taken from [24]

In the present study, the same principle of distance-dependent fluorescence quenching will be used. However, the gold nanoparticles are functionalized with a fluorophore (FITC) attached to the polymer, near enough to the gold core to allow a strong quenching. After the recognition event, a change in conformation of the polymer is expected, leading to an increased distance between the fluorophore and the gold surface, so that the quenching of the fluorescence signal is largely cancelled.

1.4. Surface modification by RAFT assisted emulsion polymerization

The reversible addition fragmentation chain transfer (RAFT) polymerization method is a controlled/living free-radical polymerization, with the advantage of the use of a wide range of monomers and reaction conditions, also providing controlled molecular weight polymers with controlled compositions and narrow polydispersities. The RAFT method was first reported by an Australian CSIRO groups in 1998 [25] for S=C(Z)S- type moieties, and was later achieved with thiocarbonylthio compounds [ZC(=S)SR] by the same group in 2005 [26, 27]. In 2008, York *et al* adapted the RAFT polymerization method to aqueous media, allowing the preparation of amphiphilic block copolymer architectures appropriate for drug and gene delivery platforms [28].

1.4.1. Reversible addition fragmentation chain transfer (RAFT) polymerization

The RAFT mechanism allows the control of polymer dimensions by targeting a specific molecular weight or chain length. The synthesis of homopolymers or block copolymers of tunable dimensions makes the RAFT polymerization a very attractive technique for drug and gene delivery applications. In addition, it can be used to synthesize various polymer architectures including multi-block, star, graft, statistical, alternating and gradient copolymers, as presented in Figure 1.6 [28].

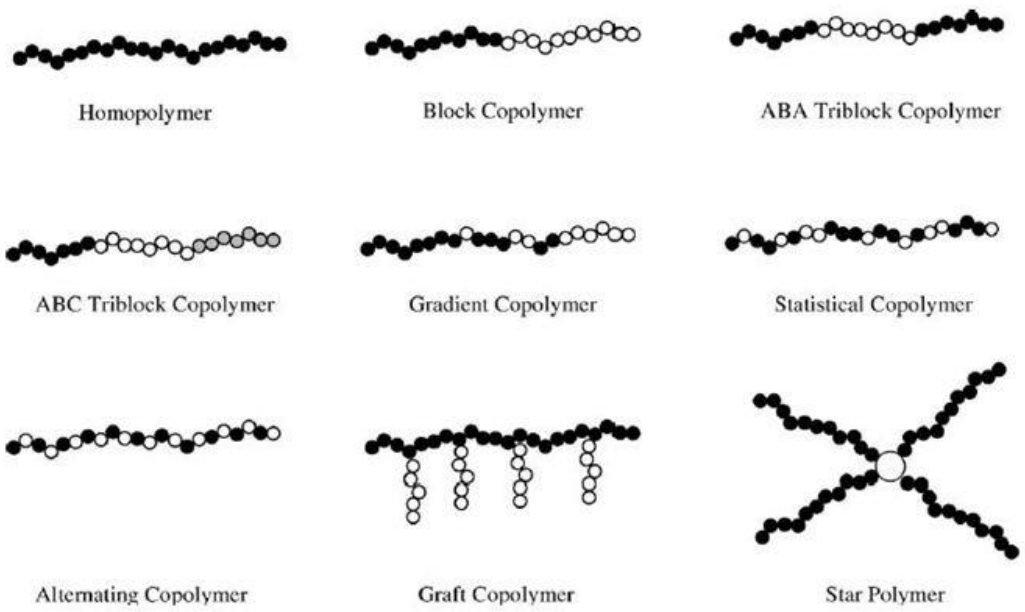

Figure 1.6: Polymer architectures available through the controlled/living radical polymerization. Taken from [28]

The RAFT process is similar to conventional free radical polymerization but incorporates a chain transfer agent (CTA) to allow controlled/living polymerization. It is based on a cycle of active and dormant chains, in a three steps method. In the first step, a polymeric active chain is formed (step I in Figure 1.7). The CTA

typically contains a thiocarbonylthio moiety that is reactive towards radicals, thus facilitating the fragmentation of the resulting intermediate radical species (step II) [28].

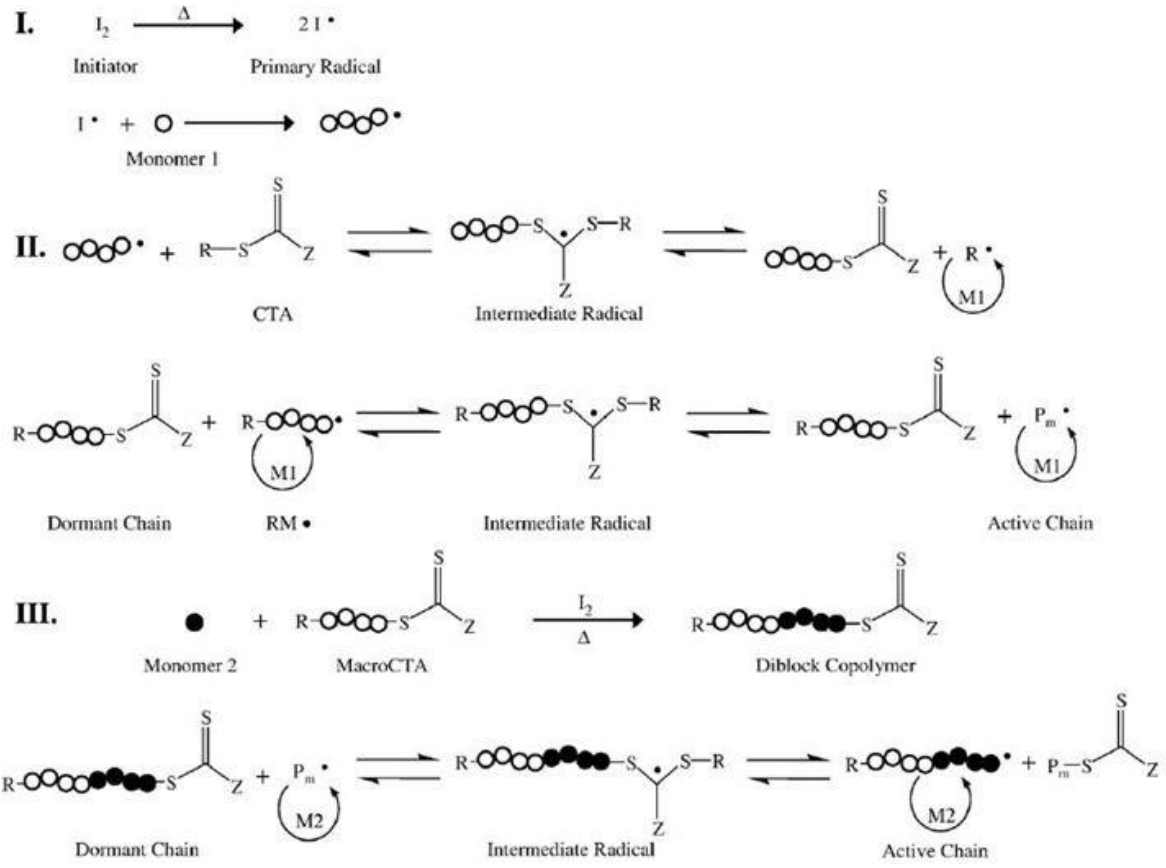

Figure 1.7: The proposed mechanism for homopolymerization (I and II) and chain extension of a macroCTA (III). Taken from [28]

The active species R$^{\bullet}$ then reacts with monomer creating RM• which can reversibly add to another thiocarbonylthio group (CTA). Eventually, the main equilibrium is reached between the propagating polymeric radical and the dormant macroCTA (also called macroRAFT agent). Fragmentation of the intermediate radical in either direction gives all polymer chains equal chances to grow, resulting in uniform chain growth. Excellent control over the molecular weight can be achieved if CTA, monomer, initiator, reaction conditions, and conversion are appropriately chosen. Preventing termination helps preserving the thiocarbonylthio chain end, which allows this "living" chain end of the polymer to be isolated and subsequently chain extended with a second monomer (step III) [28].

The surface modification of gold nanoparticles using polymers prepared via RAFT polymerization has been largely explored due to the di- and tri-thio CTA agents whose chemical affinity for Au surfaces via the sulfur atoms can be explored in surface modification procedures of this metal.

1.4.2. RAFT-assisted encapsulating emulsion polymerization (REEP) strategy

Recently, progress was made in RAFT-controlled radical polymerization in dispersed media and resulted in a new technique for the encapsulation of nanoparticles by using macromolecular RAFT (macroRAFT or MR) polymers: the RAFT-assisted encapsulating emulsion polymerization (REEP) strategy. It was first developed in 2008 by Hawkett and co-workers [29], and is based on the adsorption of macroRAFT agents onto the inorganic surface followed by the growth of RAFT polymers via emulsion polymerization. The two-step method is advantageous as it does not require the use of any extra surfactant or organic solvents, and it could easily change the nature of the polymer shell. Several authors reported the use of REEP strategy, such as Bourgeat-Lami and co-workers for the synthesis of silica/poly(MMA-co-BA) hybrid latexes [30] or by Zou *et al* for the preparation of polymer/inorganic colloidal nanocomposites: namely SiO_2-coated Gd_2O_3:Eu^{3+} nanorods [31].

During her thesis work and for the resulting publication in 2016, S. Pereira and co-workers applied this strategy to Au NPs [6, 32]. The MR agent P($PEGA_{40}$)-TTC is first synthetized from a RAFT agent: TTC-A (2-(dodecylthiocarbonothioylthio)-2-methylpropionic acid) and a monomer: PEGA (poly(ethylene glycol) methyl ether acrylate) using the initiator ACPA (4,4'-azobis(4-cyanovaleric acid)) at a reaction temperature of 70°C, as illustrated in Figure 1.8.

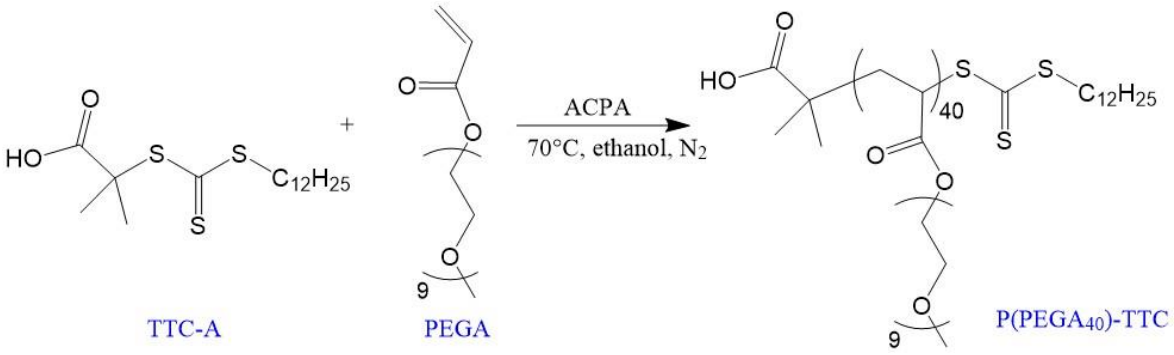

Figure 1.8: Synthesis of the MR agent P($PEGA_{40}$)-TTC via RAFT polymerization.

The REEP strategy here involves the polymer growth from the gold surface after chemisorption of the MR agent via the trithio group, thus requires two main steps. The first step is the preparation of Au NPs well-coated with the MR agent (MR@Au NPs), step 1 in Figure 1.9. The RAFT agent (TTC) has the advantage to form a strong interaction with gold due to the presence of the trithio group. The RAFT agent is thus immobilized on the surface of Au NPs. The second step is the growth of a hydrophobic polymer chain in a controlled way via RAFT emulsion polymerization from MR@Au NPs, yielding stable and robust copolymer@Au NPs, step 2 in Figure 1.9. As the macroRAFT agent in this case acts as surfactant and has an

amphiphilic character, the RAFT emulsion polymerization of a mixture of hydrophobic monomers (methyl methacrylate (MMA) and butyl acrylate (BA)) is carried out from the surface of MR@Au NPs.

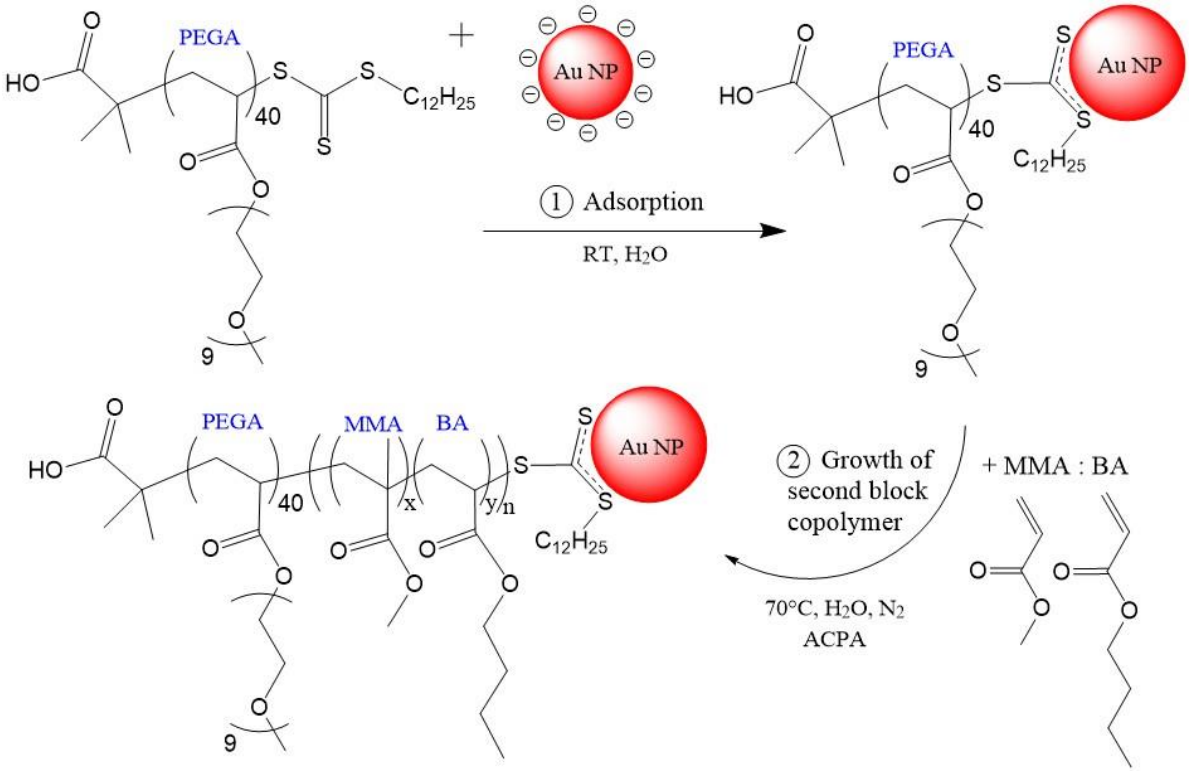

Figure 1.9: Preparation of copolymer@Au NPs via RAFT-assisted encapsulated emulsion polymerization.

An important parameter to take into consideration for the macroRAFT (MR) agent is the critical micellar concentration (CMC), which is defined by the concentration of surfactant (MR in this case) above which micelles will form in solution. Since the MR agent is amphiphilic and has two moieties: a hydrophobic C_{12} chain and a hydrophilic chain containing the repeating units of PEGA, micelles can be formed depending on the concentration used. The CMC can thus influence the adsorption of MR agent onto the surface of Au NPs. In the case of MR agent P($PEGA_{40}$)-TTC, a CMC between 0.1 and 0.3 mM was measured by S. Pereira during her thesis work [32].

1.5. Functionalization by “click chemistry”

Several routes are possible to obtain a specific functionality for a specific application. The functionalization of the polymeric macroRAFT agent described in section 1.4 with biotin will allow obtaining the desired biosensing functionality. This can be done by using the “click chemistry” reaction hereby described.

The term “click chemistry” was introduced in 2001 by K. B. Sharpless and co-workers [33], and refers to a high yielding reaction, simple to perform, and possibly conducted in easily removable solvents. It aims at bonding two functional groups by cycloaddition, namely the azide and alkyne groups. The classic 1,3-dipolar cycloaddition of alkynes to azides requires elevated temperatures and often produces mixtures of two triazoles regiomers. However, these problems can be overcome by the use of catalysts such as copper and ruthenium, as presented in Figure 1.10.

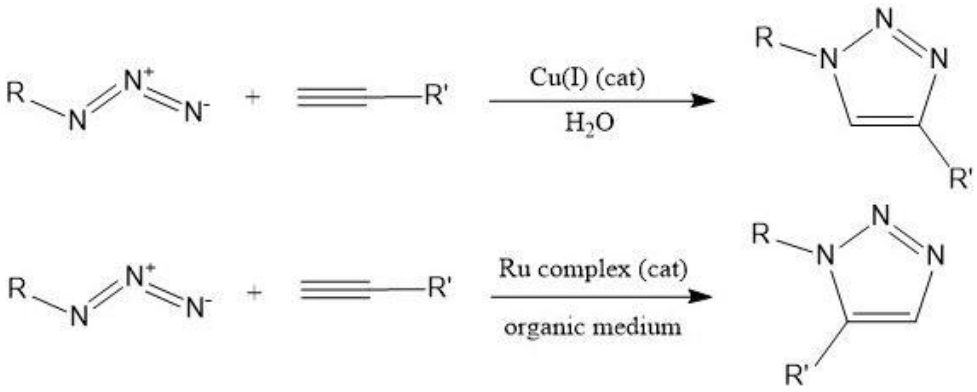

Figure 1.10: Representation of the azide-alkyne cycloaddition reactions catalyzed with Cu(I) or Ru complexes.

The copper-catalyzed reaction using Cu(I) is the most common one and is referred to as CuAAC as in Copper-Catalyzed Azide-Alkyne Cycloaddition. It allows the synthesis of 1,4-disubstituted regiomers specifically. Similarly, the ruthenium-catalyzed (RuAAC) reaction gives the opposite regiomers with formation of 1,5-disubstituted triazoles [34, 35]. The CuAAC is insensitive to solvents thus can be performed in aqueous media at room temperature, as well as physiological conditions, and is highly tolerant to functional groups. In fact, it has been proven to be a powerful tool in polymer science due to its high yields, simple reaction conditions, fast reaction times, and high selectivity [36, 37]. In 2006, the first combination of RAFT polymerization and CuAAC for the preparation of block copolymers was reported [38]. The increase of this combination of reactions is due to the advantages of RAFT polymerization to be used in mild conditions, with a wide range of monomers [39, 40]. The “click” reaction allows the functionalization of polymers with organic dyes, peptides, oligonucleotides, saccharides, proteins [32] and as in our case protein ligands such as biotin [41, 42].

1.6. Layer-by-Layer (LbL) deposition method for preparation of multilayered thin films

As compared to other techniques for the preparation of ultrathin multilayer films, the Layer-by-Layer (LbL) technique based on electrostatic interactions presents several advantages: it is an easy and inexpensive process that allows different types of materials to be incorporated. In practice, only beakers and tweezers are required to perform the deposition [43]. Other strategies exist such as the Langmuir-Blodgett (LB) and self-assembled monolayers (SAM), but both present several limitations. The Langmuir-Blodgett (LB) is a very common and straightforward approach but is not adapted to large scale application, as it requires expensive instruments and is not applicable for all types of materials. Self-assembled monolayers (SAM) method can be applied to a broader range of materials, and is based on chemisorption principle, where each layer is grafted onto the previous one. However, the technique requires chemical reactions yielding at 100% which is a difficult task to achieve. These problems are avoided by using the electrostatic attraction between the surface and adsorbed molecules in the Layer-by-Layer assembly technique [43, 44].

1.6.1. Principle of LbL deposition method

The Layer-by-Layer (LbL) deposition method was first realized by Decher and Hong in 1991 [44]. Figure 1.11 illustrates the four steps of the LbL assembly driven by electrostatic interactions. First, a substrate with a negatively charged surface is immersed in the solution of the positively charged polymer. The adsorption of a single layer leads to the neutralization of the surface charge. If a large amount of positively charged polymer is adsorbed, then an excess of positive changes is present, ending up in the reversal of the surface charge. Then, the substrate is rinsed in pure water in order to remove adhering solution of the positively charged polymer. Next, the substrate is dipped into the solution containing the negatively charged polymer. Again a monolayer is adsorbed, restoring the original negative surface charge. After a second rinsing step the process can be carried out in a cyclic fashion, yielding multilayer assemblies with the desired number of bilayers [44]. Possibly, the most significant advantage of this method is the variability of the applicable materials: not only polyelectrolytes but also charged proteins, molecules or colloidal particles such as Au NPs can be incorporated.

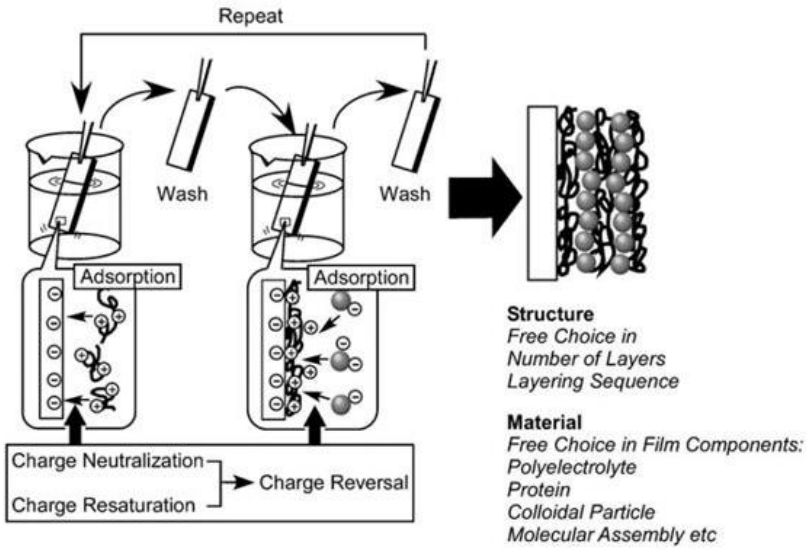

Figure 1.11: Outline of the Layer-by-Layer assembly through electrostatic interaction. Taken from [43]

As the LbL assembly is highly tunable and allows the control of materials incorporation, film thickness, composition and distribution, it can be prepared to fit a specific application. It was described by Yu *et al* in 2017, that the growth of multilayers is dominated by two possible steps: the adsorption and interlayer diffusion, as illustrated in Figure 1.12 [45]. The adsorption step is defined by the polyelectrolytes molecules linking to the charged film surface. Then, interlayer diffusion is defined by the movement of these polyelectrolyte molecules from the surface into the film.

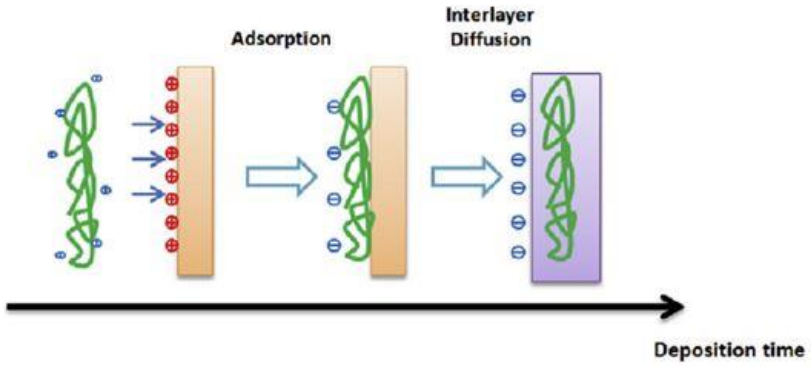

Figure 1.12: Representation of the definition of adsorption and interlayer diffusion during the deposition process. Taken from [45]

Based on these two steps, two types of growth behavior have been reported: First, the linear growth, where the thickness of the film increases with the number of bilayers. This behavior is thus controlled by adsorption, i.e. the interaction between charges from the polyelectrolytes in solution with the charges from the polyelectrolyte on the film surface. The second behavior observed is the exponential growth, based on the interlayer diffusion within the multilayers, thus giving a film growing exponentially with the number of

layers. This behavior is observed when weak and partially charged polyelectrolytes are used for the LbL assembly [45].

1.6.2. Parameters influencing the LbL deposition

The choice of polyelectrolytes for the Layer-by-Layer deposition was made from previous studies by Pereira and co-workers [32, 46], in which they describe the one-step surface functionalization of Au NPs using fluorescein isothiocyanate (FITC) and biotin. In their work, colloidal Au NPs have been surface-modified with the polyelectrolytes poly(allylamine hydrochloride) (PAH) and poly(sodium styrene sulfonate) (PSS). In the present work, a different strategy of preparing multilayered thin films using PAH, PSS and Au NPs instead of a shell@core polyelectrolytes assembly was studied.

In 2004, Jiang and co-workers used these two specific polyelectrolytes combined with gold nanoparticles for sensing application by using a spin-assisted Layer-by-Layer (SA-LbL) deposition technique [47]. They prepared polyelectrolyte multilayer structures containing gold nanoparticles with the general formula $[Au/(PAH{-}PSS)_nPAH]_m$ having well-organized microstructure, uniform surface morphology and high surface quality, as illustrated in Figure 1.13.

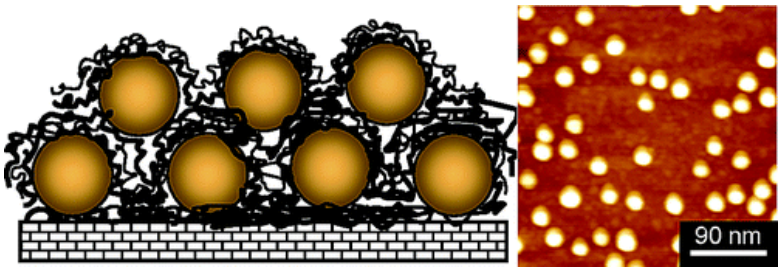

Figure 1.13: An example of multilayer film including nanoparticles.
Illustration of the film microstructure composed of two gold nanoparticle layers separated by three polymer layers, $[Au/(PAH\text{-}PSS)_1PAH]_2$ and high-resolution AFM topographical image of a gold nanoparticle monolayer prepared. Taken from graphical abstract in [47]

Not only the nature of polyelectrolyte has a strong influence on the LbL assembly, but also its molecular weight and concentration, the deposition time, pH and ionic strength of the solutions used will have an effect on the robustness and thickness of the multilayered films preparation. Yu *et al* in 2017, studied the effects of pH, molecular weight and deposition time on the film growth and surface topography in the case of the preparation of PAH/PAA (PAA being poly(acrylic acid)) multilayered thin films. The study showed that film thickness increased with deposition time (from 10 seconds to 15 minutes), the film thickness also increased with higher molecular weight PAA (MW 225 000 compared to 15 000 g/mol) due to the larger coil size of high molecular weight PAA [45].

CHAPTER 2. PREPARATION OF POLYMER@GOLD NANOSTRUCTURES VIA RAFT POLYMERIZATION

2.1. Strategy

A preliminary work was performed, aiming at optimizing the parameters of adsorption of macroRAFT (MR) agent onto the gold nanoparticles (Au NPs), in order to scale up the quantities prepared, namely increase the concentration of Au NPs, and maximize the amount of MR adsorbed per NP. This was done namely by testing different concentrations of gold and concentrations of MR agent used for the adsorption. The Au NPs were synthetized via citrate method and described in section 2.2. The macroRAFT agent used, as represented in Scheme 2.1 (A), was already prepared by S. Pereira via RAFT polymerization method [32]. The second step concerning the adsorption, as in Scheme 2.1 (B), is then performed. A study of adsorption parameters, described in section 2.3, allowed obtaining optimized MR@Au nanostructures. Using the same RAFT reaction process, the addition of hydrophobic monomers into the polymer shell was then performed, as shown in Scheme 2.1 (C), aiming at increasing the length of polymer chain, described in section 2.4.

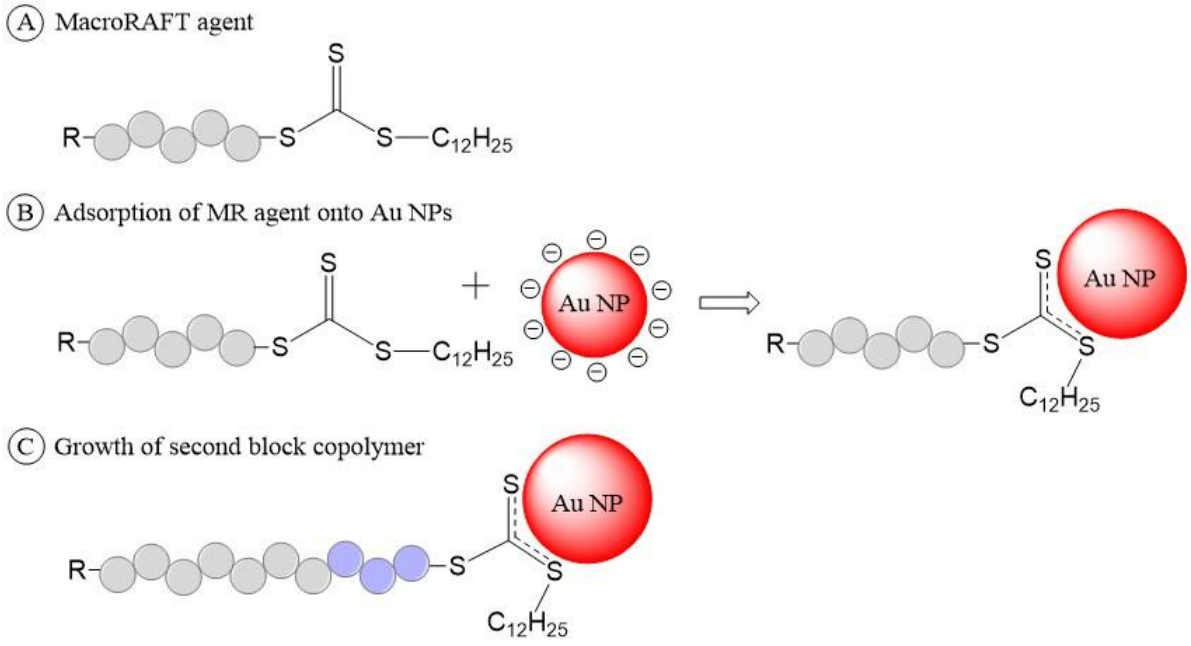

Scheme 2.1: Strategy for the preparation of copolymer@Au nanostructures via REEP

Au NPs were characterized by transmission electron microscopy (TEM), UV-Visible spectroscopy, dynamic light scattering (DLS) and zeta potential measurements. Similarly, the nanostructures MR@Au were characterized using UV-Visible spectroscopy, DLS, zeta potential measurements, and scanning electron microscopy (SEM). Additionally, the chemical composition of MR@Au NPs and copolymer@Au NPs were studied by Fourier-transform infra-red spectroscopy (FTIR). The macroRAFT@Au nanostructures obtained are non-functionalized or sometimes referred to as “blank” nanostructures. In Chapter 3, a functional MR agent will be prepared as well as functional gold colloids.

2.2. Synthesis and characterization of Au NPs

Colloidal gold solutions were synthetized by the commonly used Turkevich method (or so-called citrate method) for the preparation of colloidal gold solution [9]. The details of synthesis are given in Chapter 6, section 6.3.1.

The morphology of Au NPs was characterized by transmission electron microscopy (TEM), several images were analysed to calculate the size and distribution of particles diameter, one of these being presented in Figure 2.1 (A). The morphology of the particles is visible in TEM, showing relatively round edges with some angularities, their shape is quasi-spherical. Therefore, the measured diameter is an approximation. Moreover, whereas the particles are well dispersed in colloidal solution, once deposited on TEM grid for analysis, two or more particles might superimpose and make their distinction difficult. The diameter of particles was measured on four TEM images. The histogram in (B) shows the distribution of the sizes measured on a total of 583 nanoparticles. The measurement of diameter was done using the software ImageJ, and size distribution calculated using Origin. The mean diameter obtained is 15.0 nm, with a standard deviation of $\pm$ 3.4 nm and particle sizes going from 9.4 to 29.5 nm. The mean value is clearly larger than the maximum peak value around 13 nm, meaning that the distribution is not Gaussian.

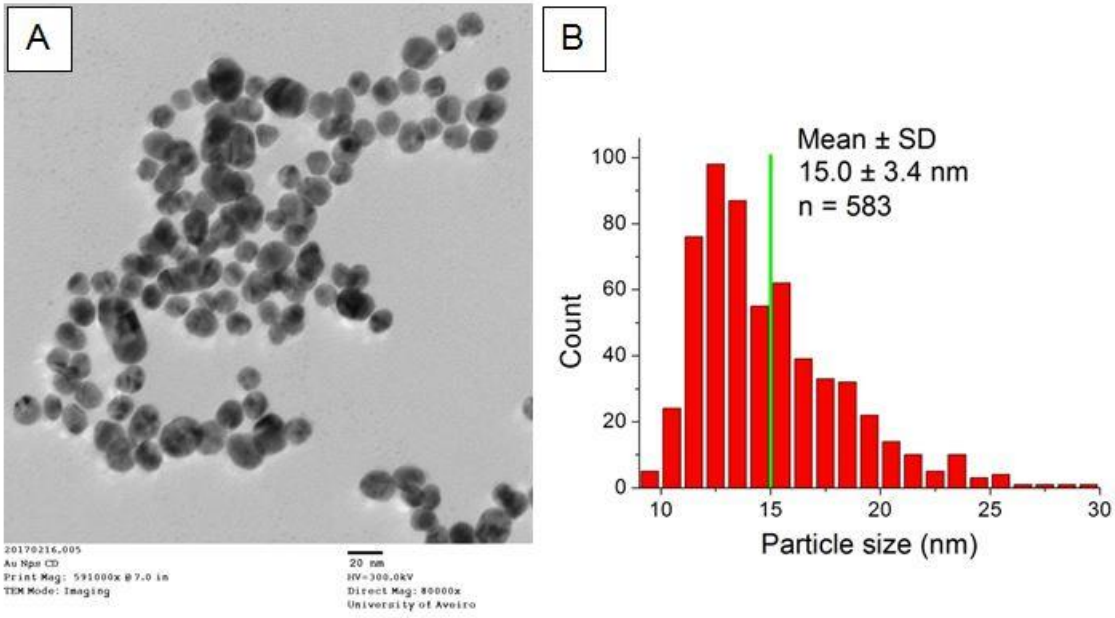

Figure 2.1: (A) TEM image of the Au NPs synthetized (B) Size distribution of particles diameter (in nm)

The UV-Visible spectrum obtained for the colloidal gold suspension is presented in Figure 2.2 (A). It shows the characteristic localized surface plasmon resonance (LSPR) peak at 521.5 nm that is typical of small particles from 10 to 20 nm in diameter. This explains the red colour of the Au NPs suspension obtained, showed in photography 2.2 (B). The narrow LSPR peak obtained indicates a narrow size distribution of particles.

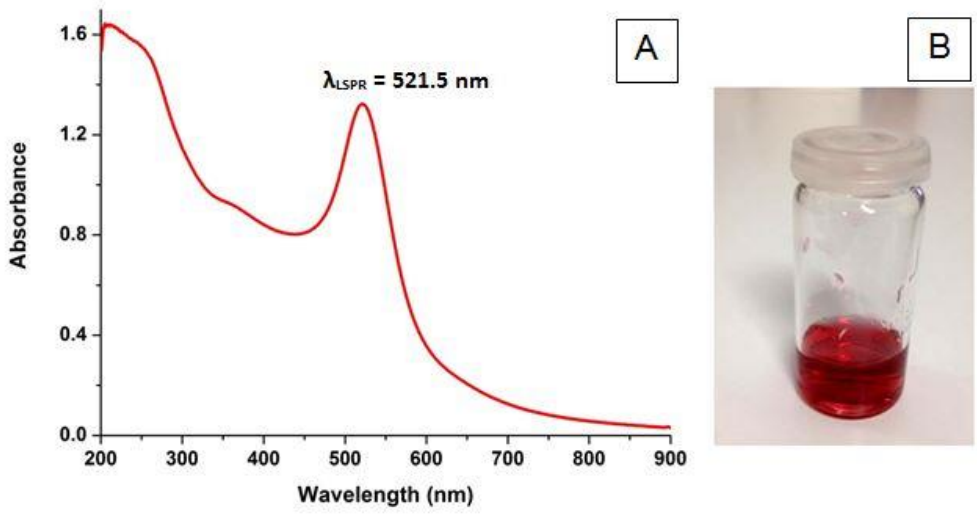

Figure 2.2: (A) UV-Visible spectrum of Au NPs, (B) Photograph of the colloidal gold solution

The method of Haiss and co-workers [48], uses the LSPR band to determine the diameter and concentration of gold nanoparticles. The authors demonstrated a linear dependence of the logarithm of the mean diameter *d* of the particles on the ratio between the maximum absorbance at LSPR wavelength (A_{LSPR}) and the absorbance at 450 nm (A_{450}), as expressed by Equation 1. This applies in the diameter range from 5 to 80 nm. The Values of B_1 (B1 = 3.00) and B_2 (B2 = 2.20) have been determined experimentally by the authors from a linear fit of the ratio A_{LSPR}/A_{450} versus *Log(d)* to a large set of Au NPs batches of known average diameter.

$$d = \exp\left(B_1 \frac{A_{LSPR}}{A_{450}} - B_2\right) \quad (1)$$

For this particular gold solution, a ratio of 1.64 was obtained from the UV-Visible spectrum, corresponding to a particle diameter *d* of 15/16 nm, which is consistent with the size obtained by TEM.

As the extinction coefficient of gold nanoparticles is dependent on particle size, the concentration of spherical nanoparticles *c* in mol/L can then be determined using Equation 2, with ε_{450} being the molar decadic extinction coefficient at 450 nm in $M^{-1}.cm^{-1}$.

$$c = {}^{A_{450}}/_{\varepsilon_{450}} \quad (2)$$

A final concentration of 2.5×10^{-9} moles of NPs per litre was determined for this particular diluted gold solution.

To evaluate the size and stability of the Au NPs in solution, dynamic light scattering (DLS) and zeta potential measurements were performed. The hydrodynamic diameter characterized by DLS measurement gives information on the inorganic core along with any coating material or solvent layer attached to the particle, and surrounding ions, as they move under the influence of Brownian motion. Thus, it is larger than the diameter of an Au NP itself when measured by TEM, as illustrated in Scheme 2.2.

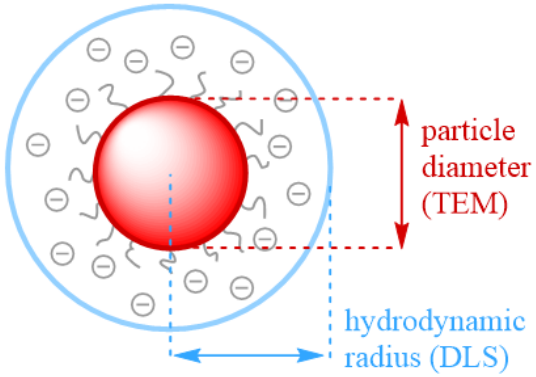

Scheme 2.2: Representation of Au NPs hydrodynamic diameter measured by DLS

In this case an average diameter of 17.1 nm is obtained, with a polydispersity index (PdI) of 0.597, which is 2 nm larger than the diameter of Au NPs measured by TEM and UV-Vis. A zeta potential (ζ) value of -39.0 mV at a pH of 6.4 was obtained. This means that the colloids were stable in aqueous solution, since a colloidal solution is stable when the absolute value of ζ is larger than 30 mV.

The presented characterization was done only for one of the stock solutions of gold, prepared at a concentration of 7.5×10^{-9} mol NPs/L, and then diluted to the desired concentration for experiments. Another stock solution was used for next section on the preliminary adsorption study (in next section 2.3) at a concentration of 7.3×10^{-9} mol NPs/L. The preparation of both Au NPs solutions was done in the same conditions and following the same synthesis method.

2.3. Study of the adsorption of macroRAFT onto Au NPs

The optimization of MR adsorption onto Au NPs was done by testing different concentrations of Au NPs and of initial concentrations of macroRAFT agent P($PEGA_{40}$)-TTC. The procedures for the adsorption and the determination of MR adsorbed are detailed in Chapter 6, in section 6.3.2.

A first study of the variation of Au NPs concentration, presented in Figure 2.3 (A), shows a linear increase of MR adsorbed with the increase of the amount of gold particles used. The concentration of initial MR for this study was kept at around 0.05 mM. The adsorption depends on the surface area of Au NPs, which increases with the number of particles. Thus, the concentration was set at $2.5x10^{-6}$ mmol NPs/L, which appeared to allow a maximal ratio of MR adsorbed per nanoparticles (graph not shown here). In addition, this allowed increasing the concentration of gold as compared to previous studies. The effect of varying the initial concentration of MR was then explored, as shown in Figure 2.3 (B). The decrease of adsorption with increasing concentrations of MR up to $2.5x10^{-2}$ mM was not expected and is not understood. The full range of concentrations studied was chosen to be lower than the critical micelle concentration (CMC) being the concentration of surfactant above which micelles form in solution. But, a possible secondary CMC might exist and thus explain this decrease in adsorption. The CMC value for P($PEGA_{40}$)-TTC was evaluated between 0.1 and 0.3 mM by DLS measurements by S. Pereira [32]. The concentration of MR was thus set at $5x10^{-2}$ mM in the stable region (from $3x10^{-2}$ to 0.11 mM), as the further increase of MR initial concentration did not seem to have a strong influence on the adsorption.

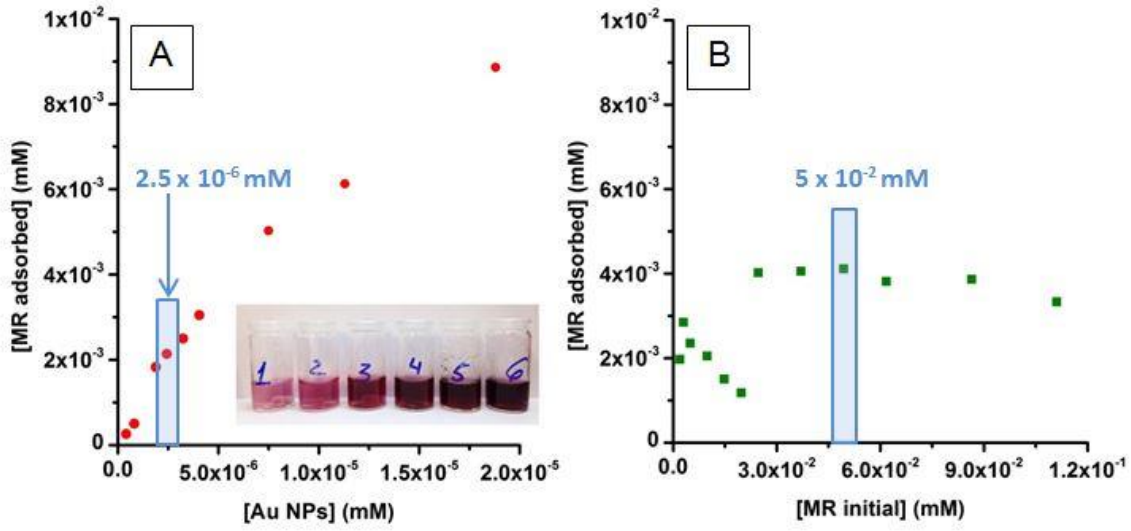

Figure 2.3: Study of the adsorption of MR agent onto Au NPs.
Effects of varying the concentration of Au NPs (A), or the initial concentration of MR agent (B). The photography in A shows the color of the 6 lower concentrations of Au NPs. The blue bars indicate the concentration retained for further experiments

2.4. Copolymerization of MMA:BA from macroRAFT@Au NPs

As discussed in Chapter 1, the MR agent can be kept "alive" due to the presence of chain transfer agent, allowing further RAFT polymerization. Thus, the strategy chosen here is to grow the polymer from the surface of MR@Au NPs using the methyl methacrylate (MMA) and butyl acrylate (BA), resulting in the copolymer@Au NPs, as illustrated in Scheme 2.3. MMA and BA were chosen for their stiffness and flexibility respectively, allowing to obtain a rigid structure capable to respond to an external stimulus.

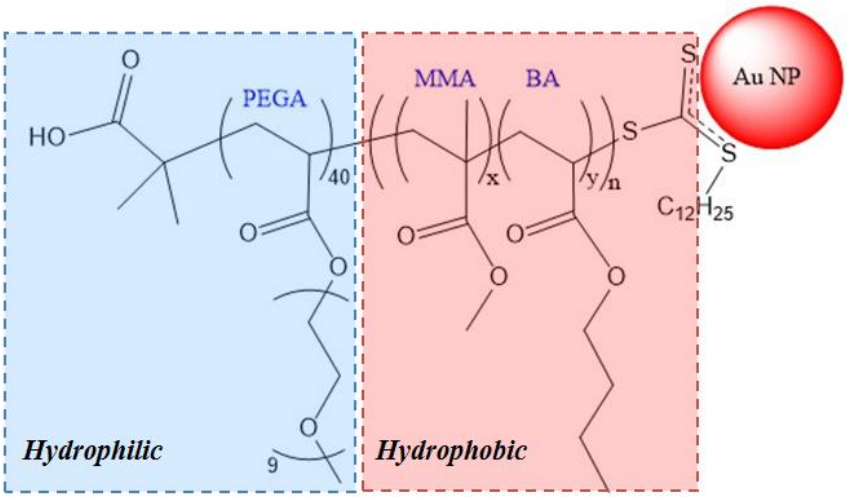

Scheme 2.3: Chemical structure of P($PEGA_{40}$)-*b*-(MMA-*co*-BA)$_n$-TTC@Au nanostructures

The addition of these hydrophobic monomers in small amounts throughout the polymerization results in stable and morphologically well-defined polymer-coated Au NPs. This strategy of controlled addition of a mixture of monomers MMA:BA (with a 10:1 w/w ratio) was previously performed and studied on P($PEGA_{40}$)-TTC (without gold) by S. Pereira [32]. The addition of monomers is done during the first hour of reaction, using VA-044 as initiator, and the temperature was set at 70°C for a total of 4h of reaction. The details of procedure are given in section 6.3.3.

The UV-Visible spectra for copolymerization reaction are given in Figure 2.4, comparing the gold reference to the nanostructures before and after copolymerization. The copolymer@Au NPs obtained show an increase of absorbance in the range 200-250 nm, which indicates the presence of copolymer in the final product. These UV-Vis spectra allow the determination of the λ_{LSPR} and gold concentration based on the Au NPs solution, using the method of Haiss *et al* as mentioned in section 2.2. They are presented in Table 2.1, along with the results of DLS, zeta potential and pH measurements.

Table 2.1: UV-Vis, DLS, zeta potential and pH measurements results obtained for gold nanostructures, before and after copolymerization

	UV-Visible		DLS		ZP	pH
Sample	λ_{LSPR} (nm)	[Au NPs] (mmol/L)	$d_{average}$ (nm)	PdI	ζ (mV)	Value
Au NPs reference	521.5	2.50E-06	17.1	0.597	-39.0	6.4
MR@Au NPs	523.5	2.50E-06	24.8	0.579	-30.0	6.9
copolymer@Au NPs	524.0	2.50E-06	25.1	0.579	-33.2	5.7

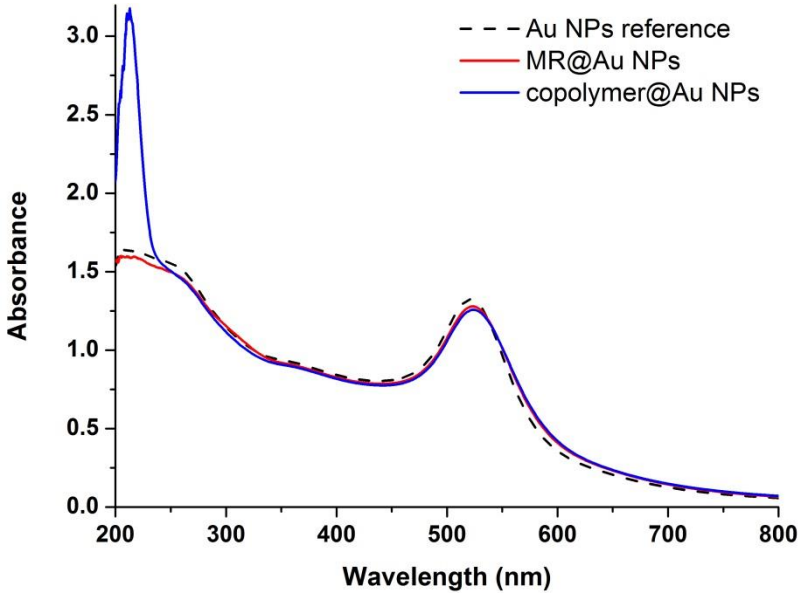

Figure 2.4: UV-Visible spectra of Au NPs, MR@Au NPs and copolymer@Au NPs

A small shift in LSPR wavelength is observed for both nanostructures, after adsorption of MR ($\Delta\lambda$ = 2 nm) and after copolymerization ($\Delta\lambda$ = 2.5 nm). This effect could be due to an interaction of the grafted polymer with the gold, or to a small degree of aggregation. DLS measurements showed an increase of hydrodynamic diameter ($d_{average}$) after MR adsorption (Δd = 8 nm). However, after copolymerization, the increase of $d_{average}$ is insignificant (0.3 nm). The high PdI values around 0.5-0.6 indicate that the samples are not homogeneous, with a broad average size distribution. The stability of colloids is assessed by zeta potential (ζ), giving good results for the gold reference as well as the gold nanostructures (with $\zeta \leq$ -30.0 mV).

The nanostructures prepared were also analyzed by scanning electron microscopy (SEM) in transmission mode, in Figure 2.5, before copolymerization (MR@Au NPs) and after (copolymer@Au NPs), where gold nanoparticles are clearly identifiable in both images. Additionally, in Figure 2.5 (A), the grey clouds surrounding the particles could most probably be the MR agent, but a well-defined shell@core structure is not observed. Similarly, the image obtained for copolymer@Au nanostructures, in Figure 2.5 (B), presents

well defined gold nanostructures. The presence of "cloud" might indicate the presence of copolymer surrounding the gold. However, signs of either coalescence or aggregation of particles are visible.

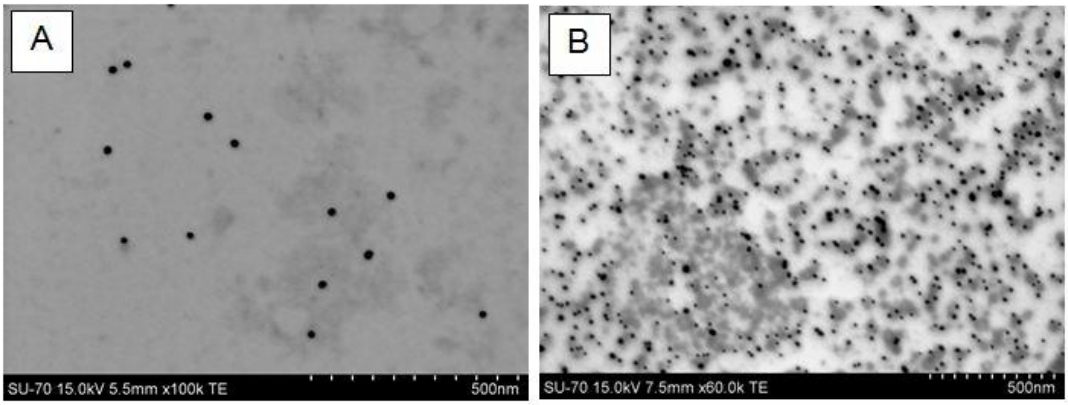

Figure 2.5: SEM images in transmission electron (TE) mode obtained for
(A) MR@Au NPs and (B) copolymer@Au NPs

Fourier-Transform Infra-Red (FTIR) spectroscopy was performed on five different samples, in Figure 2.6. The comparison of the three first samples (Au NPs, MR agent and MR@Au NPs) gives information on the adsorption of MR agent onto the gold nanoparticles. The spectrum of Au NPs presents the characteristic peaks corresponding to citrates on Au NPs [49]. In the middle to low frequency region (2000-400 cm^{-1}), the peaks at 1636 and 1385 cm^{-1} correspond respectively to the antisymmetric and symmetric stretching of COO^-, peaks at 1262 and 1092 cm^{-1} correspond to the stretching of *C-O*, and finally the peak at 801 cm^{-1} to the bending mode of COO^-. Several peaks are characteristic of the macroRAFT agent, namely at 1730 cm^{-1}, 1452 cm^{-1}, 1106 cm^{-1} and 950 cm^{-1}, corresponding to stretching of carboxylic or ester *C=O*, methylene CH_2 bend, ether group from PEG side chains and alkene *CH* bend respectively, and these can also be found in the MR@Au nanostructures. Additionally, the characteristic peaks of citrates are still found in the samples MR@Au NPs and copolymer@Au NPs, such as the peaks at 1636 and 1385 cm-1 of COO^- stretching and at 1262 and 1092 cm^{-1} of *C-O* stretch, indicating that citrates ions are still present at the surface of the gold.

Then, the copolymerization of MMA:BA by controlled addition was performed from the surface of the MR@Au nanostructures. Thus, the obtained copolymer@Au nanostructures are being compared to a sample of copolymer P($PEGA_{40}$-*b*-(MMA-*co*-BA))-TTC alone, prepared by S. Pereira during her thesis [32]. The presence of copolymer in the colloids could be indicated by the peaks at 1352 cm^{-1}, 1165-1147 cm^{-1} and 750-759 cm^{-1}, corresponding to bending of alkene *C-H*, ester *C-C(O)-C* and alkene *CH* or alkane CH_2 respectively, that are present in both copolymer and copolymer@Au NPs. Also, the region 1300-800 cm^{-1} seems to be attenuated by the presence of copolymer (the full spectra is available in Appendix A). To verify that chain extension occurred, thermogravimetric analysis (TGA) could have been performed, but the technique is destructive due to the high temperature required, and we did not have enough quantity of samples to perform this analysis.

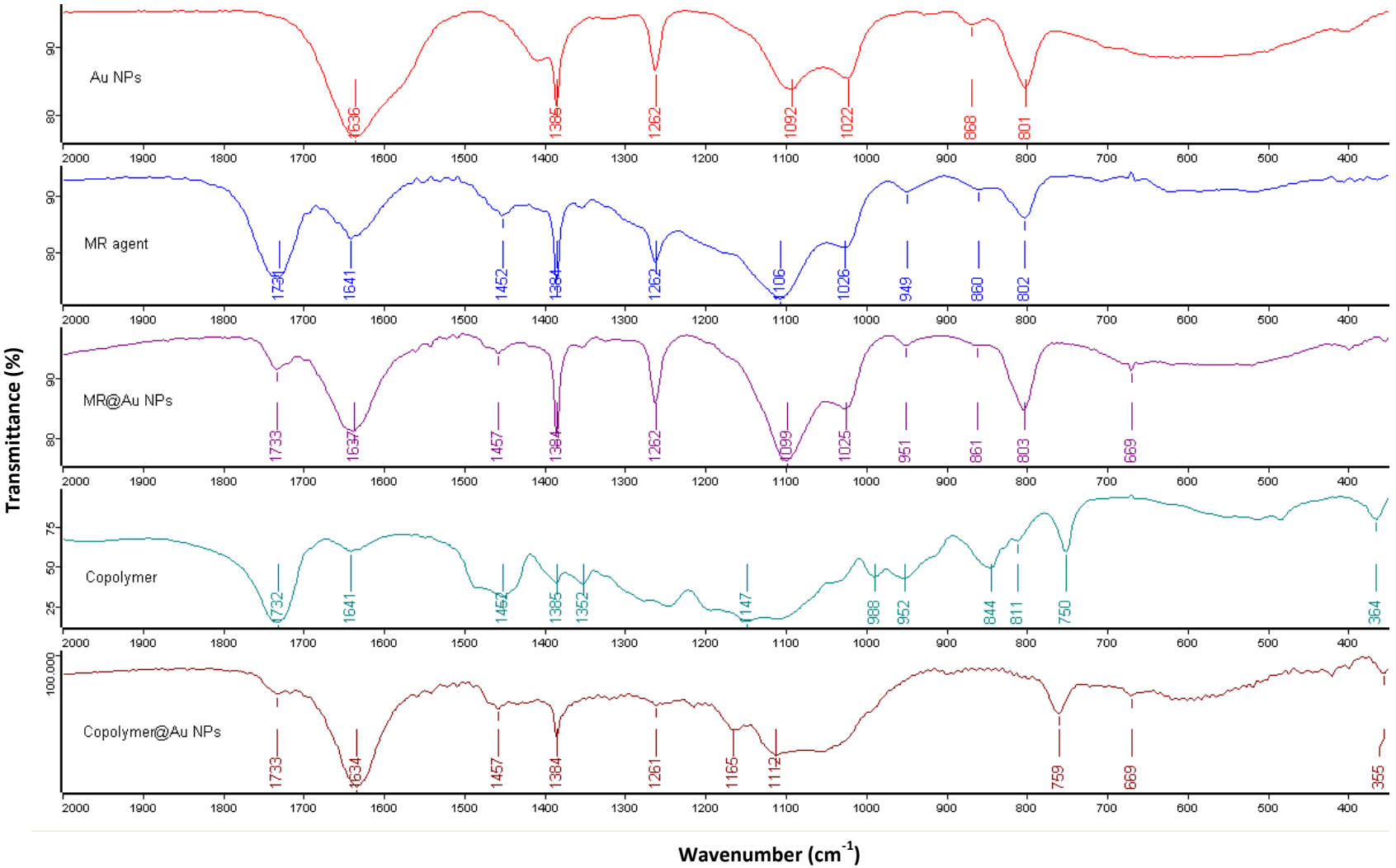

Figure 2.6: KBr-FTIR spectra of (from top to bottom) Au NPs alone, MR agent alone, MR@Au nanostructures, copolymer alone and copolymer@Au nanostructures, plotted using OPUS software after baseline correction and normalization of spectra

CHAPTER 3. PREPARATION OF FUNCTIONAL POLYMER@GOLD NANOSTRUCTURES

3.1. Strategy

Following the preparation and characterization of the MR@Au nanostructures in Chapter 2, functional macroRAFT@Au nanostructures (FMR@Au NPs) were prepared. RAFT polymerization was used to add a fluorescent monomer to an azide-modified MR agent illustrated in Scheme 3.1 (A). The "Click chemistry" reaction was then performed to attach biotin to the polymer chain from the azide group. The obtained macroRAFT is thus functionalized with a fluorophore (FITC) and biotin, as in Scheme 3.1 (B). Following the same principle as used for the preparation of the "blank" MR@Au NPs, the adsorption of biotin-FITC-functionalized MR agent onto the Au NPs was achieved, as in Scheme 3.1 (C). Finally, the controlled addition of hydrophobic monomers into the polymer chain was performed (D), in order to increase the distance between the gold core and the fluorescent moiety.

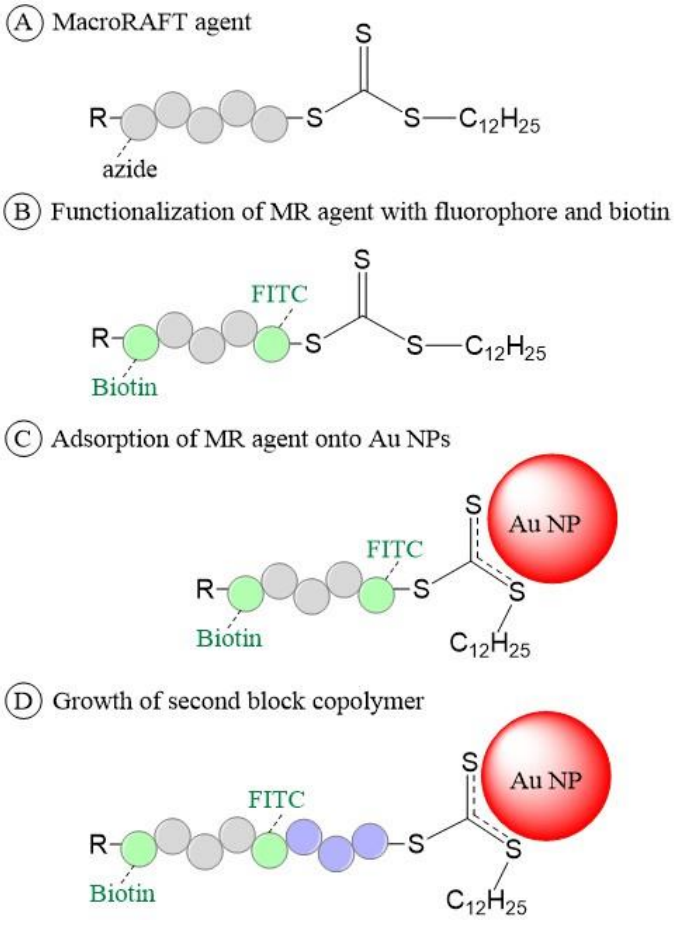

Scheme 3.1: Strategy for the preparation of functionalized copolymer@Au nanostructures via REEP

The functional macroRAFT (FMR) prepared (Scheme 3.1 (B)) was analysed by several techniques such as UV-Visible, fluorescence and FTIR spectroscopies and proton nuclear magnetic resonance (^{1}H-NMR) spectrometry to verify the presence of FITC and biotin moieties, in section 3.2. Then, two adsorptions

assays were carried out. The first one using a mixture of functional and non-functional MR agents, named [2MR:1FMR]@Au described in section 3.3 and the second one using only functional MR (FMR) agent, named FMR@Au NPs in section 3.4. Furthermore, the polymerization of hydrophobic monomers from MR agent was only evaluated via ^{1}H-NMR in section 3.3.2. Additionally, the molecular weight of these MR agents, with or without second polymer block, was estimated using gel permeation chromatography – size exclusion chromatography (GPC-SEC), this study is presented in section 3.3.2. Then, the chain extension was tested from the [2MR:1FMR]@Au NPs, section 3.3.3. The second study explored the adsorption of FMR only onto Au NPs, in section 3.4.1. The copolymerization was not studied in this case due to time limitations. Both nanostructures prepared were characterized by UV-Visible spectroscopy, DLS and zeta potential, and observed by scanning electron microscopies (SEM in transmission mode and STEM). Moreover, photoluminescence spectroscopy was performed to attest the presence of fluorescence emission for both nanostructures. Finally, biosensing tests were performed to evaluate the response of these two nanostructures towards avidin, sections 3.3.4 and 3.4.2.

3.2. Preparation of functional macroRAFT

The azide-modified MR agent used for functionalization was prepared by S. Pereira via RAFT polymerization, and is slightly different from the macroRAFT used in Chapter 2. It is composed of two repeating units of acrylic acid (AA, $DP_{AA} \leq 2$), hence named P(AA_2-*b*-$PEGA_{40}$)-TTC. The purpose of these AA units was to increase the number of carboxylic acids where the functionalization with azide group occurs. The addition of the azide group (N_3) was performed using a typical esterification reaction between the carboxyl group from the MR agent and the hydroxyl group from a 3-azido-1-propanol. The macroRAFT was thus named P($azAA_2$-*b*-$PEGA_{40}$)-TTC, or referred to as N_3-MR agent. In this section, the N_3-MR agent was first polymerized with a fluorescent monomer. The resulting MR agent is called N_3-FITC-MR. Secondly, this MR agent was further functionalized with biotin by click chemistry. Each functionalization step was followed by thorough purification of the polymer in order to remove unreacted monomers and unlinked biotin. The final functional MR agent is thus called biotin-FITC-MR.

3.2.1. Synthesis of azide-FITC-MR agent via RAFT polymerization

The azide-FITC-MR agent was prepared by RAFT polymerization of a fluorescent monomer. This fluorescent monomer was synthetized by S. Pereira by covalent bonding of 2-aminoethyl methacrylate hydrochloride (AEM) with FITC, named AEM-FITC [32]. The RAFT polymerization was performed at 44°C using the initiator VA-044. This temperature was chosen, instead of the 70°C previously used, since the azide moiety cannot sustain high temperature due to the risks of explosion [40]. Thus, the initiator VA-044 having a half-time of reaction of 10h at 44°C was chosen for the reaction [50]. Then, the N_3-FITC-MR agent was collected by precipitation using diethyl ether and this step (precipitation and decantation) was repeated several times;

details are given in section 6.4.1. Two precipitates collected from the reaction showed the presence of MR agent and FITC (see the results and discussion in section 3.2.3). Therefore, the two samples were then mixed to form the final N_3-FITC-MR agent. Moreover, during the reaction, aliquots were withdrawn: the presence of FITC was confirmed by ^{1}H-NMR, but it was not possible to follow the monomer conversion using this technique.

The theoretical chemical structure of the N_3-FITC-MRagent is given in Scheme 3.2. The product obtained from the reaction had a different aspect than the MR agent. Instead of a viscous liquid, powder-like precipitates with the orange coloration from FITC have been obtained.

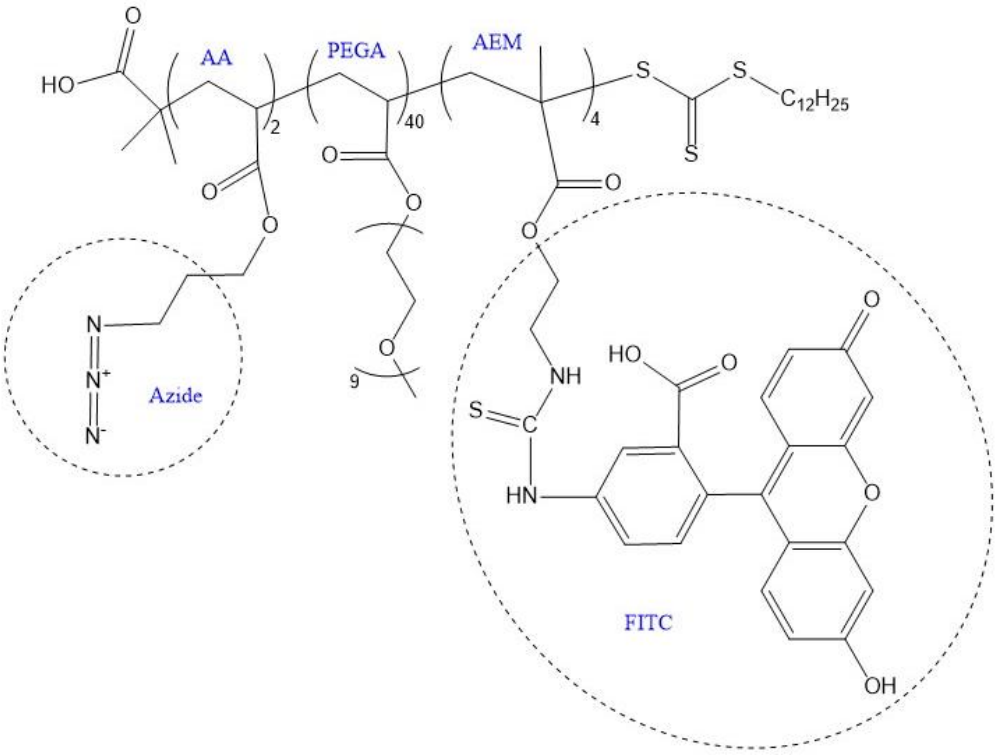

Scheme 3.2: Chemical structure of P(azAA2-PEGA40)-b-(AEM-FITC)4-TTC.
It was obtained after RAFT polymerization using VA-044 as initiator and performed at 44°C, azide and FITC moieties are highlighted by dashed circles

The FITC fluorophore was chosen because it has a maximum emission at 517 nm when excited at 495 nm, which is close to the maximal absorption of the Au NPs at 521.5 nm. Further, the Au NPs show a minimum of absorption at the excitation wavelength used (λ_{exc} = 495 nm). The chemical structure of AEM-FITC is presented in Appendix B-1 (A). The corresponding absorbance and fluorescence emission spectra for AEM-FITC were measured by S. Pereira during her study, and are given in Appendix B-1 (B). Moreover, it is important to have in mind that the pH of solution has a strong influence on the signal of fluorescein and its derivatives, a higher pH giving stronger absorbance and fluorescence emission signals. This pH dependency is given for the fluorescein compound in Appendix B-3, along with the ionized species of fluorescein in B-2.

3.2.2. Addition of alkynated-biotin to MR agent via CuAAC

The copper-catalyzed azide-alkyne cycloaddition (CuAAC) reaction allows the linkage of azide and alkyne groups, the procedure detailed in section 6.4.2. Prior to reaction, the MR agent was modified using an azide group (N_3-MR), and biotin was modified with an alkyne group (alkynated biotin) by S. Pereira [32], the click reaction is illustrated in Scheme 3.3. Thus, the cycloaddition aims at obtaining the final biotin-functionalized macroRAFT agent, the chemical structure is given in Scheme 3.4.

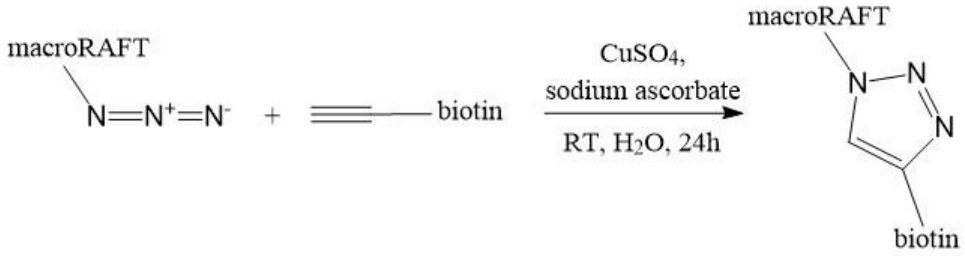

Scheme 3.3: Illustration of of the cycloaddition of azide-MR agent to alkynated-biotin via the CuAAC reaction

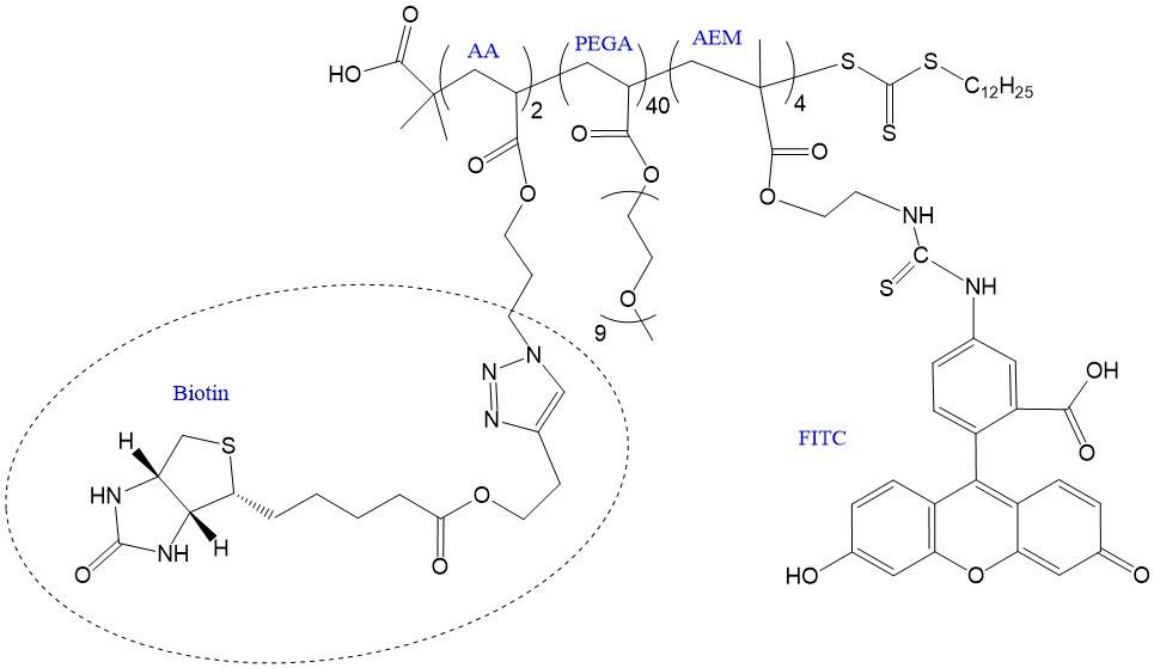

Scheme 3.4: Chemical structure of P((biotin-AA)$_2$-PEGA$_{40}$)-*b*-(AEM-FITC)$_4$-TTC

After click reaction, the solution obtained was purified by dialysis in order to eliminate the unbounded alkynated-biotin as well as other impurities (such as copper). As the MR agent has a high molecular weight, it should stay in the membrane while the other reagents are crossing out the membrane film. Details of the membrane used and procedure are given in section 6.4.3.

3.2.3. Characterization of biotin-FITC-macroRAFT agent

In this section, several characterization techniques such as proton and carbon nuclear magnetic resonance spectroscopies, infrared spectroscopy and elemental analysis were used to determine if the linkage of the two functional moieties to the macroRAFT agent was successful.

Proton nuclear magnetic resonance spectroscopy (^{1}H-NMR) was also used to check the presence of FITC and biotin in the samples, as it gives information on the hydrogen atoms present in the compound. Figures 3.1 and 3.2 present two regions of the spectra, for the samples N_3-MR, AEM-FITC and N_3-FITC-MR. Prior to analysis, these spectra have been normalized using a characteristic peak of ethylene glycol from PEGA (at 3.24 ppm). This has been chosen since the different samples have not been prepared in the same conditions, i.e. different volumes of sample and solvent d^6-DMSO. Therefore, a reference based on the d^6-DMSO peak (at 2.50 ppm) was not ideal. As the sample AEM-FITC does not contain PEGA, its intensity was adjusted to the d^6-DMSO peak as it is the only reference possible. In Figure 3.1, the characteristic peaks corresponding to FITC protons (a, b, c, d) at 6.65 and 6.62 ppm are indeed present in the spectrum AEM-FITC monomer. The signal seems to be present in one of the sample N_3-FITC-MR (blue), but is hard to detect in the second one (orange) as it is almost part of the spectrum noise. It is difficult to conclude on the presence of FITC based on this ^{1}H-NMR analysis.

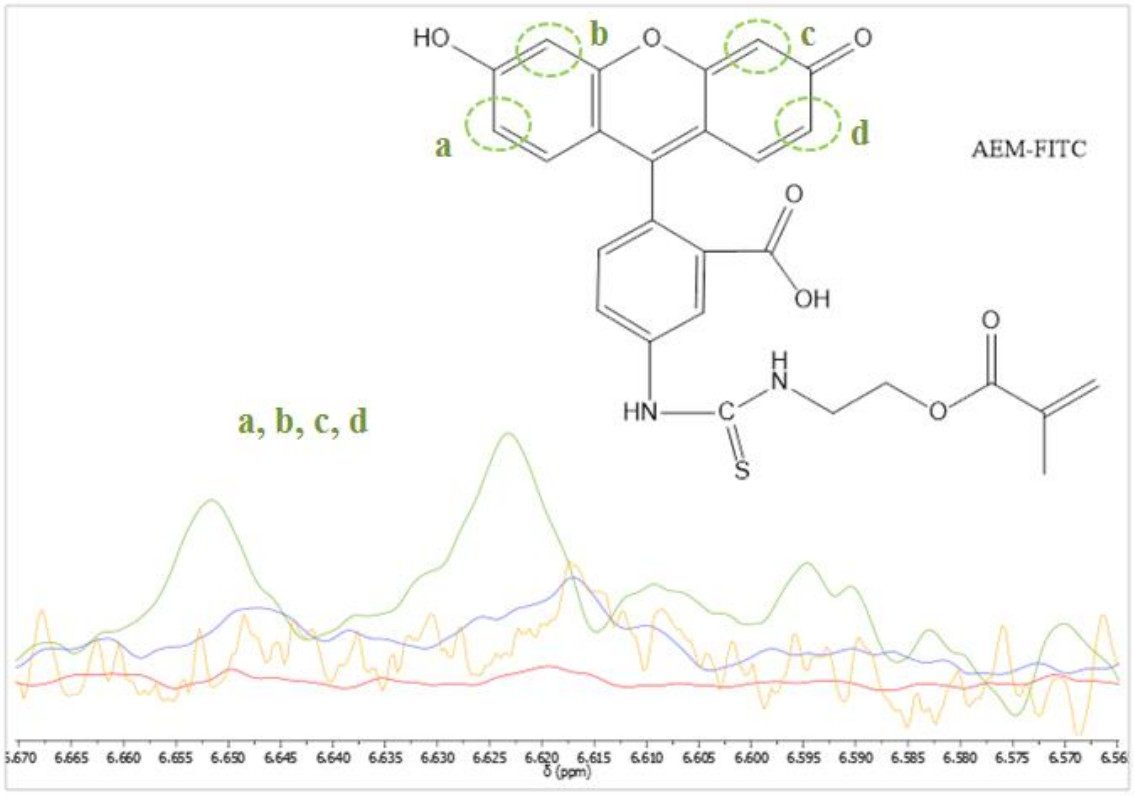

Figure 3.1: ^{1}H-NMR spectra of N_3-MR (red), AEM-FITC (green) and two samples of N_3-FITC-MR (blue and orange) in the region δ = 6.67-6.50 ppm

After the second step of the functionalization, i.e.: the click chemistry, ^{1}H-NMR was performed to confirm the presence of biotin. Figure 3.2 presents one region of the spectra, in which samples N_3-FITC-MR, alkynated-biotin and final biotin-FITC-MR are compared. Again, the normalization was done based on a characteristic peak of PEGA (at 3.50 ppm), and the alkynated-biotin was adjusted based on the d^6-DMSO peak at 2.50 ppm.

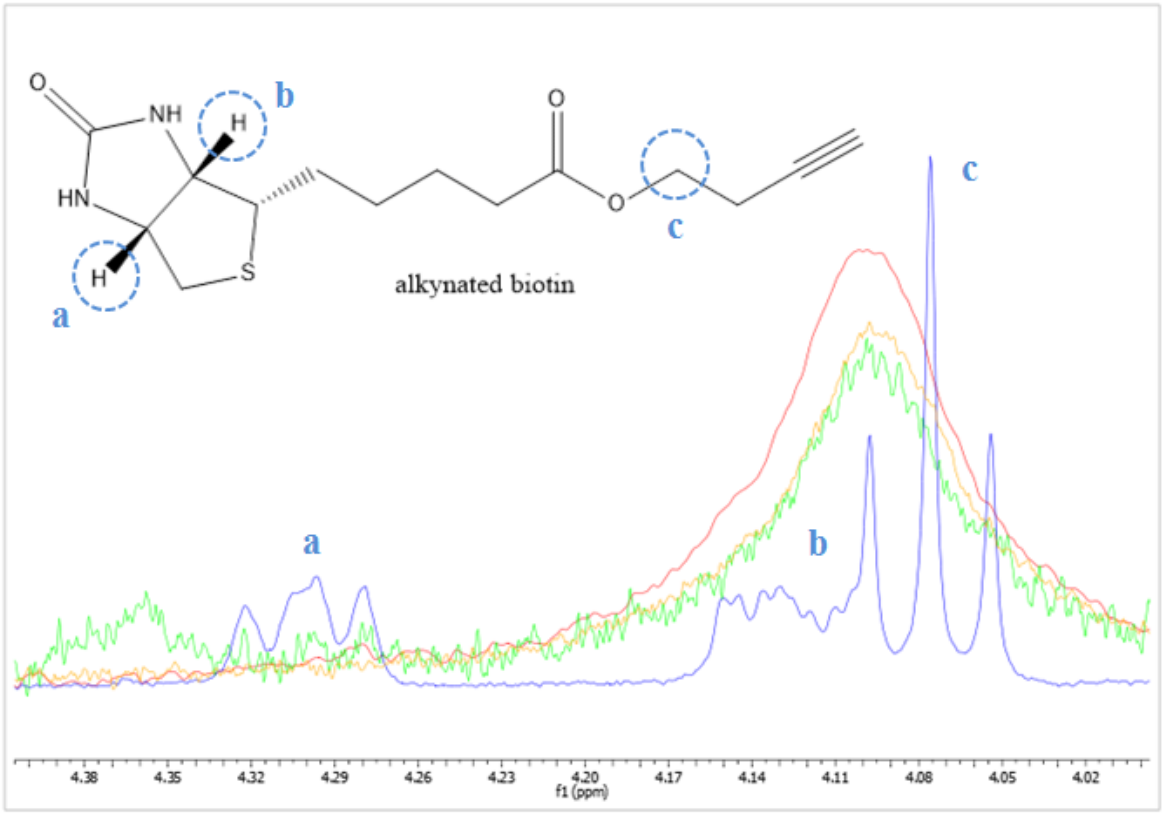

Figure 3.2: ^{1}H-NMR spectra of N_3-FITC-MR (red and green), alkynated-biotin (blue) and final biotin-FITC-MR (orange) in the region δ = 4.00-4.40 ppm

Based on the analysis of full spectra (not shown here), the characteristic peaks of biotin are only present in the alkynated-biotin sample (blue). In Figure 3.2, at around 4.10 ppm, the signal of MR agent is preventing any possible detection of biotin. The confirmation of linkage of biotin to the MR agent is not possible, suggesting that if Biotin binding has actually taken place, it was not extensive.

FTIR spectroscopy was performed on the azide-modified MR agent (N_3-MR), after addition of FITC moiety (N_3-FITC-MR), and after addition of biotin (Biotin-FITC-MR). Samples were dried and blended with potassium bromide (KBr) powder to form a pellet used for the analysis. The KBr-FTIR spectra of these three samples on a particular region (2500 to 1800 cm^{-1}), corresponding to a characteristic signal of the azide group, are presented in Figure 3.3. The spectra of the full range are available in Appendix C.

The presence of azide group in the N_3-MR agent is revealed by FTIR, as shown by the characteristic peak of azide at 2097 cm^{-1}. After polymerization with the fluorophore, the azide peak is still present with lower intensity. However, a quantitative analysis in this case is difficult, as the concentration and amount of sample in the KBr pellet has a strong influence on the IR signal. It is important to note that the presence of orange colour from the fluorescent dye is visible in solution, even after purification. After the 1,3-cycloaddition reaction between the azide and the alkynated-biotin, the peak corresponding to the azide should disappear, or at least its intensity should be reduced. However, there is no strict evidence that the amount has decreased. The presence of biotin cannot be confirmed by FTIR, but we could admit that at least part of the azide groups should have reacted with the alkynated biotin, since click chemistry is known to have a high efficiency and specificity.

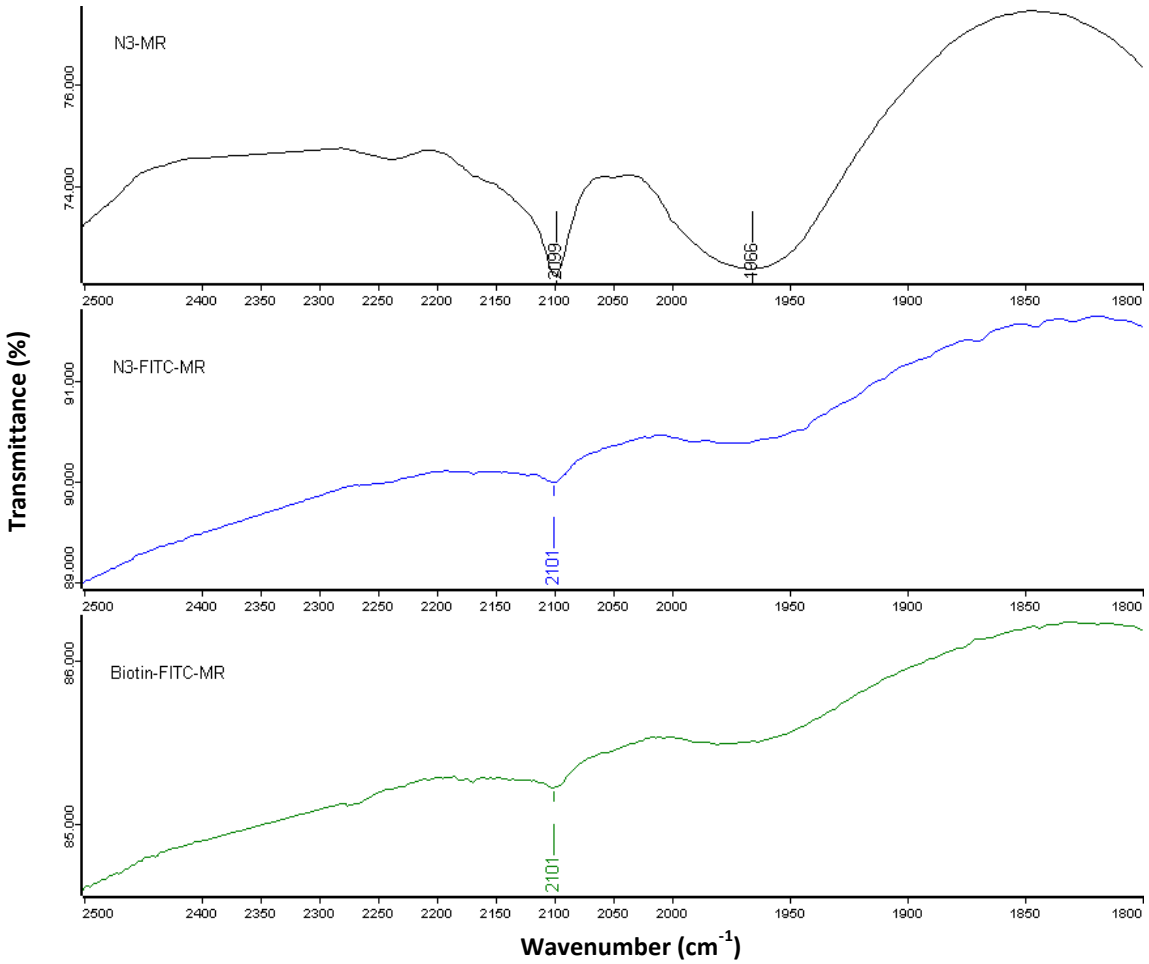

Figure 3.3: KBr-FTIR spectra of N_3-MR, N_3-FITC-MR and Biotin-FITC-MR agents (from top to bottom), on the region 2500-1800 cm^{-1}, after baseline correction and normalization

Several other characterization techniques were used in order to verify the presence of biotin. Elemental analysis was performed and did not provide realistic results, probably due to insufficient quantity of sample for a reliable analysis. In addition to ^{1}H-NMR, carbon nuclear magnetic resonance (^{13}C-NMR) was also used

but did not show signs of the presence of neither FITC nor biotin in the final sample, also possibly due to small quantities of samples.

To confirm if the azide group is still present in the MR agent functionalized with FITC and further modified with biotin, X-ray photoelectron spectroscopy (XPS) could be used. Upon deconvolution of the peaks detected for nitrogen, XPS would provide information if the 1,3 cycloaddition had indeed taken placed as it has been done by Campos *et al* [51]. Restrictions related to time and sample quantities did not allow performing this analysis during the thesis period.

In the following sections, two approaches were tested for the MR adsorption onto gold. First, a mixture of functional MR and normal or "blank" MR mixed in a [1:2] molar ratio was adsorbed. The blank MR agent being P($PEGA_{40}$)-TTC, and the functional one being the MR agent functionalized with FITC and biotin described in the present section. Then, from the [2MR:1FMR]@Au nanostructures, the addition of hydrophobic monomers was performed, as described in section 3.3.3, to increase the distance between the fluorophore and the Au NP core. Additionally, a study of the copolymerization reaction from the P(AA_2-*b*-$PEGA_{40}$)-TTC alone is also described in section 3.3.2. Later, the adsorption of functional MR (FMR) alone onto Au NPs was tested, and is described in section 3.4.

3.3. Study of copolymer@Au NPs from [2MR:1FMR] mixture

3.3.1. Adsorption of mixture [2MR:1FMR] onto Au NPs

The [2MR:1FMR] molar ratio was chosen following the results from S. Pereira thesis [32], in order to add the functionality without significant perturbation of the RAFT emulsion polymerization. Furthermore, this ratio was also thought to (i) avoid overcrowding of the surface which might compromise diffusion of monomers towards the active site, thus preventing chain extension, as well as (ii) prevent unspecific binding of other control species such as BSA during the biosensing tests which will be discussed later. Assuming that the functionalization with FITC and biotin was successful, this ratio should be enough to obtain a fluorescence signal. To make sure that the functional MR was adsorbed, a two-step adsorption of FMR and MR, in a [1:2] stoichiometry was performed. The dropwise addition of FMR was performed first and left stirring for 2 hours. Only then, the dropwise addition of twice as much MR was performed. The procedure details are given in the experimental section 6.4.4.

UV-Visible and photoluminescence (PL) spectra of the [2MR:1FMR]@Au NPs were recorded, as shown in Figure 3.4, along with the gold and [2MR:1FMR] mixture references, i.e. the solution having the same concentrations as used for the adsorption.

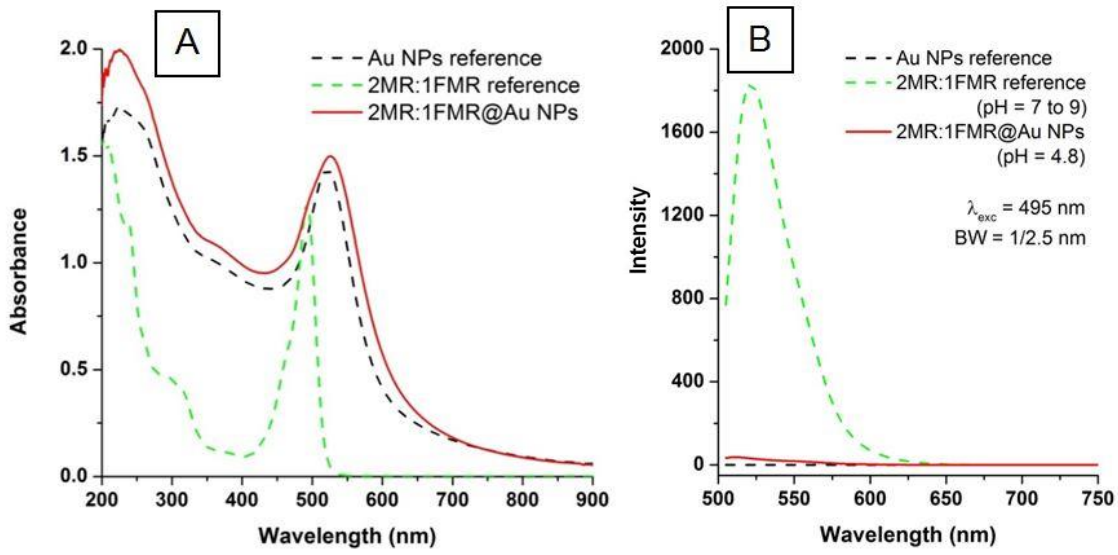

Figure 3.4: (A) UV-Vis and (B) Photoluminescence spectra of colloids [2MR:1FMR]@Au NPs, and Au NPs, and [2MR:1FMR] mixture

The UV-Vis spectra in (A) shows that the adsorption was successful, as the peak of maximum LSPR absorbance corresponding to Au NPs (λ_{LSPR}) presents a small shift ($\Delta\lambda$ = 4.5 nm) that is induced by the addition of the MR agents. Additionally, a "shoulder" is visible around 490 nm in the functional colloid spectrum, which is due to the presence of FITC, as it is aligned with the main peak (λ_{max} = 492.5 nm) of the

reference spectrum of [2MR:1FMR]. The fluorescence spectra (B) were recorded in emission mode, with parameters chosen for the detection of FITC emission, therefore using an excitation wavelength at 495 nm. The functionalized colloid show the peak of fluorescence emission from FITC ($\lambda_{max,colloid}$ = 512 nm), even though the intensity compared to [2MR:1FMR] reference is lower by a factor of nearly 50 (at $\lambda_{max,MR}$ = 521 nm). As mentioned earlier, the effect of pH of solutions should be taken into account, as it has a strong influence on the fluorescence emission of FITC (Appendix B). After recording the fluorescence spectra, the pH of the functionalized colloidal solution was measured 4.8, whereas the pH of [2MR:1FMR] reference was between 7 and 9 (unstable value), which would cause a decrease in peak intensity. This may further explain the important difference in emission signal.

To verify the presence of a shell of [2MR:1FMR], the [2MR:1FMR]@Au nanostructures were first observed with scanning electron microscopy (SEM) in transmission mode. The images collected for the functionalized colloid are shown in Figure 3.5 (A) and (B) in TE and SE modes respectively. As it can be observed, the Au NPs are well defined yet, unexpectedly, micellar structures were also observed in a different spot of the sample (C), that could suggest that the MR agent mixture was not adsorbed as well as expected. Nonetheless, expected morphologies of MR-coated Au NPs seem to also appear, as in bottom left side of Figure 3.5 (C).

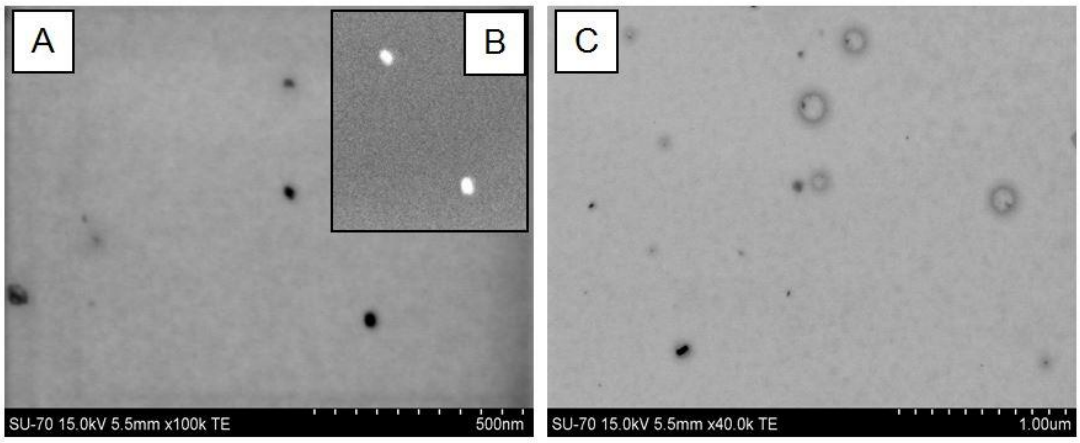

Figure 3.5: Images from SEM in transmission mode (at 15kV) with (A) and (C) transmission electron (TE) mode on two spots of the [2MR:1FMR]@Au NPs, and (B) secondary electron (SE) mode of spot in A.

In order to observe the nanostructures with more precision, scanning transmission electron microscopy (STEM) was used, as it allows working at a higher energy (200kV), and thus a higher resolution. The images obtained for [2MR:1FMR]@Au NPs are given in Figure 3.6 (A) and (B), in secondary electrons (SE) and transmission electrons (TE) modes respectively. The results obtained are consistent with previous observations in SEM, a vesicle or micelle is observed, surrounded by colloids. The presence of Au NPs has been confirmed by an energy-dispersive X-ray analysis (EDX) on the region at the bottom-right size of micelle, represented by a square on Figure 3.6 (A).

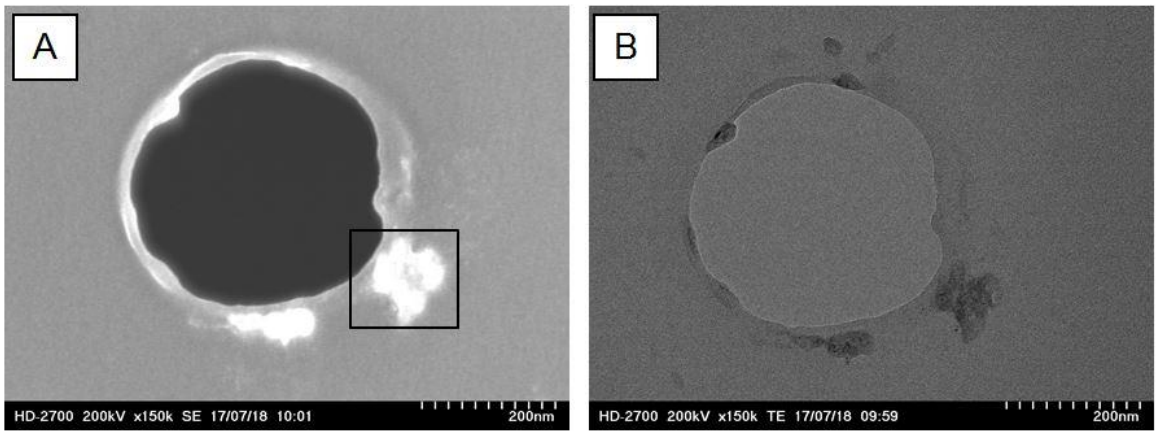

Figure 3.6: STEM images (at 200kV) of [2MR:1FMR]@Au NPs, observed in (A) SE and (B) TE

A possible explanation could be that the critical micelle concentrations (CMC) of the blank MR and functional MR are different. The CMC of macroRAFT agent was evaluated by S. Pereira during her thesis, but the CMC of the new functional MR was not, and can well be different due to the presence of biotin and FITC moieties. Therefore, it is hard to predict the behavior of the functionalized MR during and after adsorption. The functionalization steps could lower the CMC of the MR agent, thus the concentration of FMR used could preferentially create micelles. Hence, a study of the CMC of this functional MR could help understanding the phenomenon.

The hypothesis realized above is supported by DLS and zeta potential measurements performed on this colloid. Similarly to the observations of non-functionalized MR@Au NPs, the hydrodynamic diameters $d_{average}$ increased after adsorption (Δd = 4.5 nm), with high PdI values over 0.5. Yet, the stability may be lost after adsorption, as suggested by the decrease of ζ to -18.9 mV, versus -39 mV for stable Au NPs, as presented in Table 3.1.

Table 3.1: UV-Visible, DLS, zeta potential and pH measurements results obtained for [2MR:1FMR]@Au NPs

	UV-Visible		DLS (average of 3 values)		ZP	pH
Sample	LSPR (nm)	[Au NPs] (mmol/L)	$d_{average}$ (nm)	PdI	ζ (mV)	Value
Au NPs	521.5	2.72E-06	21.8	0.589	-38.6	4.3
[2MR:1FMR]@Au NPs	526.0	2.72E-06	26.3	0.551	-18.9	4.8

3.3.2. Study of the copolymerization of MMA:BA from MR agent alone

The controlled addition of hydrophobic monomers MMA:BA, was also studied on the MR agent alone P(AA_2-*b*-$PEGA_{40}$)-TTC, in order to estimate the monomer conversion and the molecular weight (MW) of the

resulting copolymer. For the colloids, the copolymerization reaction is done following the adsorption of MR onto Au NPs.

The polymerization conditions were kept identical to those used for the preparation of P($PEGA_{40}$)-*b*-(MMA-*co*-BA)-TTC described in Chapter 2, i.e. controlled addition of monomers during 1h, using VA-044 as initiator at a temperature of 70°C for a total of 4h, details of the procedure are available in section 6.4.5. The MR agent is slightly different as it has an additional two units of acrylic acid (AA). The final polymer containing MMA:BA block copolymer is presented in Scheme 3.5.

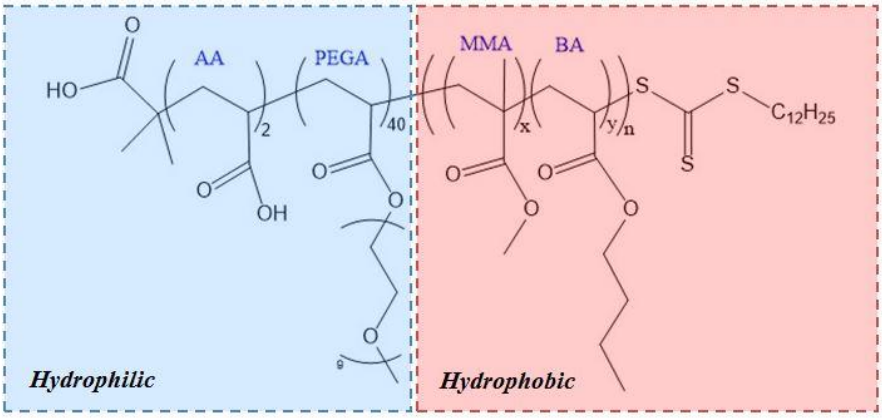

Scheme 3.5: Chemical structure of P[(AA_2-*b*-($PEGA_{40}$)-*b*-(MMA-*co*-$BA)_n$]-TTC

The reaction products were prepared for a ratio [macroRAFT]/[Initiator] of 9. The copolymerization from P($PEGA_{40}$)-TTC in the same conditions was studied previously by S. Pereira, and gave a 100% of monomer conversion, but in that case the monomer addition was performed in one shot at the beginning of the reaction. S. Pereira confirmed by GPC-SEC that the procedure also allowed the conventional radical polymerization to takes place. Therefore, in this work the monomer addition is done in a controlled way for P(AA_2-*b*-$PEGA_{40}$)-TTC. The conversion of MMA:BA monomers (with 10:1 w/w ratio) is calculated via gravimetric analysis, i.e. based on the measured mass of dried polymer withdrawn throughout the reaction, and the known mass of each reagent.

Results of the instantaneous and overall conversions are presented in Figure 3.7. Aliquots were withdrawn from the reaction solution at various times along the 4h reaction, and placed in an ice bath to stop the reaction. During, the first hour, 15 μL of monomers were added every 10 minutes, giving a total of 105 μL monomers mixture. For the remaining 3h of reaction at 70°C, aliquots were withdrawn without further addition of monomers. A final conversion rate higher than 100% was obtained, which is not plausible, but might be due to a non-complete evaporation of the solvent from the samples before weighting. It could be assumed that the reaction yielded complete conversion, which is consistent with the expected conversion rate from previous studies, i.e. the insertion of monomers in P($PEGA_{40}$)-TTC using VA-044 at 70°C for 4h has reached 100% conversion at pH 8 [32]. In these conditions and assuming a total insertion of monomers into

the MR agent, a polymerization degree (PD) of 156 was calculated. Thus, the final chemical structure of copolymer prepared would be: P[AA_2-*b*-$PEGA_{40}$-*b*-(MMA_{10}-*co*-BA_1)$_{156}$]-TTC, having a molecular weight ($\overline{Mn}$) of 34 316 g/mol (based on the experimental molecular weight P(AA_2-$PEGA_{40}$)-TTC previously obtained by ^{1}H-NMR by S. Pereira: $\overline{Mn}$ = 18 291 g/mol).

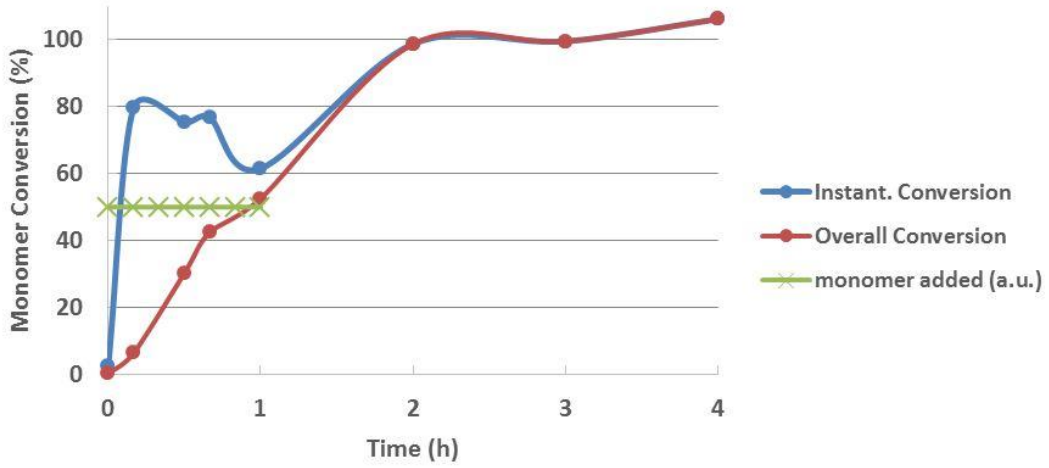

Figure 3.7: *%Conversion* during the copolymerization of MMA:BA (10:1 w/w) in the presence of P(AA_2-*b*-$PEGA_{40}$)-TTC using initiator VA-044 at 70°C for 4h (pH = 8.2)

Additionally, the hydrodynamic size of the particles in the aliquots was measured by DLS measurements, as presented in Table 3.2. The addition of monomer being performed during the first hour, the corresponding results (t0 to t4) present unstable sizes, with average diameters first increasing to near 100 nm, then dropping down to 50 nm. Together with the high values of PdI (0.6-0.7) at times below 30 min, this could suggest that a partial copolymerization took place, before reaching a stable state.

Table 3.2: DLS measurements of copolymer@Au NPs during copolymerization

		DLS (average of 3 values)	
Aliquot	Time (min)	$d_{average}$ (nm)	PdI
t0	0	78.5	0.703
t1	10	94.4	0.649
t2	30	47.4	0.098
t3	40	52.3	0.066
t4	60	57.6	0.067
t5	120	61.3	0.074
t6	180	61.0	0.064
t7	240	61.5	0.056

During the additional 3h of reaction, without further addition of monomer, a steady increase led to a plateau at 61 nm of diameter, with much lower polydispersity indexes (PdI around 0.06). These results seem to indicate that a successful copolymerization reaction took place.

In order to determine the molecular weight (MW) of the copolymer prepared, and compare it with the MR agent before addition, gel permeation chromatography – size exclusion chromatography (GPC-SEC) was performed, the graph obtained is presented in Figure 3.8, and corresponding results are presented in Table 3.3. Details of preparation of samples for GPC-SEC and procedure are available in section 6.4.6.

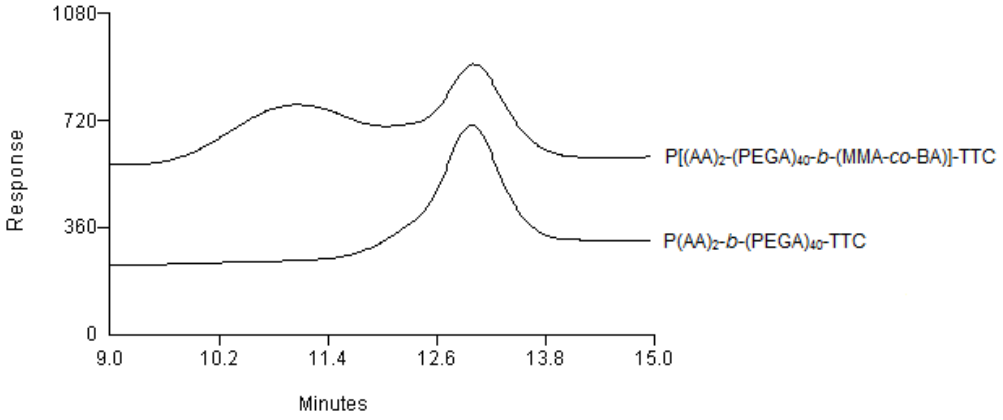

Figure 3.8: GPC-SEC chromatograph of copolymer and corresponding MR agent P(AA_2-*b*-$PEGA_{40}$)-TTC

By GPC-SEC, the MR agent P(AA_2-*b*-$PEGA_{40}$)-TTC gives an experimental molecular weight ($\overline{Mn}$) of 14 500 g/mol, which is close to the value obtained by ^{1}H-NMR. Two molecular weights are obtained for the copolymer ($\overline{Mn}$ = 11 900 and 71 300 g/mol) instead of an expected single molecular weight around 34 000 g/mol estimated by gravimetric analysis).

Table 3.3: Molecular weights obtained by GPC-SEC for MR agent P(AA_2-*b*-$PEGA_{40}$)-TTC and copolymer

Compound		P(AA_2-*b*-$PEGA_{40}$)-TTC	P[(AA_2-$PEGA_{40}$-*b*-(MMA-*co*-BA)]-TTC	
			1st peak	2nd peak
GPC-SEC	$\overline{Mw}$ (g/mol)	14 500	99 000	14 300
	$\overline{Mn}$ (g/mol)	12 500	71 300	11 900
	Đ	1.16	1.38	1.20
Mn (g/mol)		18 291 (exp_NMR)	34 316 (exp_gravi)	

This can be explained by a possible competition between the conventional free radical polymerization and controlled addition of monomers via RAFT. In controlled addition, i.e. starved conditions, molecular weight distribution is expected to give a single and rather sharp peak in GPC (with dispersity indexes Đ closer to 1,

as for peaks obtained for MR and 2nd peak of copolymer), as it allows preferential linking of the monomer to the MR agent, rather than creating free polymer MMA-BA by conventional free radical polymerization (as for 1st peak of copolymer) [32]. However, given the results obtained, the polymerization was not controlled at all and a substantial amount was polymerized by conventional radical polymerization and/or other terminating reactions must be involved. In fact, when conventional free radical polymerization is carried out in emulsions the polydispersity is not so high. Indeed it is generally around 1. Therefore, the possibility of competing side terminating reactions cannot be overlooked.

3.3.3. Copolymerization of MMA:BA from [2MR:1FMR]@Au NPs

The same controlled addition of monomers (details given in section 6.4.7) was performed from the mixture [2MR:1FMR] adsorbed onto nanoparticles, and their properties characterized by UV-Visible and PL spectroscopy. See Figure 3.9. Similarly to previous observations, the presence of the copolymer is evidenced by the increase of adsorption in the region 200 to 250 nm in UV-Visible spectra in Figure 3.9 (A), even though the intensity has not increased as much as observed for the copolymerization from MR@Au NPs (Figure 2.4).

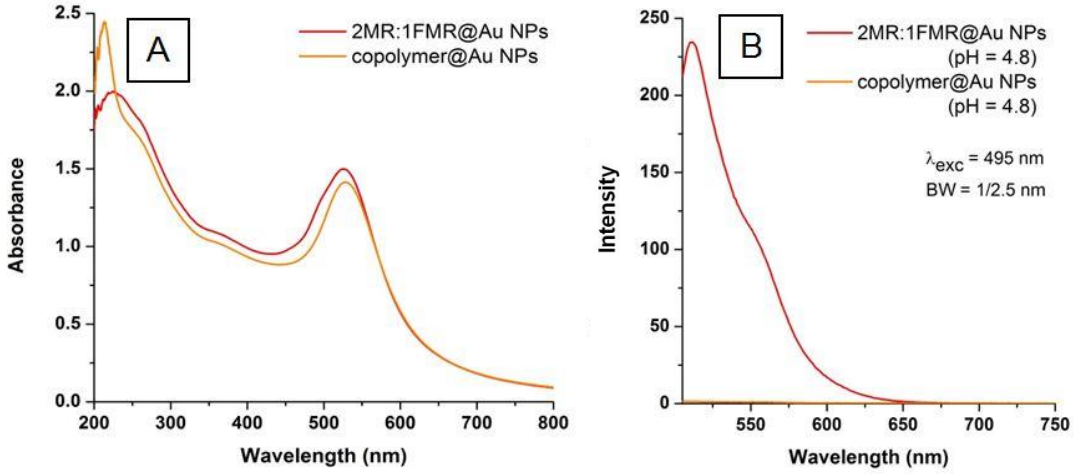

Figure 3.9: (A) UV-Visible and (B) PL spectra of [2MR:1FMR]@Au NPs and copolymer@Au NPs at pH = 4.8

The fluorescence emission has highly decreased for the copolymer@Au NPs sample, with a maximum intensity of 1.5, compared to the [2MR:1FMR]@Au NPs sample with a maximum intensity of 235. To record the spectra, the band widths have been increased compared to measurements after adsorption in section 3.3.1, to allow a better detection of the copolymer signal. The comparison of both samples in this case is easier, as a similar acidic pH (4.8) was measured for both samples, even though the pH was not stabilized using a buffer. After that, the colloids [2MR:1FMR]@Au and copolymer@Au were diluted in PBS buffer (10 mM, pH 7.4, dilution with a ratio 1:1 of colloids/PBS), to stabilize the pH and check its effect on the absorbance and fluorescence emission spectra of the nanostructures, presented in Figure 3.10.

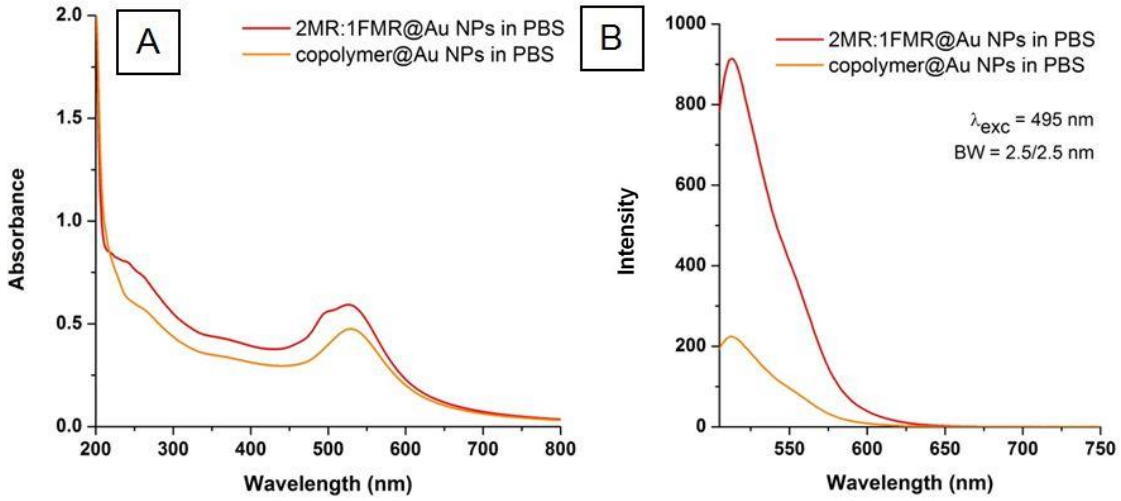

Figure 3.10: (A) UV-Visible and (B) PL spectra of [2MR:1FMR]@Au NPs and copolymer@Au NPs (in PBS buffer pH 7.4, 10 mM)

As expected from the effect of pH on fluorescence signal, both 2MR:1MR@Au and copolymer@Au colloids emissions show an important increase in Figure 3.10 (B), even at lower concentration of colloids (1:1 v/v dilution of colloids in PBS). Due to the diluted concentration of colloids, the signal of absorbance has decreased, in (A), but the LSPR wavelength of Au NPs is still detected. However, the characteristic increase at 200-250 nm corresponding to copolymer signal is not visible, which could be due to the dilution. Comparing the PL spectrum of [2MR:1FMR]@Au NPs and copolymer@Au NPs at the same pH, it was expected that the emission intensity increase after the copolymerization due to the incorporation of the hydrophobic block which should increase the distance between the core and the FITC. Yet, the possibility of some significant conformation change and/or removal of the functionalized MR (at least partial) from the colloid during polymerization could also be considered.

Table 3.4: UV-Visible, DLS, zeta potential and pH measurements for [2MR:1FMR]@Au NPs and copolymer@Au NPs

	UV-Visible		DLS (average of 3 values)		ZP	pH
Sample	LSPR (nm)	[Au NPs] (mmol/L)	$d_{average}$ (nm)	PdI	ζ (mV)	Value
Au NPs	521.5	2.72E-06	21.8	0.589	-38.6	4.3
[2MR:1FMR]@Au NPs	526.0	2.72E-06	26.3	0.551	-18.9	4.8
copolymer@Au NPs	528.5	2.72E-06	24.9	0.534	-27.5	6.1

Results obtained for DLS and zeta potential, in Table 3.4, surprisingly show a decrease in hydrodynamic diameter (Δd = 1.5 nm), and an increase in stability with copolymer@Au NPs from -18.9 mV to -27.5 mV after addition of monomers. In this case the samples were measured at a different time, presenting a

different pH (pH 6.1 for copolymer@Au NPs was measured before fluorescence analysis), which can also influence the results.

The copolymer@Au nanostructures were analyzed by STEM. In Figure 3.11 (A) and (B), in TE and SE modes respectively, a cluster/big aggregate is observed. In TE image, in (A), two Au particles are observed. However, they do not seem to be present in the corresponding SE image in (B). This could be due to a mistake in the preparation of TEM grids, as the colloidal solution may have been deposited on both sides of the grid. This would explain why the Au NPs can be seen in transmission mode as the transmitted electrons are detected, but not in secondary electrons.

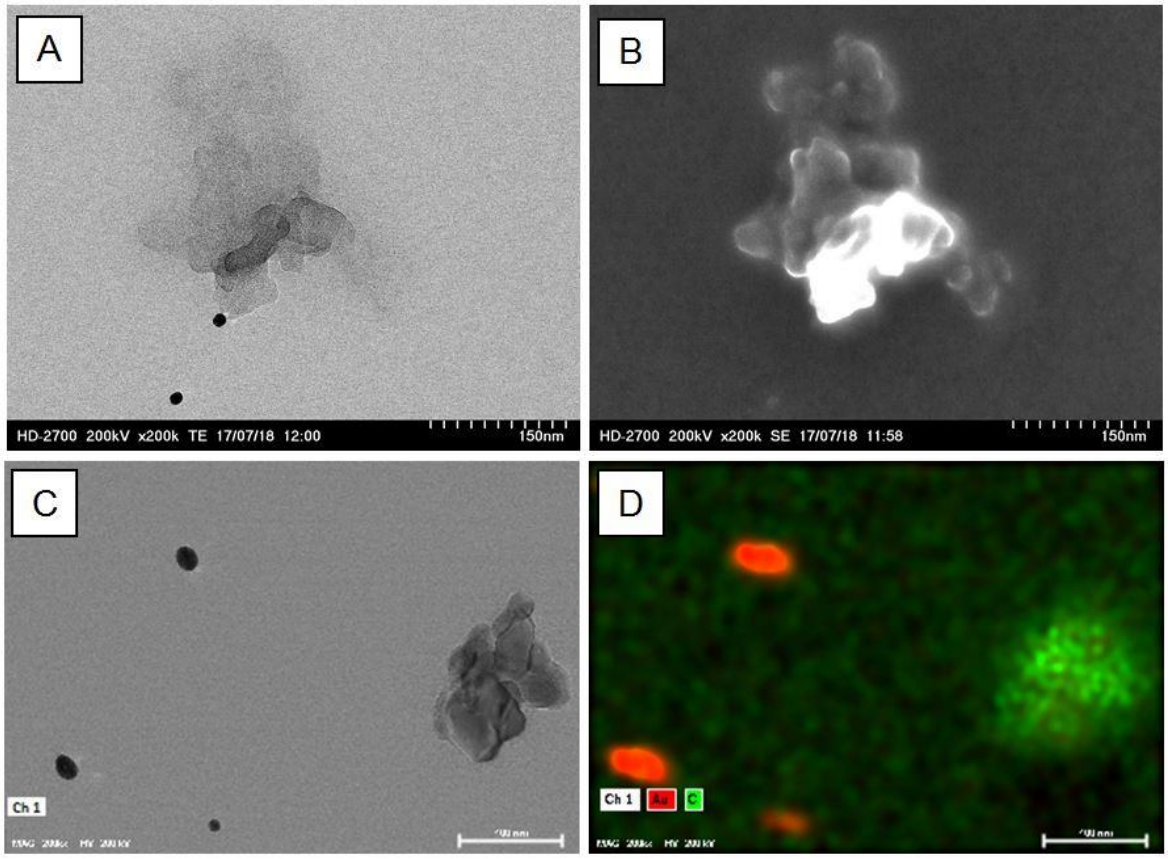

Figure 3.11: STEM images of copolymer@Au NPs (A) in SE mode (B) in TE mode, and EDX mapping (D) of image (C) showing presence of Au (red) and C (green) elements

These aggregates and particles were analyzed via EDX mapping on the region in image (C). The mapping (D) shows the presence of gold (Au) and carbon (C) elements on the particles, and presence of carbon element in the aggregates. The hypothesis put forward before the addition of the hydrophobic block could still be viable, as the aggregates could be MR and functionalized MR agents that did not adsorb properly on the surface of gold. Then, the addition of monomers would preferentially take place in the aggregates rather than encapsulate the Au NPs to yield functionalized Au nanostructures.

3.3.4. Biosensing response of copolymer@Au NPs towards Avidin

Despite of the uncertainty regarding the successful encapsulation of Au NPs, the optical response of the copolymer nanostructures prepared using [2MR:1FMR] was evaluated. The aim of these tests was to assess the response of the biotin-FITC-functionalized colloids towards avidin, which is the natural biotin receptor, as introduced in Chapter 1. Thus, the response of colloids was first tested in the presence of avidin. As a control, the response was then tested in the presence of bovine serum albumin (BSA), a different protein, to check the specific response to avidin. Finally, the colloids were tested in the presence of PBS reference, as all the colloidal solutions prepared are diluted in PBS buffer to maintain the pH at 7.4. For the copolymer@Au NPs, the optical response was tested at two incubation times: after 10 min and after 2h30. Straight after measuring the absorbance, the fluorescence emission spectrum of a particular sample was recorded using the same quartz cell. Details of the procedure are given in section 6.4.8.

The visible spectra in Figure 3.12 present relatively similar absorbance intensity after 10 min incubation (A-top), as all the colloids have the same concentration of Au NPs. After 2h30 of incubation time (B-top), the response has decreased for samples tested in Avidin and PBS reference. After 10 minutes of incubation time (A-bottom), the colloids present a relatively equal fluorescence emission for the two proteins and reference, with a slightly higher intensity in the presence of avidin.

The fluorescence response obtained after 2h30 of incubation time (B-bottom) was not as expected for several reasons. First, the response in reference sample has increased over time, rather than giving a stable response. Then, the expected response in the presence of avidin was a fluorescence quenching, thus a decrease in emission intensity, whereas the observation here is the opposite effect: an increase of fluorescence emission after 2h30 of incubation time. For both absorbance and fluorescence emission signals, the response observed in the presence of BSA (the non-specific protein) gave a rather stable signal in fluorescence emission and absorbance after 2h30.

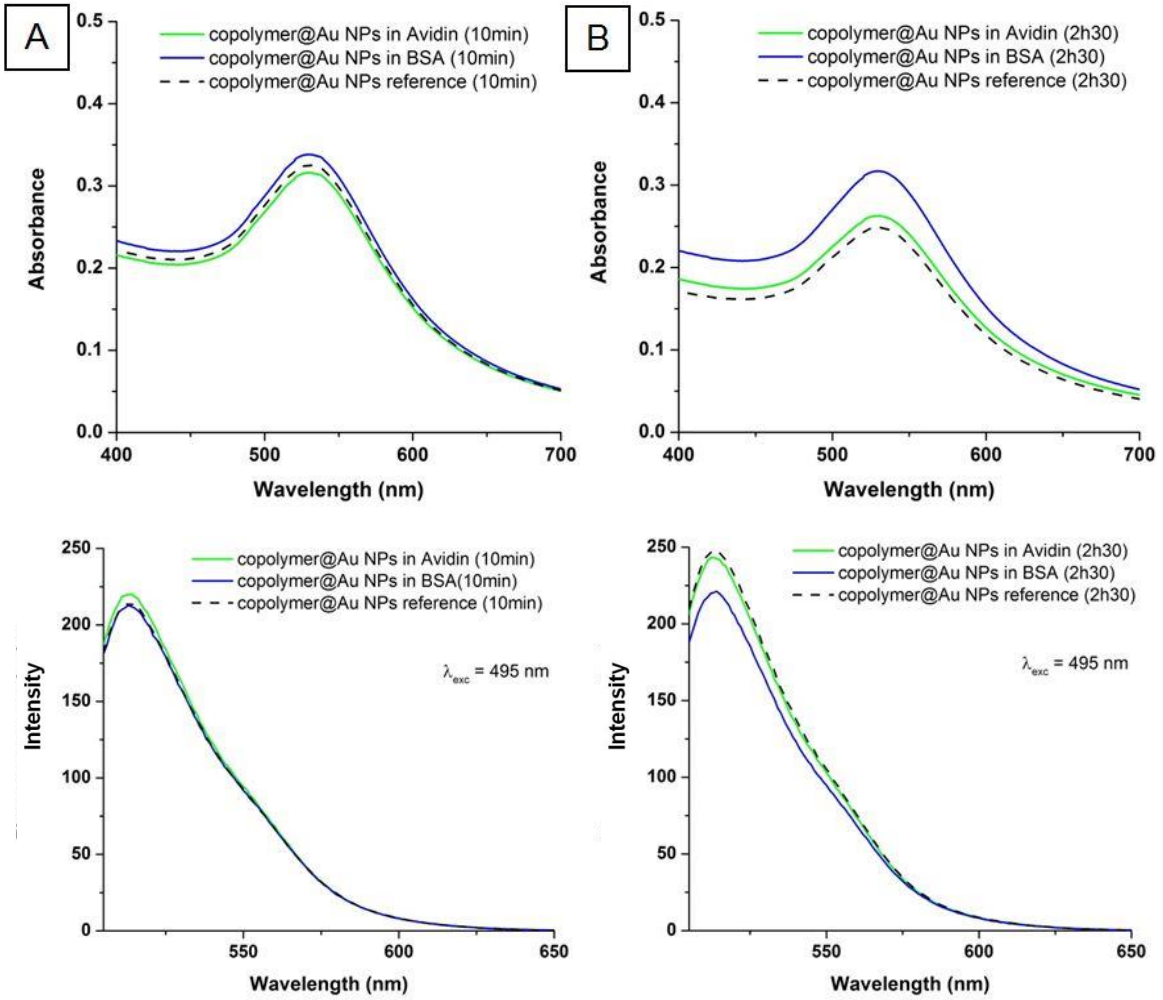

Figure 3.12: Visible (top) and PL spectra (bottom) of copolymer@Au NPs, in presence of avidin, BSA and PBS reference at (A) 10 min and (B) 2h30 of incubation time

After the observations from SEM and STEM, plus the results obtained for biosensing test with avidin, the choice of adsorbing only functional MR onto gold was made, to avoid a possible competition and aggregation of the MR agents, and eventually obtain a better adsorption of the functional MR agent as well as ensure plenty of binding sites for avidin (i.e. increase the concentration of biotin on the surface of the nanostructures).

3.4. Study of FMR@Au NPs

In this section, the adsorption of only functional MR agent (FMR) onto Au NPs was evaluated by UV-Visible and fluorescence spectroscopies, DLS and zeta potential measurement (section 3.4.1). Then, the biosensing response towards avidin was tested (section 3.4.2).

3.4.1. Adsorption of FMR onto Au NPs

The procedure followed for the adsorption is similar to the one performed on MR@Au NPs in Chapter 2, except for the use of biotin-FITC-MR agent only, rather than blank macroRAFT. The details are given in experimental section 6.4.9. UV-Vis and fluorescence spectra of FMR@Au NPs are given in Figure 3.13. The absorbance spectrum shows a maximum at LSPR wavelength, with the "shoulder" corresponding to FITC in MR agent.

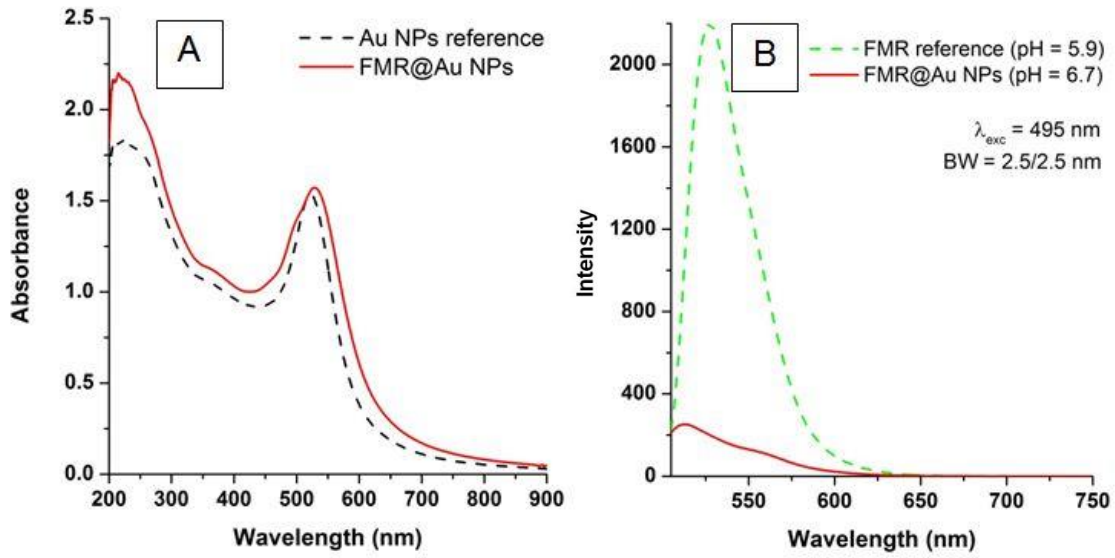

Figure 3.13: (A) UV-Visible and (B) PL spectra of FMR@Au NPs, with Au NPs and FMR references

The fluorescence emission intensity has clearly improved compared to previous colloids, as the adsorption used in this case only functionalized MR rather than a mixture. The emission for FMR@Au NPs being 6 times higher (250, Figure 3.13) than for [2MR:1FMR]@Au NPs (40, Figure. 3.4). However, this time, the pH of FMR reference was measured at pH 5.9 and that of the colloids' at 6.7. Again, this difference in pH could account for the much lower emission by the colloid versus the reference. In the present case, fluorescence emission intensity of FMR reference is 8 times higher than colloid.

Hydrodynamic sizes obtained in DLS are presented in Table 3.5, with a 8.4 nm increase in diameter after adsorption, and a decrease in stability with ζ = -20.2 mV as compared to stable Au NPs (ζ = -51.5 mV). This result confirms that the FMR agent does not confer the same stability as for the [2MR:1FMR]@Au NPs.

Table 3.5: DLS, zeta potential and pH measurements for FMR@Au NPs

	DLS (average of 3 values)		ZP	pH
Sample	$d_{average}$ (nm)	PdI	ζ (mV)	Value
Au NPs reference	15.8	0.553	-51.5	
FMR reference	187.4	0.444		5.9
FMR@Au NPs	24.2	0.515	-20.2	6.7

STEM images of FMR@Au nanostructures are presented in Figure 3.14. From SE image in (A), well-defined gold nanoparticles are observed, with a grey surrounding that could be the FMR agent. In TE image (B), the morphology of Au NPs is well observed.

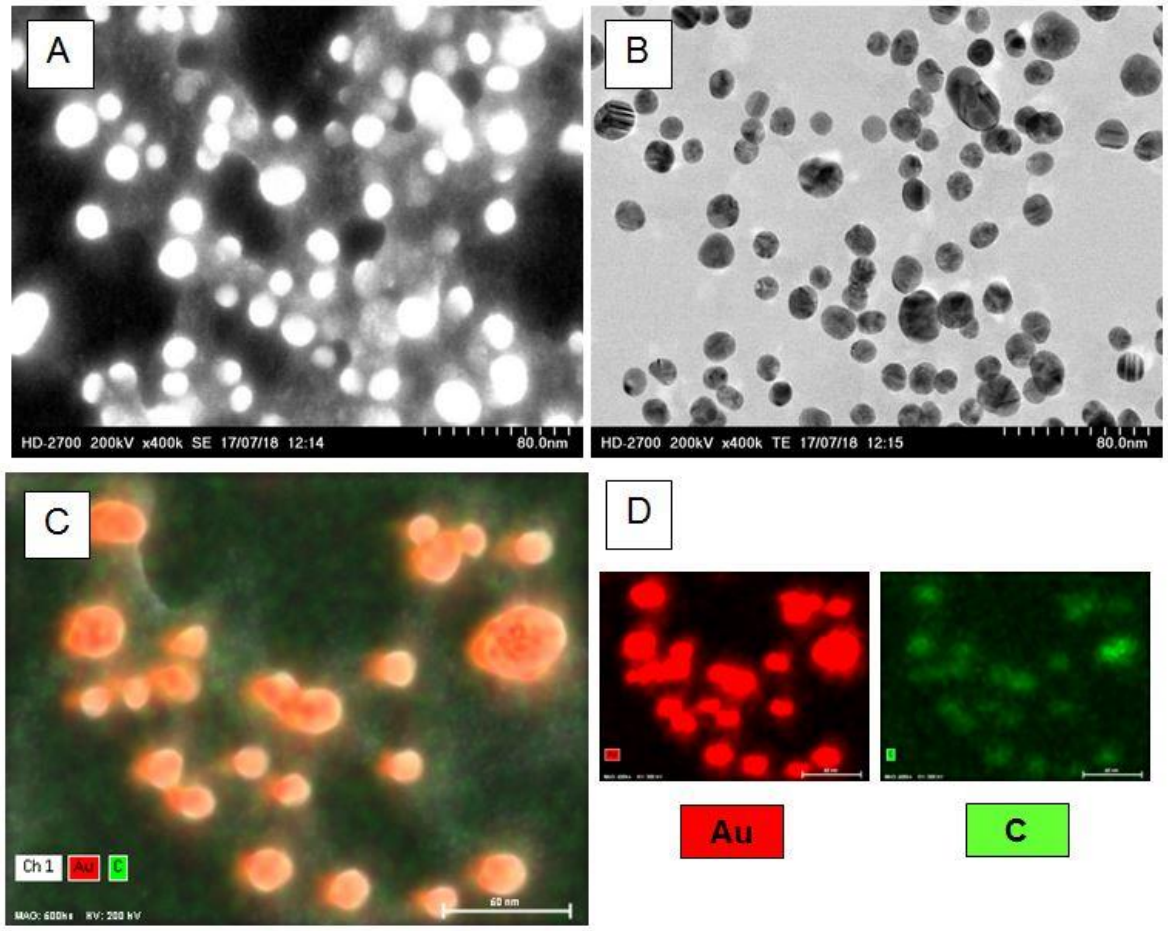

Figure 3.14: STEM images of FMR@Au NPs (A) and (B) being SE and TE mode respectively, EDX mapping performed on image (C), showing presence of Au and C elements in (D)

To confirm the presence of FMR agent, an energy dispersive X-ray spectroscopy (EDX) mapping was performed on image (C). The presence of gold element is evidenced in the particles, Au in red in (D). Carbon element is detected on the surface of the grid, as it is coated with amorphous carbon, but a higher concentration is detected around the nanoparticles, which could indicate the presence of polymer. This

technique is neither sensitive enough to detect small quantities of sulfur (S) associated with the RAFT agent and FITC nor nitrogen (N) from the biotin and FITC due to the small quantities in which they are present.

3.4.2. Biosensing response of FMR@Au NPs towards avidin

In the case of FMR@Au nanostructures, the same biosensing test as the one performed on copolymer@Au NPs prepared with [2MR:1FMR] was done. This time, there was no addition of the hydrophobic monomers to FMR@Au NPs, due to time constrains, but the colloids were centrifuged and redispersed in PBS (10mM, pH=7.4) before protein testing. The conditions of study are kept identical, except for the recording times that were done after 10 minutes and 4 hours of incubation (instead of the 2h30 for previous colloids, for practical constraints). The visible signal recorded, in Figure 3.15, shows a similar trend observed for the copolymer@Au NPs, with a decrease of absorbance for the three solutions tested after 4 hours of incubation. Similarly, the decrease is more important for avidin and reference samples.

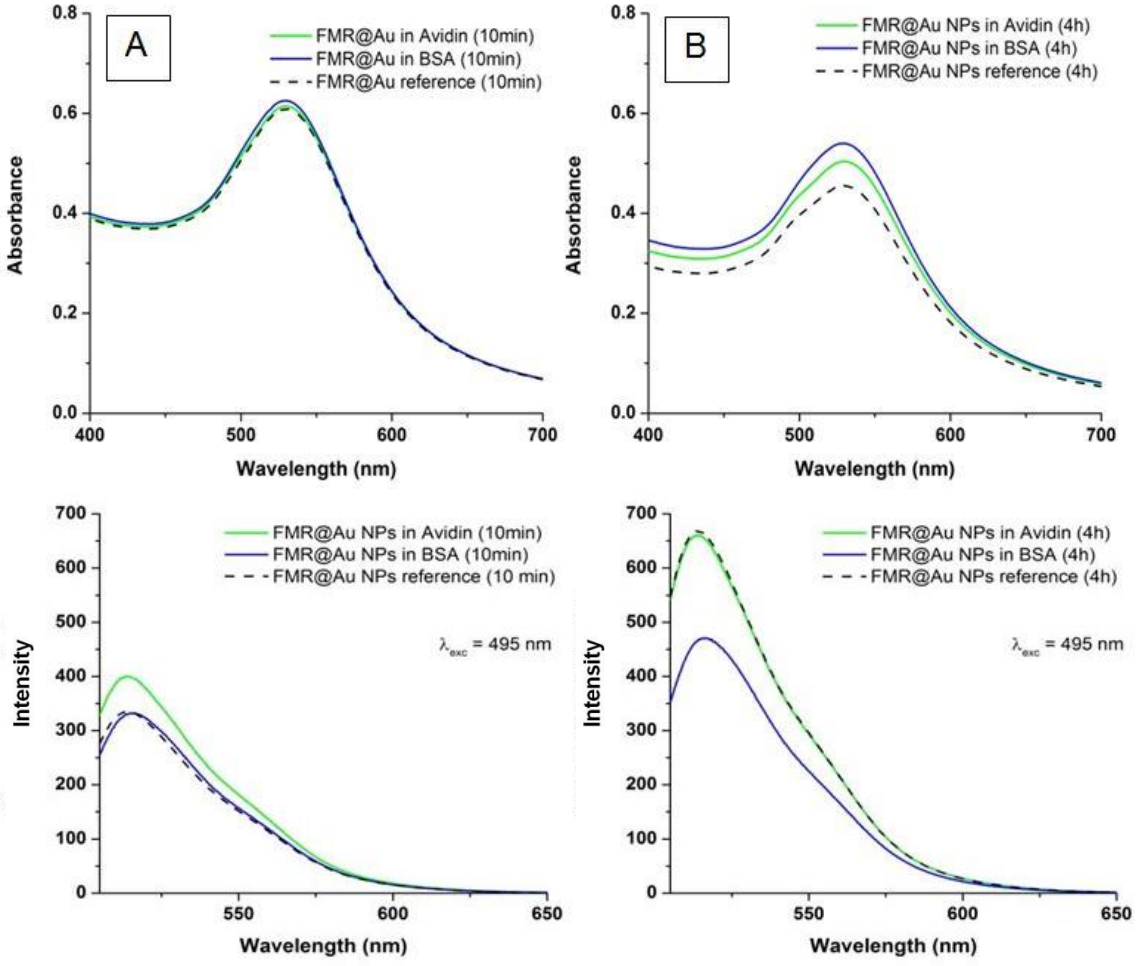

Figure 3.15: Visible (top) and PL spectra (bottom) of FMR@Au NPs, in presence of avidin, BSA and PBS reference at (A) 10 min and (B) 4h of incubation time

Similarly, the photoluminescence spectra show an increase in fluorescence emission for FMR@Au colloids tested in avidin and reference after 4h of incubation time. An increase is also visualized for the colloids in the presence of BSA protein, but with a lower intensity than for avidin and PBS reference.

After these observations, the choice was made to do a series of similar tests in a systematic way, i.e. with shorter recording times, in order to observe the behaviour of both absorbance and fluorescence emission between 10 min and 2h40 of incubation time. Therefore, the response was recorded after 10 and 20 minutes and then every 20 minutes during a total period of 2h40 for each solution tested. The visible and photoluminescence spectra are given in Figure 3.16, showing the response in the presence of avidin, BSA and PBS reference in Figure 3.16 (A), (B) and (C) respectively.

The major observations from this additional study are that the response obtained visible spectroscopy gives a similar trend for all solutions tested (avidin, BSA and PBS) with an overall decrease of absorbance and increase of fluorescence emission over time. This study confirms that there is no specific response from the nanostructures in the presence of avidin, neither a quenching of fluorescence. Additionally, the signals obtained from BSA control and PBS reference do not give a steady response over time, but a similar behaviour to that observed for avidin.

To evaluate the behaviour of colloids after being tested for biosensing, their hydrodynamic size was evaluated by DLS, as presented in Table 3.6. The results obtained show an increase in hydrodynamic sizes in the presence of avidin and BSA ($\Delta d_{average}$ = 5 nm and 2.6 nm respectively. Yet, if this was due to specific interaction between avidin and biotin, aggregation would have occurred and the PL signal should have decreased which was not the case. Instead, the presence of avidin seems to lead to an increase of the distance between the Au core and FITC suggesting the occurrence of a conformation change associated with changes in the surrounding medium. Yet, in that case, the response in the presence of BSA was expected to follow the same trend which was not the case. The stability in solution while diluted in PBS buffer in this case cannot be tested by surface potential evaluation, as the amount of NaCl (~0.1 M)) in the PBS buffer induces a charge screening.

Table 3.6: DLS measurements on FMR@Au NPs diluted in PBS after testing in avidin and BSA

	DLS (average of 3 values)	
Sample	$d_{average}$ (nm)	PdI
FMR@Au NPs	23.3	0.507
FMR@Au NPs in Avidin	28.3	0.466
FMR@Au NPs in BSA	25.9	0.495
FMR@Au NPs in reference (PBS)	23.2	0.515

In view of the inconclusive results obtained and the lack of evidence regarding the presence of biotin and/or the occurrence of the click reaction, a new literature research was carried out in order to find possible side reactions that might jeopardise this functionalization step. Indeed, a paper by Perrier *et al*, dating from 2008, reports the limitations of carrying out controlled radical polymerizations in the presence of azide groups [52]. In this work, the authors verified that 1,3-cycloadditions may take place between the azide and the double bonds of different types of monomers, including meth(acrylates). Yet, the reactivity of methyl methacrylate was identified as lower, when compared to other types of monomers. Hence, the incorporation of the AEM-FITC may have actually taken place and the UV-Vis spectra are in agreement with that hypothesis. However, this type of side reactions are still thought to be a major limitation and the subsequence reaction between azide and the alkynated biotin via 1,3-cycloaddition may have been compromised. In view of this finding, it has to be concluded that a distinct synthetic strategy has to be adopted in order to functionalize this type of nanostructures.

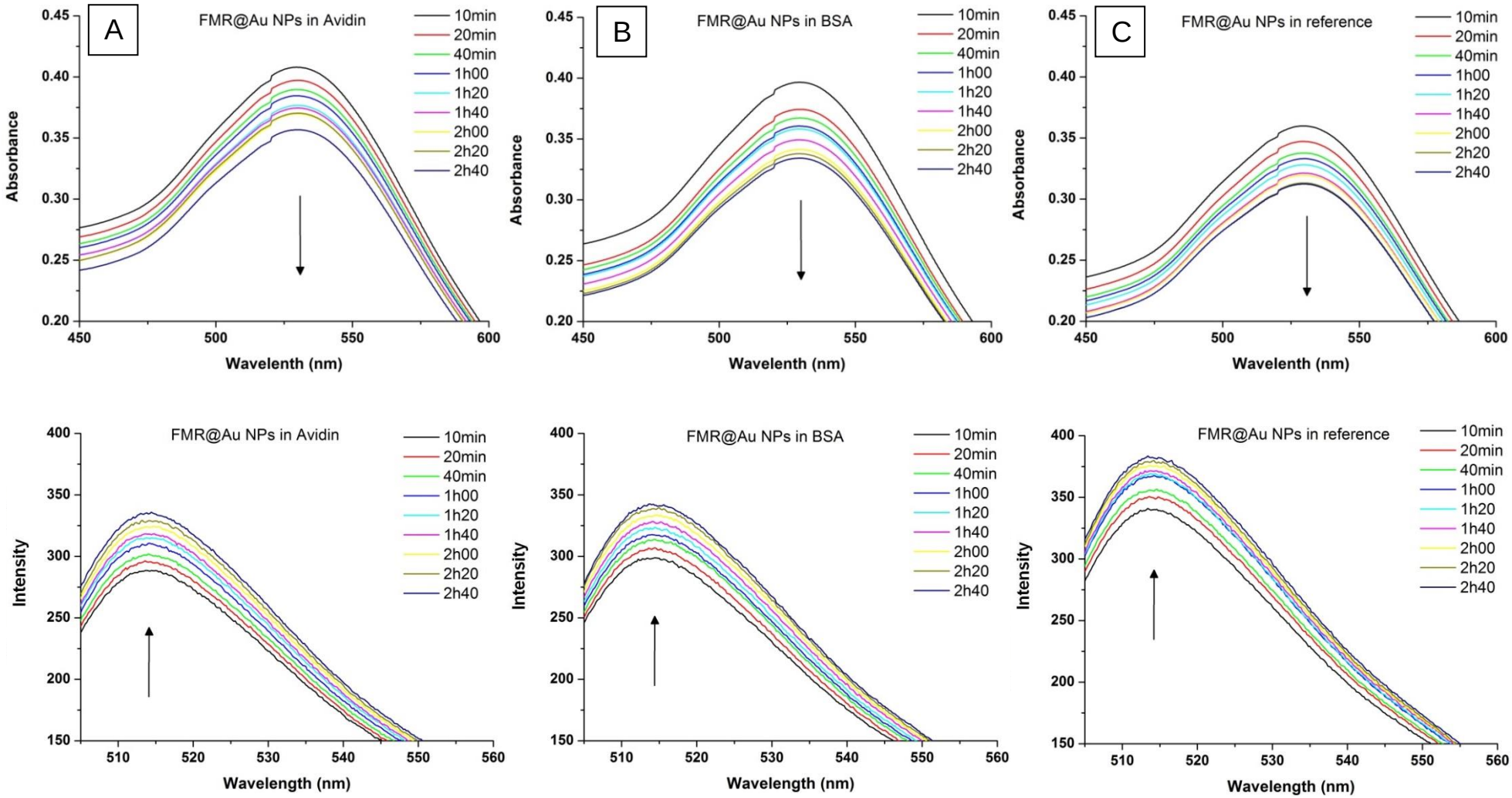

Figure 3.16: Visible and corresponding photoluminescence spectra (top to bottom) of FMR@Au NPs in the presence of (A) avidin, (B) BSA and (C) PBS reference

CHAPTER 4. PREPARATION OF MULTILAYERED THIN FILMS VIA LAYER-BY-LAYER METHOD

4.1. Introduction

In parallel to the work done regarding the encapsulation of Au NPs in Chapter 2 and 3, the preparation of multilayered thin films embedding these nanostructures was studied. In a preliminary study, the deposition of the polycation poly(allylamine hydrochloride) (PAH) and the polyanion poly(styrene sulfonic acid sodium salt) (PSS) of different molecular weight was studied, in order to get familiar with the Layer-by-Layer (LbL) deposition procedure, described in section 4.2.1. Then, the same deposition was performed using the "blank" copolymer@Au NPs prepared as negative charged layer and PAH as the positive layer, i.e. (PAH/copolymer@Au NPs), by studying of the number of bilayers, described in section 4.2.2. Additionally, the deposition of PAH/Au NPs bilayers on the previously coated (PAH/PSS) slides was also tested, in order to evaluate the improvement of thin film quality, namely uniformity on a pre-coated surface. Following these observations, a strategy for the possible configuration of multilayered films was outlined, as described in section 4.3. Using this configuration, the effect of deposition time for polyelectrolytes and gold nanostructures was studied in section 4.4.

4.2. Study of Layer-by-Layer method

4.2.1. Preparation of (PAH/PSS) multilayered thin films

The choice of polyelectrolyte concentration was based on previous studies from Pereira and co-workers [32, 46]. Here, two molecular weights (MW) were tested for PAH: 15 000 and 56 000 g/mol, and one for PSS: 70 000 g/mol, details of the preparation of solutions are available in section 6.5.1. Two glass slides were prepared and the polyelectrolytes deposited using the Layer-by-Layer method: (PAH_{15}/PSS_{70}), (PAH_{56}/PSS_{70}), details of the method are given in section 6.5.2. Figure 4.1 illustrates the LbL method for one bilayer of the two polyelectrolytes, the desired number of bilayers was achieved by repeating these four steps. In this case, the deposition of 2 to 3 bilayers was done.

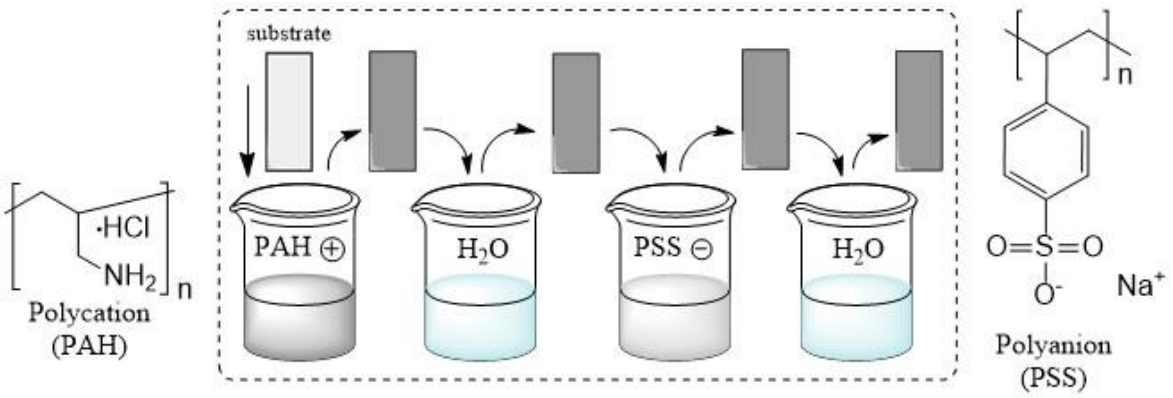

Figure 4.1: Illustration of the Layer-by-Layer deposition of one bilayer of PAH and PSS polyelectrolytes

4.2.2. Preparation of (PAH/copolymer@Au NPs) multilayered thin films

First, the LbL deposition was tested with PAH solution of MW 56 000 g/mol and previously prepared copolymer@Au NPs, in Chapter 2. The deposition of bilayers (PAH_{56}/copolymer@Au NPs) via Layer-by-Layer method is illustrated in Figure 4.2.

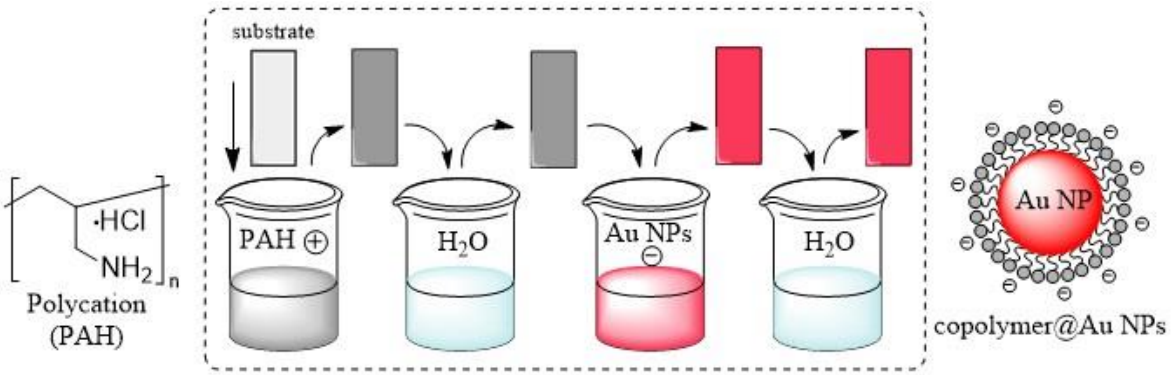

Figure 4.2: Illustration of the Layer-by-Layer deposition of one bilayer of PAH and copolymer@Au NPs

The deposition can be evaluated by visible spectroscopy, as even the first bilayer of Au nanostructures can be detected due to the presence of LSPR wavelength, as presented in spectra of each of the six bilayers deposited, in Figure 4.3.

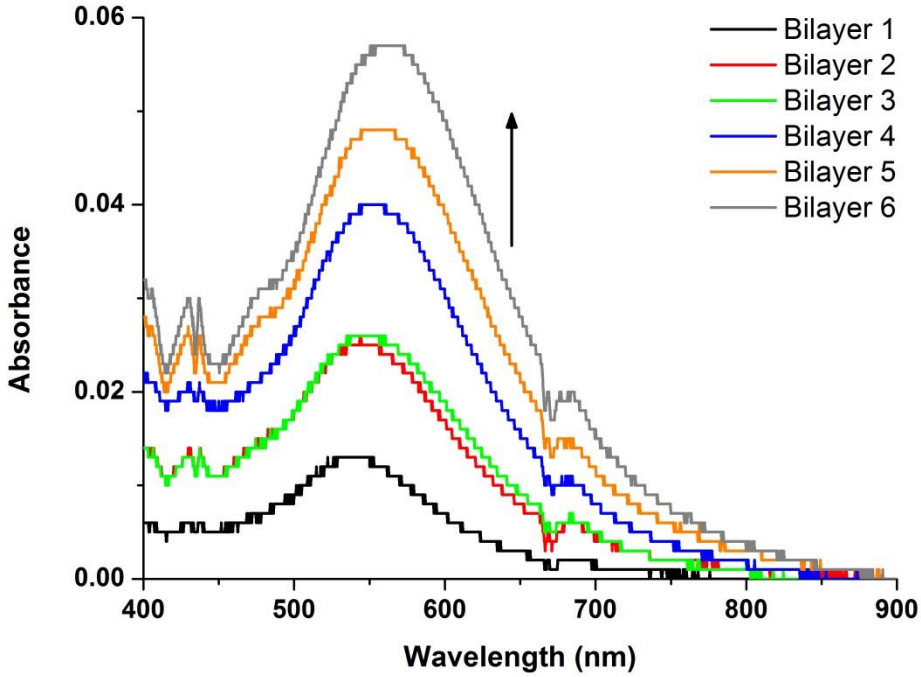

Figure 4.3: Visible spectra of six (PAH/copolymer@Au NPs) bilayers deposited

The increase of absorbance after deposition of each bilayer indicates a successful coating of gold nanostructures onto the substrate. However, a shift in λ_{LSPR} from around 540 to 560 nm ($\Delta\lambda \approx 20$ nm) was observed, that could indicate aggregation of the gold nanostructures. Indeed, after LbL deposition, the colloidal solution presented a purple/blue color showing that strong aggregation of gold colloids had taken place. This could be due to insufficient washing and drying of the slides between steps of PAH and copolymer@Au NPs deposition, thus causing aggregation in the solution. This can be overcome by increasing the number and time of washing and drying steps.

Additionally, the films obtained did not present homogeneous deposition of copolymer@Au nanoparticles. The use of precursor bilayers of polyelectrolytes before deposition of nanoparticles can improve the homogeneity of the adsorption of gold nanostructures. Therefore, the presence of precursor bilayers of PAH/PSS prior to nanostructures deposition was studied in this case with both MW configurations: (PAH_{15}/PSS_{70}), (PAH_{56}/PSS_{70}) using the glass slides prepared in section 4.2.1. The difference in MW of PAH solution did not seem to influence the coating, as was evidenced by visible spectroscopy (not shown here). However, a visual improvement of the homogeneity for both configurations was observed, as compared to the coating without precursor bilayers. Therefore, the choice was made to use the MW of 56 000 g/mol of PAH solution, and to keep the PSS with a MW of 70 000 g/mol for the preparation of 3 precursor bilayers.

As was introduced in Chapter 1, another parameter that can improve the homogeneity and thickness of the film is the ionic strength (or salt concentration) of the solutions used. Thus, the ionic strength of solutions was adjusted to 10 mM NaCl for the next preparation of multilayered films.

4.3. Configuration of multilayered thin film assembly

Conclusions from these studies allowed outlining a strategy for the LbL film configuration, as illustrated in Scheme 4.1. The first step, (1) in Scheme 4.1, consists of the deposition of several (*n*) precursor bilayers of PAH/PSS in order to create a robust, homogeneous and highly charged surface. Then, the second step, (2) in Scheme 4.1, concerns the deposition of bilayers (*m*) of PAH/Au nanostructures onto the pre-coated surface. The final goal was to deposit functionalized copolymer@Au NPs as last layer, in step (3), on top of the previously coated substrate, in order to obtain a robust bio-detector containing the functional moieties at the surface for detection purpose.

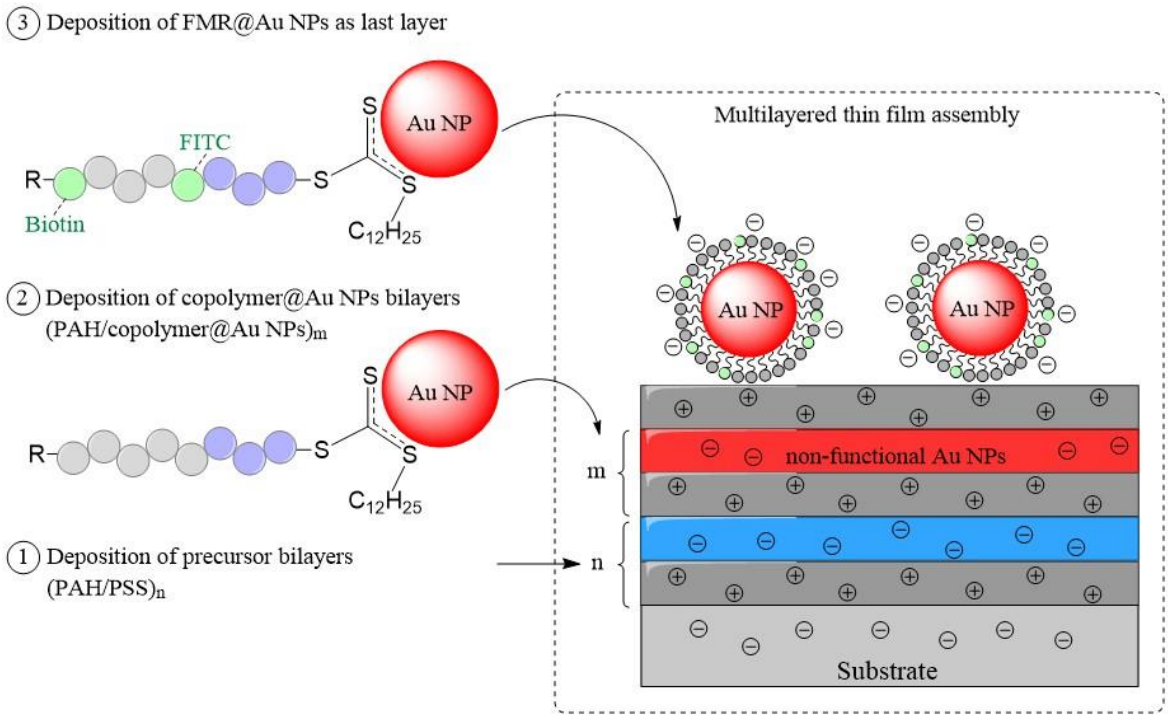

Scheme 4.1: Strategy for the preparation of multilayered thin films of $(PAH/PSS)_n$ $(PAH/copolymer@Au\ NPs)_m$ (PAH/FMR@Au NPs) via Layer-by-Layer deposition method

The LbL deposition was to be tested on quartz substrates for the detection of fluorescence signal. Unfortunately, due to the inconclusive results obtained on the functionalized colloids and time constraints, this last deposition was not performed. In the case of successful functionalization of colloids and positive results for the functional colloids, the next steps would have been to test the response of multilayered thin films prepared towards avidin.

4.4. Study of multilayered thin films of (PAH/copolymer@Au NPs) varying deposition time

Following the conclusions from LbL deposition tests in section 4.2, the parameters were chosen to be improved on the washing and drying steps, to avoid aggregation of gold solution. Moreover, the ionic strength of polyelectrolytes was chosen to be modified to 10 mM NaCl to enhance the layer thickness and homogeneity, the details of the procedure are given in section 6.5.3. In this section, the successive deposition of 4 bilayers of (PAH_{56}/copolymer@Au NPs) onto a pre-coated substrate with 3 bilayers of (PAH_{56}/PSS_{70}) will be presented, as illustrated in Scheme 4.2. The present study was focusing on the effect of the deposition time of gold colloidal solution.

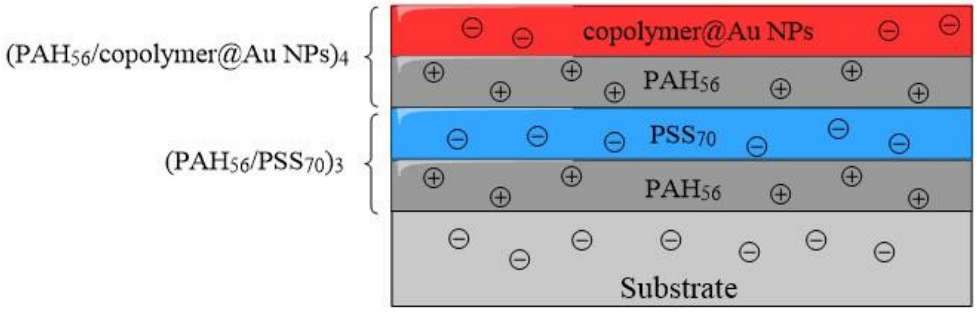

Scheme 4.2: Multilayered film assembly via Layer-by-Layer deposition of precursor bilayers $(PAH/PSS)_3$ and bilayers of $(PAH/copolymer@Au\ NPs)_4$

The visible spectra obtained for this study are presented in Figure 4.2, with three deposition times chosen at 5, 10 and 20 minutes. An increase of absorbance with increasing deposition time is clearly observed, as highlighted in Figure 4.2 (D). In a similar way to preliminary study, shifts in λ_{LSPR} are observed for all deposition times tested: from around 530 to 540 nm for 5 min deposition time ($\Delta\lambda_{5min} \approx 10$ nm), from 535 to 540 nm for 10 min ($\Delta\lambda_{10min} \approx 5$ nm), and from 530 to 550 nm for 20 min ($\Delta\lambda_{20min} \approx 20$ nm), but in this case the solution of copolymer@Au NPs used did not present a visible colour change. Thus, the aggregation might take place on the substrate rather than in the colloidal solutions.

In conclusion, the absorbance intensity increases linearly with the number of gold bilayers. Also, increasing the deposition time has a positive influence on the intensity. In the present case, the 10 minutes deposition time seems to be a good compromise, at it makes the preparation of the film possible in a relatively short time, while significantly increasing the signal compared to 5 minutes. Moreover, it seems to cause less aggregation, with smaller variation of the LSRP. Other parameters such as the pH of solutions would be interesting to study, as it also has an influence on the deposition, but time restrictions did not allow performing an in-depth study of the Layer-by-Layer method.

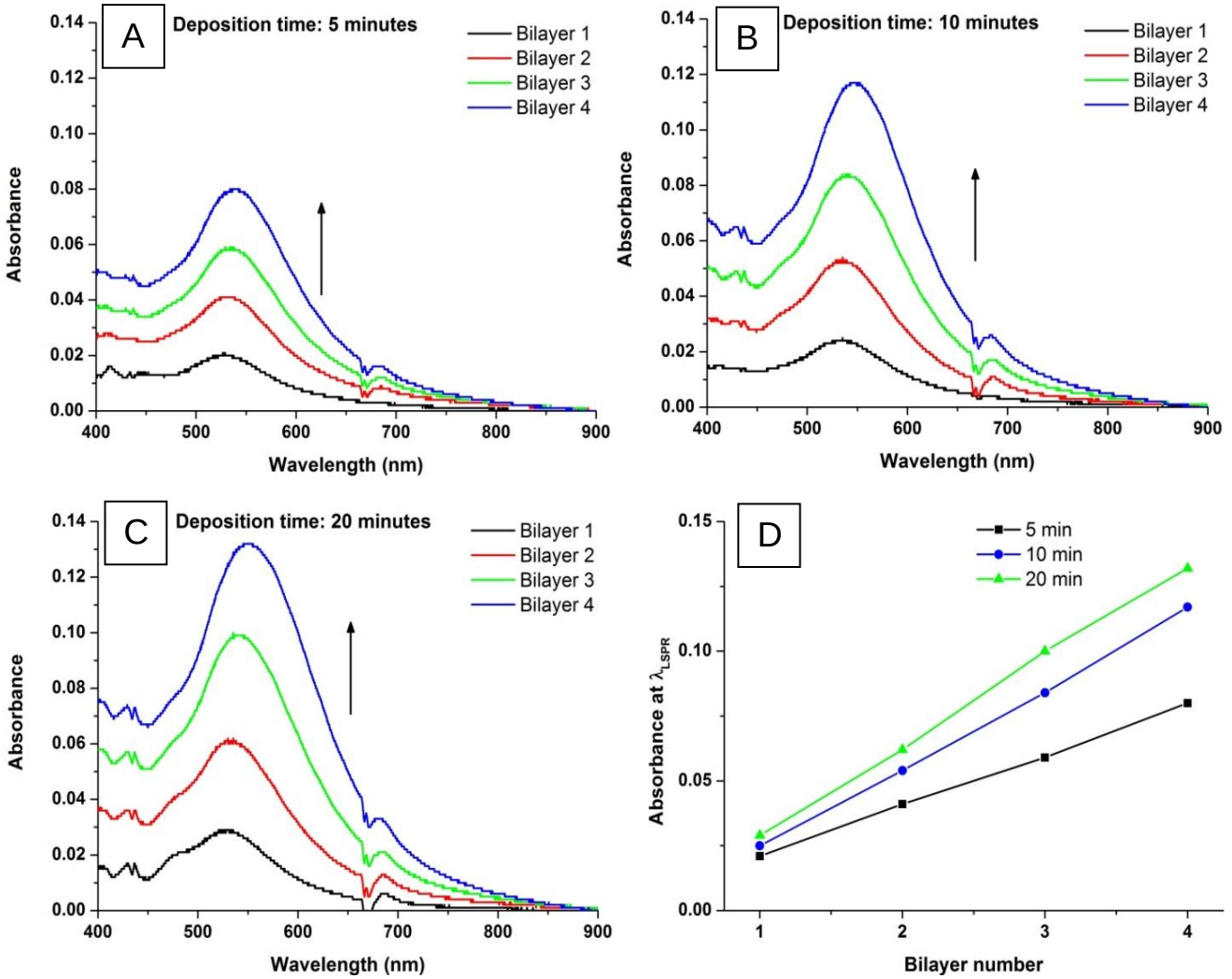

Figure 4.4: Visible spectra of 4 bilayers of (PAH/MR@Au NPs) at deposition times (A) 5 minutes, (B) 10 minutes, (C) 20 minutes, and (D) the linear correlation between absorbance at λ_{LSPR} and number of bilayer

CHAPTER 5. CONCLUSIONS AND FUTURE WORK

The synthesis of gold nanoparticles and the adsorption of macroRAFT agents at their surface were successfully achieved in the case of blank MR agent. Furthermore, by adjusting the amount of Au NPs and MR it was possible to scale up the amount of nanostructures prepared. The following conditions have been selected for this scale up: $2.5x10^{-6}$ mmol of Au NPs per liter and $5.0x10^{-2}$ mM of initial concentration of MR agent.

The encapsulation of MR@Au NPs via REEP using MMA and BA was also successfully achieved and verified by UV-Visible spectroscopy, DLS, zeta potential measurements and STEM. However, notice should be made that GPC-SEC analyses of the corresponding block copolymers prepared under the same reaction conditions but in the absence of Au NPs have shown that the polymerization is not controlled as the molecular weight distribution is bimodal. Hence, conventional free radical polymerization and possibly other chain transfer reactions must take place in parallel with the RAFT polymerization.

The preparation of the functionalized MR containing FITC and biotin moieties was not clearly confirmed by the techniques used during this work (proton and carbon NMR, FTIR, elemental analysis). Moreover, according to the literature, the incorporation of the AEM-FITC may have been limited due to parallel 1,3-cycloadditions between the double bond of this monomer and the azide. Consequently, the subsequence reaction between azide and the alkynated biotin via 1,3-cycloaddition may also have been compromised. In view of this finding, XPS analysis should be carried out to clarify this issue Moreover, a distinct synthetic strategy has to be considered to functionalize this type of nanostructures.

As regards the adsorption of FMR onto Au NPs and subsequent encapsulation via REEP, two adsorption strategies were tested. The first one, by attempting to adsorb a mixture of functional and non-functional MR agent, seems to have permitted the creation of micelles or aggregates. The determination of the CMC of the functional MR agent could confirm this hypothesis. Encapsulation of the Au NPs via REEP was therefore inconclusive. In turn, the second strategy, aiming at adsorbing only the functional MR agent at the surface of Au NPs showed improved structures, yet, due to time restrictions encapsulation of FMR@Au via REEP was not tested.

The response of the functionalized nanostructures to avidin did not show any specific response to avidin, as both tests in the presence of reference and avidin showed the behaviour opposite to what was expected. An increase of the fluorescence intensity was observed instead of the fluorescence quenching expected. In view of the doubts regarding the functionalization of the MR, namely in what concerns the incorporation of biotin, it was not possible to explain the results obtained.

Concerning the layer-by-layer deposition method, the study of effects such as of the polyelectrolytes molecular weights, salt concentration, washing and drying steps as well as the deposition time, allowed the

optimization of the deposition of gold nanostructures. Moreover, the presence of precursor bilayers of PAH/PSS prior to deposition of gold increased the films homogeneity. Nevertheless, it might be worth evaluating the effect of pH on the deposition of these materials in future works.

CHAPTER 6. EXPERIMENTAL PROCEDURES

6.1. Chemicals

In Chapter 2, the synthesis of gold nanoparticles was done using hydrogen tetrachloroaurate (III) trihydrate, 99.9+% ($HAuCl_4.3H_2O$, Sigma-Aldrich) and sodium citrate tribasic dehydrate, ≥99% ($Na_3C_6H_5O_7.2H_2O$, Sigma-Aldrich). The preparation of macroRAFT agent solutions in Chapters 2 and 3, and addition of FITC monomers in Chapter 3, were done using previously prepared MR agents (P($PEGA_{40}$)-TTC and P($azAA_2$-*b*-$PEGA_{40}$)-TTC) and AEM-FITC from S. Pereira, using VA-044 as initiator and 1,3,5-trioxane as internal standard (99.5+%, Acros). The click chemistry was done using previously prepared alkynated-biotin, copper sulfate ($CuSO_4$) and sodium ascorbate ($C_6H_7NaO_6$). The biosensing tests were performed using avidin from egg white, ≥98%, bovine serum albumin (BSA). For Chapters 3 and 4, a phosphate buffer saline (PBS) solution (10 mM) was prepared with NaCl (137 mM), KCl (2.7 mM), Na_2HPO_4 (10 mM) and KH_2PO_4 (1.8 mM). In Chapter 4, the Layer-by-Layer deposition was performed using the polyelectrolytes poly(allylamine hydrochloride) of MW= 15 000 g/mol and 56 000 g/mol (PAH) and poly(styrene sulfonic acid sodium salt) of MW=70 000 g/mol (PSS). Ionic strength was modified using sodium chloride (NaCl, 0.01 M). For all reactions, the adjustment of pH was done using sodium hydroxide (NaOH, 0.1 and 0.01 M) and hydrochloride acid (HCl, 0.1 and 0.01 M). The cleaning of glassware and glass/quartz slides was done using nitric acid (pure), aqua-regia (2:1 v/v mixture of hydrochloric acid and nitric acid) or piranha (3:1 mixture of sulfuric acid (H_2SO_4) and hydrogen peroxide (H_2O_2)) solutions. Ultrapure water used for dilutions throughout the project was obtained from a MilliQ water purification system (Millipore, Billerica, MA).

6.2. Instrumentation

The UV-Visible spectra of solutions (colloids or polymers) were recorded using quartz cells of different volumes (maximum volumes of 3 mL and 1.4 mL) and a JASCO V-560 UV-Visible spectrometer, using distilled water as reference. The UV-Visible spectra of glass slides to follow the LbL deposition were recorded on a PG instruments T60 UV-Visible spectrometer, using a black self-made support. The fluorescence spectra of colloids and polymers were recorded using quartz cells with four transparent faces of different volumes (maximum volumes of 3 mL and reduced volume 1.4 mL) on a JASCO FP-8300 spectrofluorometer. Transmission electron microscopy (TEM) images were obtained using a Hitachi H-9000 microscope operating at 300kV. Scanning electron microscopy (SEM) in transmission mode images were obtained using a Hitachi SU-70 operating at an acceleration voltage of 15kV. Scanning transmission electron microscopy (STEM) images, with transmission and secondary electron detection, were obtained using a Hitachi HD2700C operating at 200kV. The samples for TEM, SEM and STEM were prepared by placing a drop of diluted colloidal solutions on a copper grid coated with amorphous carbon film and left to evaporate. The zeta potential and dynamic light scattering (DLS) measurements were carried out using ZetaSizer Nano ZS Model Zen 3500 from Malvern. The colloidal solutions were analysed as prepared, the aliquots from the

copolymerization study were diluted before analysis. Centrifugations of the colloidal solutions were performed in a Force 1618 Microcentrifuge and a Thermoscientific Megafuge 16R at room temperature, with a speed of 15600 g for 30 minutes. ^{1}H-NMR and ^{13}C-NMR spectra were recorded on a BRUKER Avance 300 spectrometer by diluting or dissolving the sample in d^{6}-DMSO solvent. GPC-SEC analysis was performed on a PL-110 GPC instrument equipped with a two PLMIXED 300x7.5 mm column and refractive index (RI) detector. The columns, injector system and the detector were maintained at 50°C during the analysis. Before sample analysis, the methylation of the carboxyl groups from the polymers was performed using trimethylsilyldiazomethane. The methylated polymers (5 mg) were dissolved in 0.6 mL of THF (CHROMASOLV® Plus, for HPLC > 99.9%, Aldrich) and 20 µL of toluene was added as internal standard. 100 µL of polymer solutions were pumped at a flow rate of 0.9 mL/min. The columns were calibrated with polystyrenes standards (Polymer Laboratories, UK) in the range of MW = 2 960 - 66 000 g/mol. KBr-FTIR spectra were recorded using a BRUKER Tensor 27 and analysed using OPUS software. The dried samples were crushed with KBr powder and pressed into pellets using a metallic press for two minutes.

6.3. Experimental procedures of Chapter 2

6.3.1. Synthesis of Au NPs via citrate method

10 mL of sodium citrate solution (38.8 mM) were added to 100 mL of $HAuCl_4.3H_2O$ solution (1 mM) previously brought to 90°C using an oil bath under vigorous stirring (250 rpm). After 1h, heating was switched off and stirring was kept overnight. Prior to use, the colloidal solutions were centrifuged for 30 minutes at 15 000 g. The supernatant was removed and the precipitates were redispersed in 1mL of ultrapure water. Au NPs with a diameter of around 15 nm were obtained and the concentration of solutions was calculated by UV-Vis spectroscopy [48]. The stock solution used for the preliminary project work (Chapter 2, section 2.3) had a concentration of 7.52 x10^{-9} mol NPs/L, the stock solution used for the rest of the project was a mixture of two batches prepared following the procedure described above, giving a final concentration of 7.33 x10^{-9} mol NPs/L.

6.3.2. Adsorption of MR onto Au NPs

The MR agent P(PEGA$_{40}$)-TTC was used as prepared by S. Pereira. A volume of 30 mL of MR solution (from stock solution of concentration 0.15 mM) was prepared and the pH was adjusted to 7-8 using NaOH (0.1 and 0.01 M). The solution was added dropwise, under stirring (300 rpm), to a dispersion of Au NPs and left under stirring overnight, at room temperature. The Au NPs dispersion used was diluted (10x) from the stock solution with 2 mL of ultrapure water. The mixture obtained was centrifuged 30 minutes at 15 600 g, the supernatant was collected and the precipitates redispersed in the same volume of ultrapure water. Both

studies (varying Au NPs and initial MR agent were prepared in the same conditions, only changing the respective concentrations.

The determination of the adsorbed concentration was done by comparing the UV-Vis spectra of initial MR agent (C_0) and spectra of supernatants (C_{sup}) after adsorption. The concentration of MR agent adsorbed (C_{ads}) is thus given by $C_{ads} = C_0 - C_{sup}$. The correlation between spectra and concentrations is obtained using a calibration curve prepared by S. Pereira [32], based on the height of the absorbance peak of MR agent at 309 nm.

6.3.3. Copolymerization of MMA:BA from MR@Au NPs via RAFT polymerization by controlled addition of monomers

Prior to use for all copolymerization reactions, the solution mixture of MMA:BA (10:1 w/w) was previously prepared and purified using an alumina column by S. Pereira. The pH of MR@Au NPs (adsorption being prepared the day before copolymerization), was adjusted to 7-8 using NaOH (0.1 or 0.01 M) and 2 mL of solution of initiator (VA-044, 0.5 mg/mL) was added the reaction vessel containing 25 mL of the colloidal solution. The mixture was purged with nitrogen for 30 minutes in an ice bath under stirring. The polymerization was started by placing the reaction vessel at 70°C. The mixture of monomers (10 MMA: 1BA w/w) was added in a controlled way: 15 μL of mixture was added before the polymerization started and then 15 μL were added each hour during 1 hour. Afterwards the copolymerization continued for 3 more hours. Then, the reaction vessel was placed in an ice bath in contact with oxygen to stop the polymerization. The resulting colloids were centrifuged 30 minutes at 15 600 g, the supernatant was collected and the precipitates redispersed in the same volume of ultrapure water.

6.4. Experimental procedures of Chapter 3

6.4.1. Functionalization of azide-modified MR agent with FITC via RAFT polymerization

Synthesis of the macroRAFT agent P(AA_2-*b*-$PEGA_{40}$)-TTC and functionalization with an azide group was performed by S. Pereira. The macroRAFT agent P($azAA_2$-*b*-$PEGA_{40}$)-TTC was used as received, and functionalized with a fluorescent monomer: 2-aminoethyl methacrylate - fluorescein isothiocyanate (AEM-FITC). The AEM-FITC used was previously prepared by S. Pereira using aminoethyl metacrylate hydrochloride (AEM) and fluorescein isothiocyanate (FITC). Details of preparation are given in her thesis work [32]. The polymerization of AEM-FITC into MR agent was done using RAFT polymerization, using VA-044 as initiator at 44°C for duration of 7h30. The azide-modified MR agent (900 mg) was first dissolved in ethanol. To this solution, 100 mg of AEM-FITC and 3 mg of 1,3,5-trioxane were added. Then, 5 mg of the

initiator VA-044, previously dissolved in water and kept in an ice bath, was added to the reaction vessel. The mixture was kept in an ice bath under stirring and purged using nitrogen for 30 minutes. Then, the reaction was started by placing the reaction vessel in an oil bath at 44°C. After 7h30, the water and nitrogen flows were stopped and the reaction, in N_2 atmosphere, was left under stirring overnight. The following day, the reaction solution was precipitated by dropwise addition of 100 mL of diethyl ether, while left in ice bath and stirring. After decantation, the supernatant was discarded and the precipitates were recovered using ethanol. Three precipitations were done: the first one straight after end of reaction, the second one after 4h, and the last one after more than 72h.

6.4.2. Copper-catalyzed alkyne-azide cycloaddition (CuAAC) - Click chemistry

A biotin functionalized with an alkyne group (alkynated-biotin or biotin-CCH) was previously prepared by S. Pereira. The alkynated-biotin obtained was used as received. For the CuAAC reaction, 250 µL of alkynated-biotin (1.67 mM, aqueous solution with 10% d^6-DMSO for a better solubilisation of biotin) was added to 10 mL of N_3-FITC-MR agent (0.055 mM) solution under stirring. Then 42 µL of copper sulfate $CuSO_4.5H_2O$ (2.5 mM) and 42 µL of sodium ascorbate (5 mM) were added to the mixture and left to stir for 24h at room temperature. The ratios used for reaction were: 1 [azide] : 0.5 [alkyne] : 0.125 [$CuSO_4$] : 0.25 [sodium ascorbate].

6.4.3. Purification of macroRAFT agent – Dialysis

After CuAAC reaction left for 24h, a volume of 10.4 mL of reaction solution is obtained. This solution is then place in a dialysis membrane (6-8000 MWCO, from Spectra/Por) for purification, i.e. removal of any unreacted reagents (monomers, solvents, etc). As the volume per length characteristic of the membrane is 1.7 mL/cm, a length of 20 cm of membrane was cut, to allow the closing of membrane by nods on each side, thus giving a minimum effective length of 6.5 cm. The membrane was first soaked for 30 minutes in distilled water. Then, it was filled with the reaction solution and closed by nods and clips. The membrane was left to soak in 1 litre of distilled water (+0.1% of d^6-DMSO-d6 solution to help the solubilisation of biotin) under stirring for several days. Each day, the mixture water-d^6-DMSO was changed, and a sample was withdrawn and checked via UV-Vis spectroscopy upon removal of FITC coloration. The total duration of dialysis was more than 100 hours.

6.4.4. Adsorption of [2MR:1FMR] onto Au NPs

The procedure for adsorption is identical to the one performed in 6.3.2, except the use of MR agent. For the correct adsorption of mixture [2MR:1FMR], two sequential adsorption reactions are performed. The pH of both solutions of MR and FMR was adjusted with NaOH (0.1 M). First, 9 mL of the solution of FMR (0.055 mM) is added dropwise to 3 mL of Au NPs ($2.5x10^{-6}$ mM), and left to stir for 2h. Then, 18 mL of the MR

agent (0.055 mM) was added to the reaction vessel, the reaction was then left overnight to stir at room temperature.

6.4.5. Synthesis of copolymers via RAFT polymerization based on MR agent

The procedure for copolymerization reaction is identical to the one described in 6.3.3, i.e. the addition of MMA:BA mixture (10:1 w/w) for 1h, using VA-044 as initiator for a total reaction time of 4h. The only change in the procedure is the MR agent used, here being the P(AA_2-*b*-$PEGA_{40}$)-TTC (instead of copolymerization from MR@Au NPs in section 6.3.3). Thus, the temperature used in the case of azide-modified MR agent is 44°C. Aliquots are withdrawn from the reaction solution at various times along the 4h reaction, and placed in an ice bath to stop the reaction. During, the first hour, 15 µL of monomers are added every 10 minutes, giving a total of 105 µL monomers mixture. For the remaining 3h of reaction at 70°C, aliquots are withdrawn without further addition of monomers.

6.4.6. Preparation of samples for GPC-SEC analysis – Methylation

Prior to the following methylation procedure, the polymers are dried to obtain a mass of around 5 mg. The following methylation procedure was performed by Pr. A. Barros and D. Evtyugin. The polymers were modified by methylation of the carboxylic group using trimethylsilyldiazomethane. The process was based on a published protocol [53]. 5 mg of each sample was first dissolved in 0.6 mL of a tetrahydrofuran (THF) solvent. The yellow solution of trimethylsilyldiazomethane was added dropwise to the polymer solution. Upon addition, bubbles appeared. The addition was continued until the solution stopped bubbling. The solution was then dried under nitrogen flow to remove solvent. 5 mg of the dried samples was dissolved in 1 mL of THF and filtered through a 0.3 µm membrane prior to GPC analyses.

6.4.7. Copolymerization of MMA:BA from [2MR:1FMR]@Au NPs via RAFT polymerization by controlled addition of monomers

The procedure for copolymerization reaction is identical to the one described in 6.3.3, i.e. the addition of MMA:BA mixture (10:1 w/w) for 1h, using VA-044 as initiator for a total reaction time of 4h at a temperature of 44°C. This time, the copolymerization was performed from the surface of [2MR:1FMR]@Au NPs.

6.4.8. Biosensing response of copolymer@Au NPs towards avidin

Prior to the biosensing tests, a 4 mL mixture (1:1) of colloidal solution of copolymer@Au NPs and PBS buffer (pH 7.4, 10 mM) was prepared to stabilize the pH at 7.4. Volumes of 805 µL of this colloidal solution are placed in three separate Eppendorf vials. Then, 23 µL of test solution: avidin (0.5 mg/mM) or BSA (0.5

mg/mM) or PBS reference, are added to the Eppendorf containing the colloids. The Eppendorf is shaken for a few seconds, and UV-Visible and fluorescence spectra are recorded 10 minutes after mixture. After 2h30, a second spectrum is recorded. The order of spectrum recording is as follows: avidin (10 min), BSA (10 min), PBS (10 min), avidin (2h30), BSA (2h30) and PBS (2h30).

6.4.9. Adsorption of FMR onto Au NPs

The procedure for adsorption was kept identical to the one performed for MR in 6.3.2, except for the use of functionalized MR agent, i.e. biotin-FITC-MR agent, instead of the "blank" MR agent.

6.4.10. Biosensing response of FMR@Au NPs towards avidin

The procedure for the first biosensing test is kept identical to the one described in section 6.4.8, except the colloids were centrifuged and redispersed prior to tests, to keep the same dilution as the one used for copolymer@Au NPs in 6.4.8. Also, the recording times (or incubation time) of UV-Vis/fluorescence spectra in this case are 10 minutes and 4 hours after mixtures. Similarly, the order of spectrum recording is as follows: avidin (10 min), BSA (10 min), PBS (10 min), avidin (4h), BSA (4h) and PBS (4h).

For the additional biosensing tests, performed in a systematic way, each solution tested (avidin, BSA and PBS reference) was done in a sequence, meaning that the order of spectra recording is as follows: avidin (10 min to 2h40), BSA (10 min to 2h40) on the first day, and PBS (10 min to 2h40) on the second day.

The DLS measurements were performed the day following biosensing tests: therefore being 2 days after contact time for FMR@Au NPs in avidin and 1 day after contact for FMR@Au NPs in PBS and BSA.

6.5. Experimental procedures of Chapter 4

6.5.1. Preparation of polyelectrolytes solutions

Solutions of PAH (MW 15 000 and 56 000 g/mol) and PSS (MW 70 000 g/mol) polyelectrolytes of concentration 2 mg/mL were prepared. A volume of 100 mL of each polyelectrolyte solution was prepared by dissolution of 200 mg of solute in ultrapure water, and left stirring overnight at room temperature. For section 4.2, the solutions were used as prepared for the Layer-by-Layer deposition. For section 4.3, the ionic strength was adjusted to 10 mM by addition of NaCl during the preparation of polyelectrolyte solutions.

6.5.2. Layer-by-Layer deposition of (PAH/PSS) and (PAH/MR@Au NPs)

For section 4.2, microscopy glass slides (2.5x8 cm), were cut to 2.5x2 cm pieces. The cleaning of slides was done using 12 mL of "Piranha" solution, prepared by adding 3 mL of hydrogen peroxide to 9 mL of sulfuric acid (ratio 3:1) in an ice bath (piranha solution has to be handle with extreme care). The slides were dipped for 30 to 45 minutes in piranha solution, and then washed several times with distilled water.

The LbL deposition of (PAH/PSS), in section 4.2.1, was performed by dipping the slide successively in vials containing: 20 mL of PAH solution (MW 15 000 or 56 000 g/mol) for 4 minutes, 20 mL of ultrapure water for 1 min, 20 mL of PSS (MW 70 000 g/mol) or MR@Au NPs for 4 min, and 20 mL of ultrapure water for 1 min. Finally, the slide was dried using gentle air flow. The process was repeated upon the desired number of bilayers. The deposition of (PAH/MR@Au NPs), in section 4.2.2, was performed following the procedure above, using PAH (MW 56 000) and MR@Au NPs instead of PSS polyelectrolyte.

6.5.3. Layer-by-Layer deposition of $(PAH/PSS)_3$ $(PAH/MR@Au\ NPs)_4$

For section 4.3, the glass slides were cleaned using pure nitric acid instead of piranha solution. The deposition times chosen for the study were 5, 10 and 20 minutes.

The 3 precursor bilayers (PAH/PSS) were deposited using polyelectrolytes PAH (MW 56 000 g/mol) and PSS (MW 70 000 g/mol) with adjusted ionic strength with 10 mM NaCl. The washing step was also modified, by adjusting the ionic strength of ultrapure water at 10 mM NaCl. To improve the washing of polyelectrolytes, three of the prepared water solutions (10 mM NaCl) were used for each washing step, by dipping the slides during 3 minutes, plus two times 1 min with new and clean ultrapure water (10 mM NaCl). The drying step was also improved by drying after each washing step. The same procedure was used to deposit the 4 bilayers of (PAH/MR@Au NPs). For each slide used, the solutions of polyelectrolytes in beakers were changed with new stock polyelectrolytes (10 mM NaCl), except for the gold solution that was kept for all depositions in section 4.3, due to an insufficient amount of solution.

REFERENCES

1. Nič M, Jirát J, Košata B, Jenkins A, McNaught A (2009) IUPAC Compendium of Chemical Terminology. IUPAC, Research Triagle Park, NC

2. Kirsch J, Siltanen C, Zhou Q, Revzin A, Simonian A (2013) Biosensor technology: recent advances in threat agent detection and medicine. Chem Soc Rev 42:8733.

3. Holzinger M, Le Goff A, Cosnier S (2014) Nanomaterials for biosensing applications: a review. Front Chem 2:63.

4. Doria G, Conde J, Veigas B, Giestas L, Almeida C, Assunção M, Rosa J, Baptista P V. (2012) Noble Metal Nanoparticles for Biosensing Applications. Sensors 12:1657–1687.

5. Upadhyayula VKK (2012) Functionalized gold nanoparticle supported sensory mechanisms applied in detection of chemical and biological threat agents: A review. Anal Chim Acta 715:1–18.

6. Pereira SO, Barros-Timmons A, Trindade T (2017) A Comparative Study of Chemical Routes for Coating Gold Nanoparticles via Controlled RAFT Emulsion Polymerization. Part Part Syst Charact 34:1600202.

7. Liz-Marzán LM (2004) Nanometals: formation and color. Mater Today 7:26–31.

8. Faraday M (1857) The Bakerian Lecture: Experimental Relations of Gold (and Other Metals) to Light. Philos Trans R Soc London 147:145–181.

9. Turkevich J, Stevenson PC, Hillier J (1951) A study of the nucleation and growth processes in the synthesis of colloidal gold. Discuss Faraday Soc 11:55.

10. Frens G (1973) Controlled Nucleation for the Regulation of the Particle Size in Monodisperse Gold Suspensions. Nat Phys Sci 241:20–22.

11. Kimling J, Maier M, Okenve B, Kotaidis V, Ballot H, Plech A (2006) Turkevich Method for Gold Nanoparticle Synthesis Revisited. J Phys Chem B 110:15700–15707.

12. Zeng S, Yong K-T, Roy I, Dinh X-Q, Yu X, Luan F (2011) A Review on Functionalized Gold Nanoparticles for Biosensing Applications. Plasmonics 6:491–506.

13. Link S, El-Sayed MA (1999) Size and Temperature Dependence of the Plasmon Absorption of Colloidal Gold Nanoparticles. J Phys Chem B 103:4212–4217.

14. Huang X, El-Sayed MA (2010) Gold nanoparticles: Optical properties and implementations in cancer diagnosis and photothermal therapy. J Adv Res 1:13–28.

15. Saha K, Agasti SS, Kim C, Li X, Rotello VM (2012) Gold Nanoparticles in Chemical and Biological Sensing. Chem Rev 112:2739–2779.

16. Sepúlveda B, Angelomé PC, Lechuga LM, Liz-Marzán LM (2009) LSPR-based nanobiosensors. Nano Today 4:244–251.

17. Anker JN, Hall WP, Lyandres O, Shah NC, Zhao J, Van Duyne RP (2008) Biosensing with plasmonic nanosensors. Nat Mater 7:442–453.

18. Raschke G, Kowarik S, Franzl T, Sonnichsen C, Klar TA, Feldmann J, Nichtl A, Kurzinger K (2003) Biomolecular Recognition Based on Single Gold Nanoparticle Light Scattering. Nano Lett 3:935–938.

19. Dulkeith E, Morteani AC, Niedereichholz T, Klar TA, Feldmann J, Levi SA, van Veggel FCJM, Reinhoudt DN, Möller M, Gittins DI (2002) Fluorescence Quenching of Dye Molecules near Gold Nanoparticles: Radiative and Nonradiative Effects. Phys Rev Lett 89:203002.

20. Aslan K, Pérez-Luna VH (2004) Quenched emission of fluorescence by ligand functionalized gold nanoparticles. J Fluoresc 14:401–405.

21. Aslan K, Pérez-Luna VH (2006) Nonradiative interactions between biotin-functionalized gold nanoparticles and fluorophore-labeled antibiotin. Plasmonics 1:111–119.

22. Kato N, Caruso F (2005) Homogeneous, Competitive Fluorescence Quenching Immunoassay Based on Gold Nanoparticle/Polyelectrolyte Coated Latex Particles. J Phys Chem B 109:19604–19612.

23. Hsieh B-Y, Chang Y-F, Ng M-Y, Liu W-C, Lin C-H, Wu H-T, Chou C (2007) Localized Surface Plasmon Coupled Fluorescence Fiber-Optic Biosensor with Gold Nanoparticles. Anal Chem 79:3487–3493.

24. You C-C, Miranda OR, Gider B, Ghosh PS, Kim I-B, Erdogan B, Krovi SA, Bunz UHF, Rotello VM (2007) Detection and identification of proteins using nanoparticle–fluorescent polymer “chemical nose” sensors. Nat Nanotechnol 2:318–323.

25. Chiefari J, Chong YK (Bill), Ercole F, Krstina J, Jeffery J, Le TPT, Mayadunne RTA, Meijs GF, Moad CL, Moad G, Rizzardo E, Thang SH (1998) Living Free-Radical Polymerization by Reversible Addition−Fragmentation Chain Transfer: The RAFT Process. Macromolecules 31:5559–5562.

26. Moad G, Rizzardo E, Thang SH (2005) Living Radical Polymerization by the RAFT Process. Aust J Chem 58:379.

27. Moad G, Rizzardo E, Thang SH (2006) Living Radical Polymerization by the RAFT Process—A First Update. Aust J Chem 59:669.

28. York A, Kirkland S, McCormick C (2008) Advances in the synthesis of amphiphilic block copolymers via RAFT polymerization: Stimuli-responsive drug and gene delivery☆. Adv Drug Deliv Rev 60:1018–1036.

29. Nguyen D, Zondanos HS, Farrugia JM, Serelis AK, Such CH, Hawkett BS (2008) Pigment Encapsulation by Emulsion Polymerization Using Macro-RAFT Copolymers. Langmuir 24:2140–2150.

30. Bourgeat-Lami E, França AJPG, Chaparro TC, Silva RD, Dugas P-Y, Alves GM, Santos AM (2016) Synthesis of Polymer/Silica Hybrid Latexes by Surfactant-Free RAFT-Mediated Emulsion Polymerization. Macromolecules 49:4431–4440.

31. Zou H, Melro L, de Camargo Chaparro T, de Souza Filho IR, Ananias D, Bourgeat-Lami E, dos Santos AM, Barros-Timmons A (2016) Adsorption study of a macro-RAFT agent onto SiO2-coated

Gd2O3:Eu3+ nanorods: Requirements and limitations. Appl Surf Sci 394:519–527.

32. Pereira SO (2016) New polymerization routes for plasmonic nanostructured assemblies. PhD thesis, Universidade de Aveiro, Departamento de Química

33. Kolb HC, Finn MG, Sharpless KB (2001) Click Chemistry: Diverse Chemical Function from a Few Good Reactions. Angew Chemie Int Ed 40:2004–2021.

34. Himo F, Lovell T, Hilgraf R, Rostovtsev V V., Noodleman L, Sharpless KB, Fokin V V. (2005) Copper(I)-Catalyzed Synthesis of Azoles. DFT Study Predicts Unprecedented Reactivity and Intermediates. J Am Chem Soc 127:210–216.

35. Boren BC, Narayan S, Rasmussen LK, Zhang L, Zhao H, Lin Z, Jia G, Fokin V V. (2008) Ruthenium-Catalyzed Azide−Alkyne Cycloaddition: Scope and Mechanism. J Am Chem Soc 130:14900–14900.

36. Binder WH, Sachsenhofer R (2007) "Click" Chemistry in Polymer and Materials Science. Macromol Rapid Commun 28:15–54.

37. Golas PL, Matyjaszewski K (2010) Marrying click chemistry with polymerization: expanding the scope of polymeric materials. Chem Soc Rev 39:1338–1354.

38. Quémener D, Davis TP, Barner-Kowollik C, Stenzel MH (2006) RAFT and click chemistry: A versatile approach to well-defined block copolymers. Chem Commun 5051–5053.

39. Ranjan R, Brittain WJ (2007) Combination of Living Radical Polymerization and Click Chemistry for Surface Modification. Macromolecules 40:6217–6223.

40. Li Y, Yang J, Benicewicz BC (2007) Well-controlled polymerization of 2-azidoethyl methacrylate at near room temperature and click functionalization. J Polym Sci Part A Polym Chem 45:4300–4308.

41. Wang X, Liu L, Luo Y, Zhao H (2009) Bioconjugation of Biotin to the Interfaces of Polymeric Micelles via In Situ Click Chemistry. Langmuir 25:744–750.

42. Jin J, Wu D, Sun P, Liu L, Zhao H (2011) Amphiphilic Triblock Copolymer Bioconjugates with Biotin Groups at the Junction Points: Synthesis, Self-Assembly, and Bioactivity. Macromolecules 44:2016–2024.

43. Ariga K, Hill JP, Ji Q (2007) Layer-by-layer assembly as a versatile bottom-up nanofabrication technique for exploratory research and realistic application. Phys Chem Chem Phys 9:2319.

44. Decher G, Hong J (1991) Buildup of ultrathin multilayer films by a self-assembly process, 1 consecutive adsorption of anionic and cationic bipolar amphiphiles on charged surfaces. Makromol Chemie Macromol Symp 46:321–327.

45. Yu J, Meharg BM, Lee I (2017) Adsorption and interlayer diffusion controlled growth and unique surface patterned growth of polyelectrolyte multilayers. Polymer (Guildf) 109:297–306.

46. Pereira SO, Trindade T, Barros-Timmons A (2015) Biotinylation of optically responsive gold/polyelectrolyte nanostructures. Gold Bull 48:3–11.

47. Jiang C, Markutsya S, Tsukruk V V. (2004) Compliant, Robust, and Truly Nanoscale Free-Standing Multilayer Films Fabricated Using Spin-Assisted Layer-by-Layer Assembly. Adv Mater 16:157–161.

48. Haiss W, Thanh NTK, Aveyard J, Fernig DG (2007) Determination of Size and Concentration of Gold Nanoparticles from UV−Vis Spectra. Anal Chem 79:4215–4221.

49. Wulandari P, Nagahiro T, Fukada N, Kimura Y, Niwano M, Tamada K (2015) Characterization of citrates on gold and silver nanoparticles. J Colloid Interface Sci 438:244–248.

50. Sigma Aldrich Sigma-Aldrich Thermal Initiators: Decomposition Rate and Half-Life. http://www.sigmaaldrich.com/content/dam/sigma-aldrich/docs/Aldrich/General_Information/thermal_initiators.pdf.

51. Campos JM, Ferraria AM, Botelho do Rego AM, Ribeiro MR, Barros-Timmons A (2015) Studies on PLA grafting onto graphene oxide and its effect on the ensuing composite films. Mater Chem Phys 166:122–132.

52. Ladmiral V, Legge TM, Zhao Y, Perrier S (2008) “Click” Chemistry and Radical Polymerization: Potential Loss of Orthogonality. Macromolecules 41:6728–6732.

53. Couvreur L, Lefay C, Belleney J, Charleux B, Guerret O, Magnet S (2003) First Nitroxide-Mediated Controlled Free-Radical Polymerization of Acrylic Acid. Macromolecules 36:8260–8267.

54. ThermoFischer Probes Useful at Near-Neutral pH. https://www.thermofisher.com/pt/en/home/references/molecular-probes-the-handbook/ph-indicators/probes-useful-at-near-neutral-ph.html.

APPENDICES

Appendix A: KBr-FTIR spectra of Au NPs, MR agent, MR@Au NPs, copolymer and copolymer@Au NPs

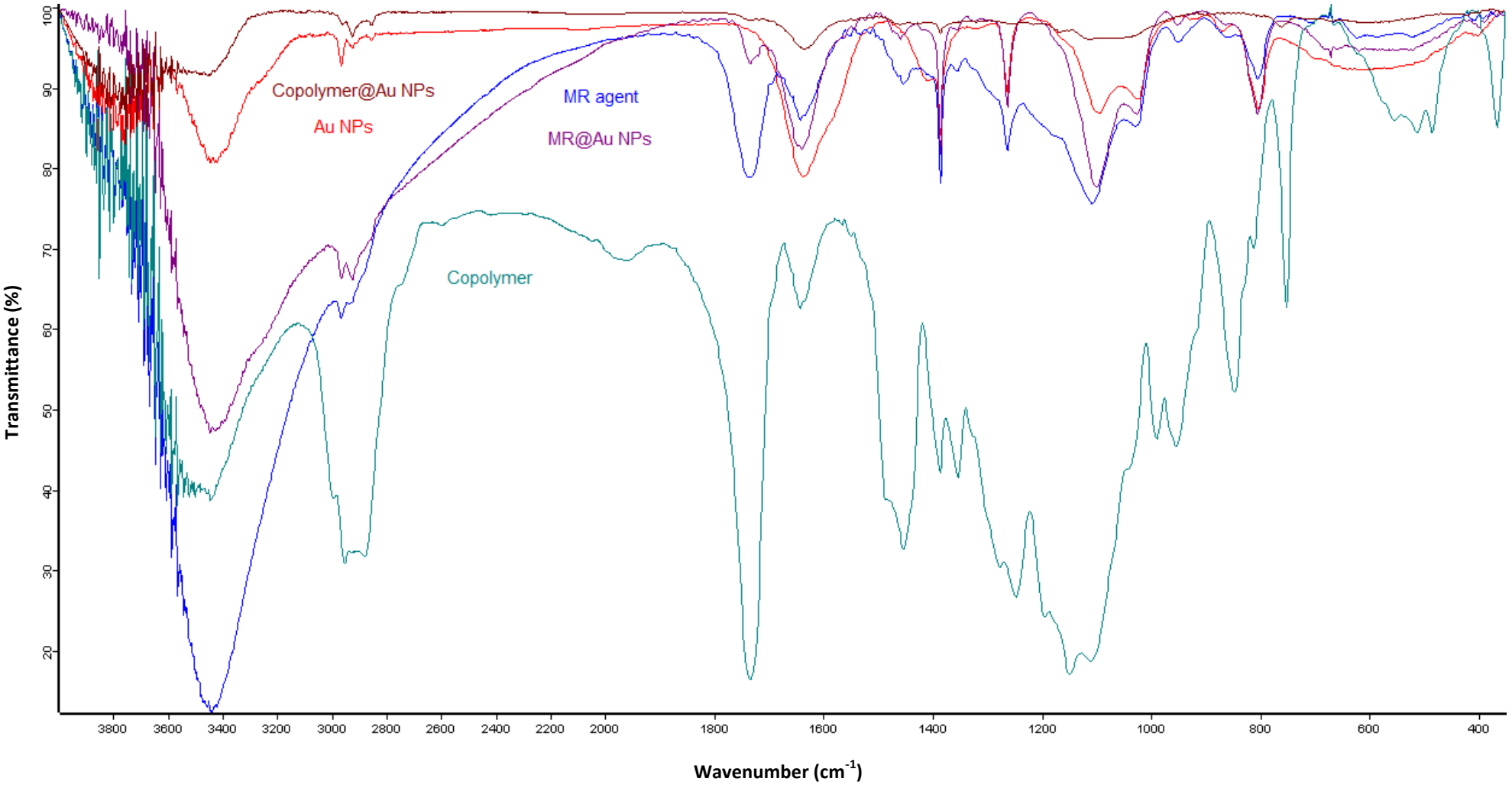

Figure A: KBr-FTIR spectra of Au NPs, MR agent, MR@Au NPs, copolymer and copolymer@Au NPs

Appendix B: AEM-FITC and fluorescein absorbance and fluorescence emission

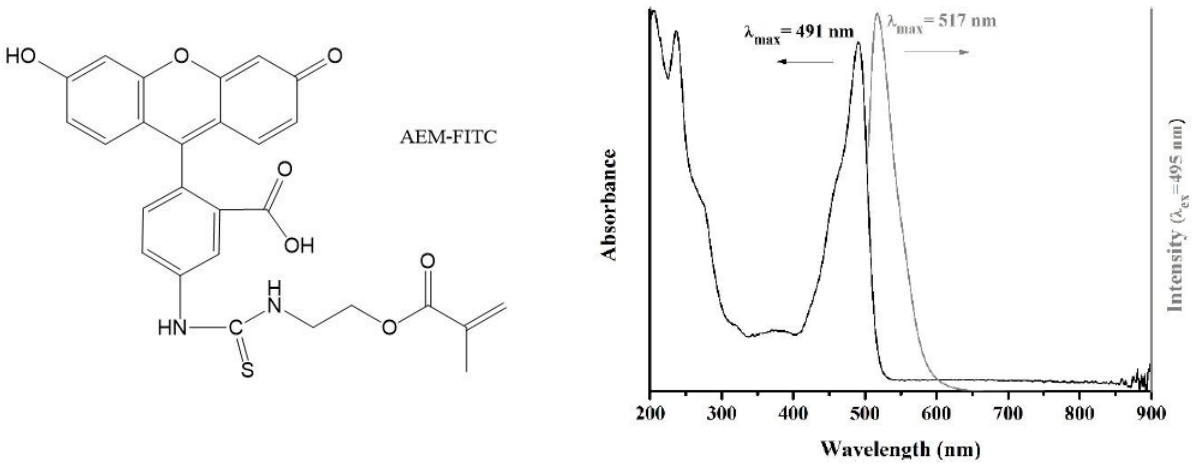

Figure B-1: (A) Chemical structure (neutral from) of fluorescein isothiocyanate (AEM-FITC), (B) Absorbance and fluorescence emission of AEM-FITC [32]

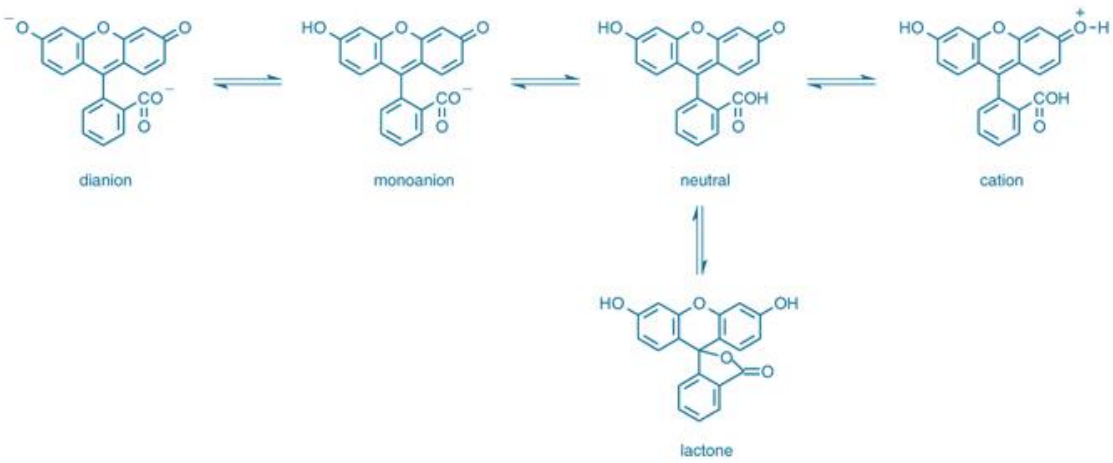

Figure B-2 : Ionization equilibria of fluorescein [54]

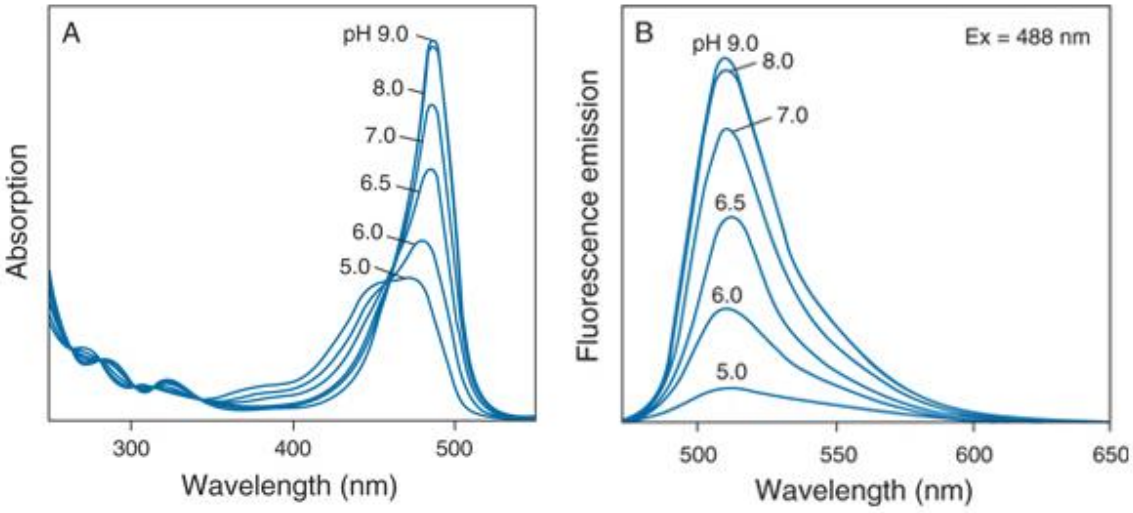

Figure B-3: pH dependent spectra of fluorescein: A) Absorbance spectra B) Emission spectra [54]

Appendix C: KBr-FTIR spectra of N_3-MR, N_3-FITC-MR and Biotin-FITC-MR

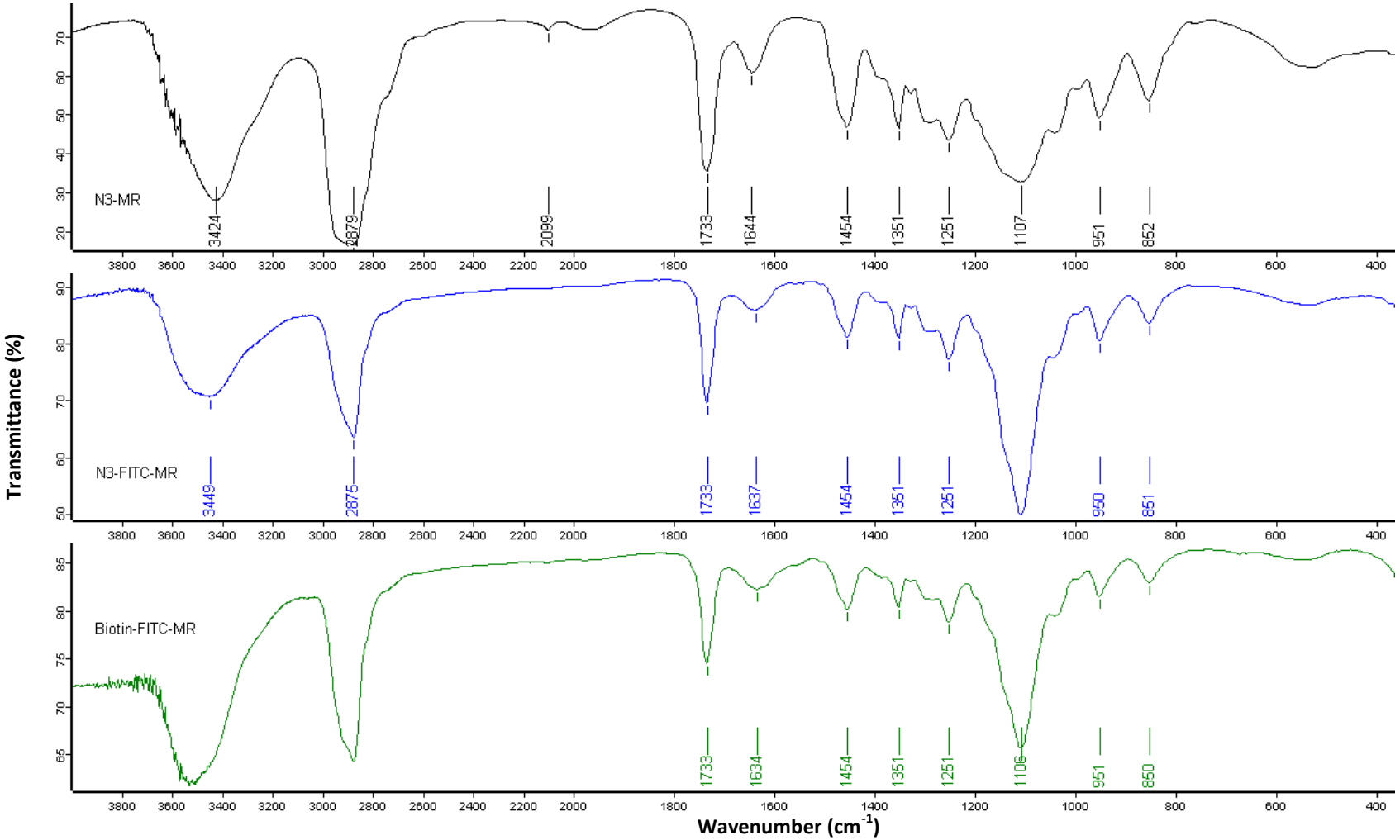

Figure C: KBr-FTIR spectra of N_3-MR, N_3-FITC-MR and Biotin-FITC-MR